2018-01-01

Integrated Immunoassays On Paper/polymer Hybrid Microfluidic Devices For Low-Cost Detection Of Disease Biomarkers

Sanjay Sharma Timilsina
University of Texas at El Paso, sanjaytimilsina@gmail.com

INTEGRATED IMMUNOASSAYS ON PAPER/POLYMER HYBRID MICROFLUIDIC DEVICES FOR LOW-COST DETECTION OF DISEASE BIOMARKERS

SANJAY SHARMA TIMILSINA

Doctoral Program in Chemistry and Biochemistry

APPROVED:

XiuJun (James) Li, Ph.D., Chair

Mahesh Narayan, Ph.D.

Juan Noveron, Ph.D.

Jianying Zhang, Ph.D.

Charles H. Ambler, Ph.D.
Dean of the Graduate School

Dedication

To my Family
with love

INTEGRATED IMMUNOASSAYS ON PAPER/POLYMER HYBRID MICROFLUIDIC DEVICES FOR LOW-COST DETECTION OF DISEASE BIOMARKERS

by

SANJAY SHARMA TIMILSINA

DISSERTATION

Presented to the Faculty of the Graduate School of

The University of Texas at El Paso

in Partial Fulfillment

of the Requirements

for the Degree of

DOCTOR OF PHILOSOPHY

Department of Chemistry and Biochemistry

THE UNIVERSITY OF TEXAS AT EL PASO

May 2018

Acknowledgments

In my five years of studying at the University of Texas at El Paso (UTEP), I am privileged that I have met many wonderful people who invested and shared their time, talent and wisdom to help me pursue my dream of being a researcher.

I would like to express my deepest gratitude to my mentor and chairman of my committee Dr. XiuJun (James) Li for introducing me to the research field of microfluidic lab-on-a-chip for bioanalysis and 3D cell culture. As my teacher and mentor, he has taught me more than I could ever give him credit for his guidance, encouragement, and constant support. His dedication and motivation to research will continue to inspire me as he is everything one could look for in a good mentor. Dr. Li is always pleased to provide opportunities for his students to give presentations in all kinds of conferences and provide strong recommendation letters whenever needed. His helpful guidance has equipped me with competency in research, improved my scientific writing skills, and made me able to produce notable scientific publications. I also appreciate Dr. Li's concern for my professional development. Thank you for being a good mentor and for guiding me on the right path.

I am indebted to my committee members: Dr. Mahesh Narayan, Dr. Juan Noveron, and Dr. Jianying Zhang who provided me extensive professional guidelines. With distinct scientific backgrounds, they have provided numerous helpful advice, insight, comments, and suggestions about scientific research with their kindness and valuable time to help improve my research projects.

I appreciate the support of my colleagues in the Li Research Group. I would like to thank those who helped me in my publications: Dr. Maowei Dou, Dr. Guanglei Fu, and Wan Zhou. I would like to thank Meihan Li who helped me with the reusable hybrid plug-and-play device. Similarly, I would like to thank Ziyuan Ma who helped me to develop electrochemical assay in the hybrid device. I would also like to thank Elisabeth Hirth and Man Luo who performed LAMP on the paper-based device and Maria Romero-Creel who performed 3D cell culture in the

hybrid device along with me. I am grateful to all of those with whom I have had the pleasure to work during my stay at UTEP including, Dr. Sai, Dr. Prasad, Dr. Wei, Dr. Zhang, Dr. Gilberto, Juan Sanchez, Pamela Hernandez, Misael, Oscar, Hamed, Sergio, Zayra, Jin, Lei Ma and all the Li group members for their readiness to help and for the nice working atmosphere they created.

I would like to thank all the professors and staff from Department of Chemistry and Biochemistry of UTEP for all their hard work and dedication, providing me the knowledge and means to complete my degree. I would like to express my special thanks to Dr. Mito for letting me use the FTIR for my project.

Nobody has been more significant to me in the pursuit of my research project than the members of my family and friends. I want to thank my dear parents, my wife, my brother, my sister-in-law, my grandparents, and all my dear family and friends for their true love, encouragement, and firm support. It was impossible for me to continue my graduate study without them, whose love and guidance are with me in whatever I pursue.

The funding agencies that supported my dissertation research are very much appreciated. I would like to acknowledge the financial support of the NIH/NIAID under award number R21AI107415, the NIH/NIGMS under award number SC2GM105584, and the NIH/NIMHD/RCMI under award number 5G12MD007593-22. Financial support from the Emily Koenig Meningitis Fund from the Philadelphia Foundation, Emily's Dash Foundation, the Medical Center of the Americas (MCA) Foundation, the U.S. NSF-PREM program (DMR 1205302), the NIH BUILD program, University of Texas System for the STARS Award, and the IDR Program at the University of Texas at El Paso, is also gratefully acknowledged.

Abstract

Infectious diseases and cancers have been the major cause of global death and disability causing a significant impact on global health and economies. Enzyme-linked immunosorbent assay (ELISA) is one of the most widely used laboratory diagnostic methods for infectious diseases and cancer. ELISA detects proteins based on their binding to immobilized antibodies or antigen. Even though most ELISAs performed today in 96-well plates are well suited for high throughput assays, performing ELISA in low-resource settings is limited by several factors, such as long incubation time, large volumes of precious reagents, and well-equipped laboratories. Herein, we have developed multiple simple, miniaturized poly(methyl methacrylate) (PMMA) and paper/PMMA hybrid microfluidic devices for the detection of infectious diseases and cancer biomarkers in low-resource settings.

At first, we developed a surface modified PMMA microfluidic microplate, where the protein was covalently bound either to the carboxylated PMMA surface using carbodiimide chemistry or to the amine dense PMMA surface functionalized with polylysine. Immobilization efficiency of proteins on the surface of the modified PMMA was remarkably increased due to the covalent binding of the protein, thereby improving the sensitivity of ELISA and decreasing the background noise. The surface modified PMMA microplate, where the protein can be covalently immobilized within 20 min was used for the ultrasensitive multiplex detection of various biomarkers including Immunoglobulin G (IgG), Hepatitis B surface antigen (HBsAg), and Hepatitis B core antigen (HBcAg) with limits of detection (LODs) of 200 pg/mL, 180 pg/mL, and 300 pg/mL, respectively. The results of the assay can be viewed by the naked eye or scanned through a simple desktop scanner for quantitative analysis within 90 min as compared to 18 hours in traditional microplates. The surface modified microplate was found to be at least 10-fold more sensitive than traditional microplates with much less reagent consumption.

To avoid the complicated surface modification steps, we also developed a novel paper/PMMA hybrid microfluidic microplate using a porous, 3D paper in flow-through microwells. The use of low-cost chromatography paper in the funnel-shaped microwells

facilitated the rapid immobilization of protein within 10 min as compared to overnight incubation in traditional microplates. In addition, it also helped in the efficient washing, decreasing the background noise. The top reagent delivery channels can transfer reagents to multiple microwells, avoiding repeated manual pipetting or the use of costly robots. Results of these colorimetric ELISA could be observed by the naked eye within an hour. LODs of 1.3 ng/mL and 1.6 ng/mL for IgG and HBsAg were achieved without any specialized equipment, which was comparable to commercially used microplate ELISA. Likewise, for the device to be used in high-end laboratories and hospitals, the hybrid device was redesigned to make it compatible with traditional microplate readers. Chemiluminescence ELISA of HBsAg, HBcAg, and Hepatitis C virus core antigen (HCVcAg) was performed in the hybrid device with LODs of 50 pg/mL, 35 pg/mL, and 10 pg/mL, respectively, using commercial microplate reader to read the device. Our hybrid device was found to be 100-fold more sensitive than 96-well commercial microplate, even with the reduced amount of sample (5 μL as compared to 50 μL) and assay time (1 hr compared to 18 hr).

To further increase the sensitivity of the device and to measure low-concentration analytes, we developed a reusable, cost-effective, and eco-friendly PMMA/paper hybrid plug-and-play (PnP) device for analyte enrichment and detection. The sample flowed back and forth through the low-cost 3D paper substrate within PMMA channels, thereby, enriching the amount of analyte adsorbed and dramatically decreasing the incubation time. After the enrichment assay, the paper substrate can be replaced so that the device can be reused. LODs, 10-fold better than commercial microplate reader and a wide linear range of five and six orders of magnitude was obtained for IgG and HBsAg, respectively. Finally, we demonstrated the broader application of our microfluidic approach by developing paper in PMMA pond hybrid microfluidic device for simultaneous detection of cancer biomarkers including prostate-specific antigen (PSA) and carcinoembryonic antigen (CEA). The porous 3D paper kept in between the flow-through reservoir and pond, helped in rapid immobilization of protein and efficient washing, thus increasing the sensitivity and decreasing the noise. Sandwich type immunoassay was performed

accordingly in the hybrid device, where the reagent is delivered automatically to the paper-substrate through the reagent delivery channel. LOD of 0.32 ng/mL for CEA and 0.20 ng/mL for PSA was obtained, which is sensitive enough to detect clinical cut off value of 5 ng/mL and 4 ng/mL for CEA and PSA, respectively.

We envisage that these simple polymer/paper hybrid microfluidic microplates can be used in both underdeveloped and developed countries for low-cost, sensitive, and high-throughput bioassays of infectious diseases, cancer biomarkers, and other bio-molecules.

Table of Contents

List of Tables

List of Figures

Chapter 1: Introduction

- This chapter introduces infectious diseases and cancer.
- Current technologies for detection of disease biomarkers and their drawbacks are described in this chapter.
- The chapter also describes the application of microfluidic lab-on-a-chip for low-cost detection of disease biomarkers.
- Finally, the research objectives are explained in the chapter.

1.1 Infectious diseases

Acute infectious diseases caused by pathogenic organisms such as bacteria, viruses, fungi, and parasites have been a major cause of global death and high disability rates throughout the human history, especially in underdeveloped and developing countries.[7, 8] They can directly or indirectly transmit from one person to another. Our defense against these diseases has been facing problems like recognition of the pathogens or viruses' species, strains, virulence factors, and antimicrobial susceptibilities in a timely manner.[9] We are currently in a very fragile balance with respect to the continual emergence of new infectious diseases and the reemergence of old infectious diseases, together with the potential for their global spread. The emergence of 335 infectious diseases between 1940 and 2004 in global human population has generated an extremely significant impact on global health and economies.[10, 11] Infectious diseases have been one of the leading causes of death and out of 58.8 million annual deaths, roughly 25% (15.0 million) deaths are due to infectious diseases.[7, 12]

1.1.1 Hepatitis B virus

Hepatitis B virus (HBV), a DNA virus from Hepadnaviridae family, is capable of establishing persistent reservoir in the form of covalently closed circular DNA in hepatocytes. Permanent elimination of these viruses is extremely low.[13] These viruses are highly transmissible as they are extremely replicable which leads to assembly of concentrated viral particles in body fluids and blood of the infected person. The continual presence of hepatitis B surface antigen (HBsAg) for at least 6 months in serum is the diagnostic confirmation of chronic hepatitis B (CHB), which is a necro-inflammation in the liver due to the extended presence of HBV.[14] HBV, which is one of the major causes of chronic hepatitis damage and hepatocellular carcinoma, has approximately 2 billion infection cases with 1.2 million deaths every year.[15, 16] 5-15% of the

people in developing and underdeveloped countries carry HBV.[17] In addition, CHB is the leading risk factor for hepatocellular carcinoma (HCC), which results in 746,000 deaths per year.[18] There is a high ecological correlation between areas of HBV prevalence and HCC incidence and mortality.[19] To prevent the transmission of HBV, testing of HBsAg has been recommended for hemodialysis patients, pregnant woman, person exposed to HBV (e.g. infants born to HBV-infected mother, sex partners of infected persons, persons exposed to infectious blood or body fluids), donors of blood, organs and tissues, HIV-positive persons, injection drug users, and high-prevalence populations (high rate of endemic HBV).[20] Marcellin *et al*. found that liver cirrhosis was reversible with sustained suppression of HBV by long-lasting treatment with tenofovir in patients with advanced fibrosis or cirrhosis.[21] Early detection of biomarkers for HBV remains a key to fight against the disease and resulting carcinoma.

1.1.2 Hepatitis C virus

Hepatitis C Virus (HCV), the causal agent for a chronic liver infection which was originally identified as non-A non-B hepatitis, is a single-stranded RNA virus.[22] It is a member of the Flaviviridae family and has six major genotypes (1-6) and a series of subtypes. There is a worldwide distribution of genotypes 1-3 while genotypes 4 and 5 appear predominantly in Africa, and genotype 6 in Asia. It has been estimated that worldwide there were 54,000 deaths and 955,000 disability adjusted life-years associated with an acute HCV infection.[23] It has also been assessed that 3-4 million persons are newly infected every year, 170 million people are chronically infected and are at risk of developing liver disease including cirrhosis and liver cancer. Each year 350,000 deaths occur due to all HCV-related causes.[24] Out of 500,000 new cases of liver cancer that occur each year, more than 100,000 (22%) are attributed to the infection of HCV. HCV has been considered one of the major health problems of global concern

because studies have shown that estimated 80% of acute hepatitis C can progress as a chronic infection. Furthermore, 10–20% of HCV infection can develop complications of chronic liver disease including liver cirrhosis, and finally, 1–5% develop liver cancer[25].

1.2 Cancer

Cancer, the uncontrolled growth of abnormal cells in the body with the potential to invade or spread to other parts of the body through the blood and lymphatic system, figures among a leading cause of death worldwide accounting for 8.2 million deaths in 2012, according to World Health Organization (WHO).[26,27] Cancerous cells often invade the surrounding tissues and can metastasize to distant parts of the body through the blood and lymphatic system. Cancer is the second leading cause of death in the US, exceeded only by heart disease, accounting for nearly 1 of every 4 deaths.[28] Besides, it is expected that annual cancer cases will rise from 14 million in 2014 to an astonishing figure of 22 million within next 2 decades. The majority of countries with top incidence rates are developing countries, however, highest mortality rate occurs in developing countries. The higher mortality in developing countries is due to late diagnosis, barriers to diagnosis and medical care.[29] Much of the burden of cancer such as incidence, morbidity, and mortality mainly occurs in developing countries.[30]

1.2.1 Prostate Cancer

Prostate cancer begins as the cells in the prostate gland start growing uncontrollably and are mostly adenocarcinomas. Prostate cancer is the fourth most common cancer if both sexes are combined and the second most common cancer in men, and the most common cancer in men in the developed countries.[31] Worldwide, in 2012 an estimated 1.1 million people were diagnosed with prostate cancer, which accounts for 15% of the cancers diagnosed in men. Out of 1.1

million, nearly 70% (759,000) occurred in more developed regions. The total prostate cancer mortality in men is estimated to be 307,000 which represents 6.6% of the total male cancer mortality and is the fifth leading cause of death from cancer.[32] Prostate cancer is primarily considered as the disease of elderly men, as 85% of all the cases are diagnosed in men who are older than 65 years. Similarly, 90% of all the deaths due to prostate cancer are in men over the age of 65 years.[33] Prostate cancer incidence remains highest in developed countries like Australia, New Zealand and North America (largely because of the widespread practice of prostate-specific antigen (PSA) testing and subsequent biopsy in those regions) and remains low in the Asian population, eastern and South-Central Asia. Age, ethnic origin, and a positive family history are the strongest known risk factors. Genes that cause prostate cancer can be inherited and some of those genes show high penetrance. Advanced prostate cancer requires androgen-deprivation treatment which can reduce symptoms in about 70–80% of patients but most tumors relapse within 2 years to an incurable androgen-independent state.[34]

1.2.2 Colorectal cancer

Colorectal cancer starts in the colon or the rectum and usually begins as growth called a polyp on the inner lining of the rectum or colon. The intestinal epithelium is a hotspot for malignant transformations such as colorectal cancer because it has a very high turnover rate. Although, there are some types of cancer which are known to run in certain families, however, most cancers are not hereditary.[35] Colorectal cancer is the second most common cancer in women with around 614,000 cases, which is around 9.2% of total cancer cases. In men, it is the third most common cancer with 746,000 cases, that is 10.0% of the total cases[32]. Incidence is more common in developed regions (55%) such as Australia and New Zealand while lowest in underdeveloped regions like Western Africa. However, mortality is higher in less developed

region due to poor prognosis. Total mortality is estimated to be 694,000 per year in both sexes, which is 8.5% of the total death due to cancer.[32] According to a recent study, the global burden of colorectal cancer is expected to increase by 60% to more than 2.2 million new cases and 1.1 million deaths by 2030.[36]

1.3 Current technologies for detection of disease biomarkers

A biomarker is a diagnostic indicator for assessing the risk or the presence of a disease. It is a characteristic that can be measured and evaluated as an indicator of normal biological processes, pathogenic processes or pharmacologic responses to a therapeutic intervention. It can include mRNA expression profiles, circulating DNA and tumor cells, proteins, proteomic pattern, lipids, metabolites, imaging methods or electrical signals. These signals/biomarkers may be obtained from sources such as urine, blood, and tissues.[37]

In 1800s, it was found that identifiable microorganisms cause specific diseases, which led to pathogen-specific medical diagnosis of today's era. Microbiological culture in a laboratory setting is commonly used as a significant approach to identify a variety of infectious diseases.[38] However, limitations of microbiological culture including a long diagnostic time up to a week to identify the organism and low-sensitivity especially for patients who have received antibiotic pre-treatment limit their use.[39-41] Gram stain is used as preliminary identification of bacterial species but should be employed by combining the other diagnostic tools such as traditional microbiological culture and molecular techniques. The sensitivity is low and the technique requires well-trained personnel, as it is mostly limited by poor staining.[42]

Similarly, a biopsy is a procedure to remove a piece of sample or tissue from any suspected part of the body to analyze in a laboratory for diagnosing cancer. A biopsy is usually performed if there are any signs or symptoms of cancer or if an area of concern is noticed by the

doctor after X-ray or other scanning tests. Recent discoveries in the field of genetics and molecular biology have revolutionized our understanding of cancer initiation and progression. Likewise, the knowledge that "genetic changes drive cancer progression" has provided a variety of molecular markers for early detection of cancer.[43] Newer technologies have transformed the field of molecular diagnosis for cancer.

Due to the high fatality and the high number of infections caused by untreated infectious disease and cancer, especially in rural and resource-limited settings, a simple, low-cost, rapid, and highly sensitive approach for immediate detection of infectious diseases and screening of cancers is in great need. WHO has developed a list of general characteristics that make a diagnostic test appropriate for resource-limited sites, abbreviated as ASSURED, and includes: Affordable by those at risk, Sensitive, Specific, User-friendly, Rapid treatment and robust use, Equipment-free, and finally Delivered to those who need it.[44]

1.3.1 Quantitative real-time polymerase chain reaction (qPCR)

Quantitative real-time polymerase chain reaction (qPCR) is a laboratory molecular biology technique used to monitor and quantify the PCR amplification of the target DNA. Detection can be achieved by using either non-sequence-specific fluorescent dyes that intercalate with any double-stranded DNA or sequence-specific fluorescent dyes. PCR remains the most widely adopted nucleic acid amplification method with applications in clinical, biological, agricultural, environmental, and forensic analysis. qPCR has been widely employed for infectious disease diagnosis.[46-48]

Measurement of HBV DNA is a direct measurement of the viral load, which can show the replication activity of the virus. HBV DNA assays can be carried out by real-time PCR. PCR has a limit of detection (LOD) of 10–20 IU/mL. Serum HBV DNA concentrations range from

undetectable to more than 10^9 IU/mL during the course of chronic HBV infection.[16] Hepatitis C Virus RNA is detectable in serum as soon as 1 week after the initial exposure. Thus, nucleic acid testing (NAT) remains the gold standard for diagnosis of HCV infection by PCR and is in routine use.[49]

The laboratory setup for performing NAT requires expert technical staffs, expensive reagents, dedicated procedure areas, and availability of pristine serum or plasma samples. In addition, qPCR requires laborious and time-consuming sample preparation process such as DNA purification, and specialized instruments in a well-equipped laboratory such as qPCR, centrifuges, fluorescent microscopes, and so on, which limits the broad application of qPCR in low-resource settings.

1.3.2 Enzyme-linked immunosorbent assay (ELISA)

ELISA, one of the most widely used laboratory methods in medical diagnostic and research applications, is based on the binding of antibodies and antigens[50]. It is used for detecting and quantifying substances such as peptides, proteins, antibodies, and hormones. ELISA can detect the etiologic agents of diseases directly from clinical samples, which is very useful for rapid detection of uncultivable or fastidious microorganisms. Depending upon the structure and characteristics of target substances, ELISA can be performed in a variety of ways such as Direct, Indirect, Sandwich, and Competitive ELISA as shown in Figure 1.1.[1]

For direct ELISA, the antigen or antibody to be measured is directly coated to the surface of the plate. After blocking the unbound surface, an enzyme-tagged antibody is added (Figure 1.1). The plate is incubated, followed by the washing of any unbound antibodies. Finally, the appropriate substrate for the enzyme is added and the signal is measured to determine the amount of antigen/antibody.

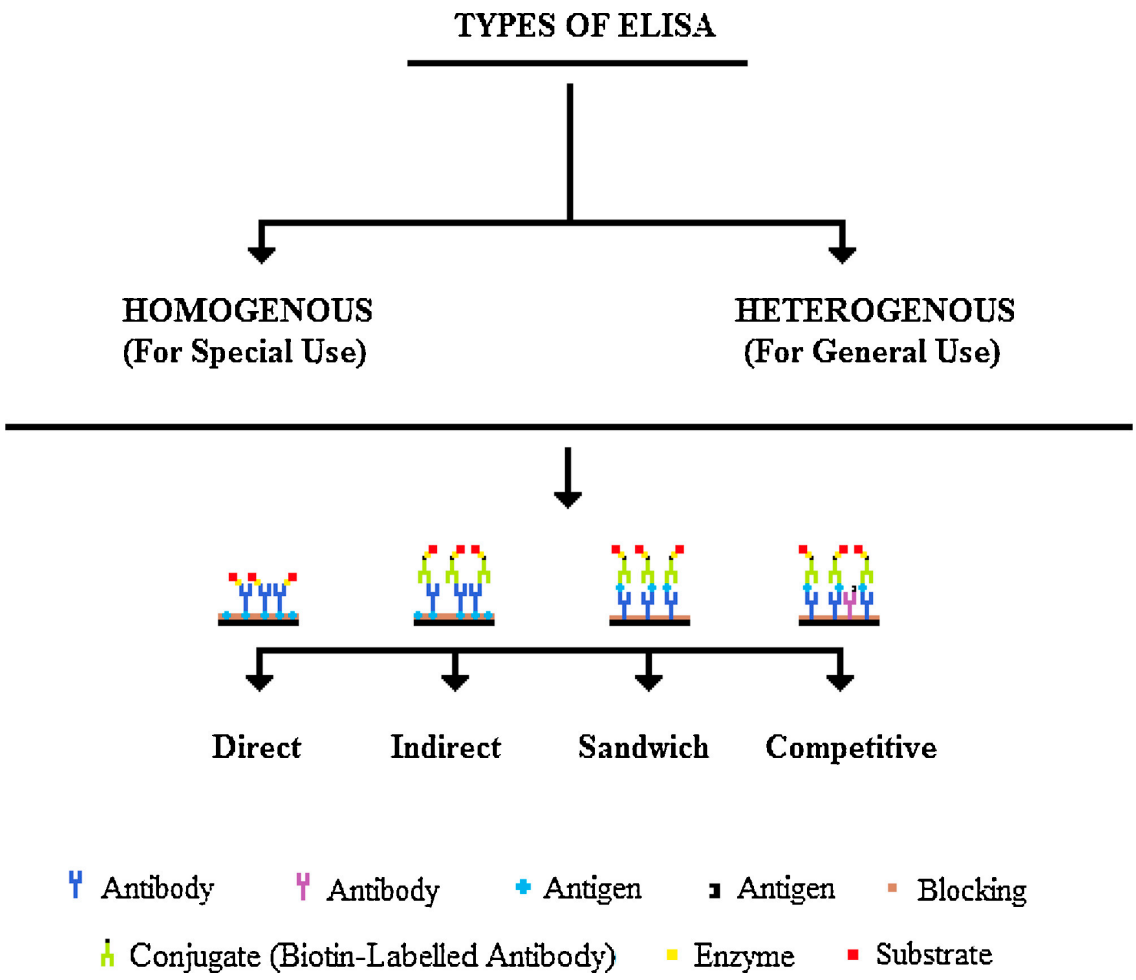

Figure 1.1: Schematic of different types of ELISA. (Source: Adapted with permission from Aydin 2015. Copyright © 2015, Elsevier).[1]

In case of indirect ELISA, the antigen to be measured is first added to the surface of the plate and blocked. The antibody against the antigen is then added to the plate so that the antibody binds to the coated antigen (Figure 1.1). Afterward, a secondary antibody coated with the enzyme is added, which binds with the primary antibody. Finally, a suitable substrate for the enzyme is added to produce a signal that can be used to determine the amount of antigen.

For sandwich ELISA, capture antibodies are first added to the plate and blocked with blocking buffer. Antigens to be measured are then added to the plate and incubated, followed by washing to remove unbound antigens (Figure 1.1). Enzyme-tagged antibodies are then added to

the plate followed by washing. After the addition of appropriate substrate, the signal is measured to determine the amount of antigen.

Finally, in case of competitive ELISA, the surface of the well is coated with the antigen-specific antibody. The antigens to be measured (untagged sample) and enzyme tagged antigens are placed into the plate simultaneously (Figure 1.1). The fixed amount of the tagged and unknown concentration of the untagged antigen (sample) compete with each other to bind to the antibody. After washing, the substrate is added and the signal is measured. Unlike other types of ELISA, there is an inverse proportion between the concentration of the antigen and the signal.

During the past few years, commercial ELISA assays for the quantification of HBsAg concentrations have been approved in Europe and many countries in Asia for the detection of HBV.[16] Similarly, for the detection of HCV, antigenic characterization has shown that the Hepatitis C Virus core antigen (HCVcAg) has the potential for the diagnostic marker, and several assays that rely on detecting the presence of the HCVcAg alone or in combination with anti-HCV in serum or plasma have been developed commercially.[49]

ELISA has also been widely used for the detection of cancer biomarkers. Carcinoembryonic antigen (CEA), is an important tumor marker responsible for clinical diagnosis of over 95% of all colon tumors, 50% of breast tumors, as well as tumors of the lung, pancreas, ovaries, and others of epithelial tissue origin, especially of the gastrointestinal tract, and is widely measured using ELISA.[51] Likewise, PSA level in the serum measured using ELISA and digital rectal examination (DRE) are the recommended methods for the detection of prostate cancer.[33]

Even though most ELISAs today which are performed in 96-well plates are well suited for high throughput assays, they take several hours to complete because of the hour-long

incubation and blocking time.[52] Similarly, other critical issues include consumption of large volume of precious samples and reagents, dependence on laboratory settings, making conventional ELISA not suitable for Point of care (POC) detection. In addition, highly complicated and specialized instruments have to be utilized to automate assays in a high-throughput format, like robotic pipettors, plate washers, and optical detectors. Furthermore, most detection methods require bulky and expensive equipment, which further limits their application in POC detection and in developing countries.

1.4 Microfluidic lab-on-a-chip

The microfluidic technique (Lab-on-a-chip (LOC), or micro total analysis system (μTAS)) developed in the 1990s offer unique opportunities for various biomedical applications.[53] It is a miniaturized system that can integrate one or several functional units in a small device.[54] They are mostly produced by the microfabrication techniques. Due to the microliter volume of the microchannels, there is a significant decrease in analysis time from hours to minutes and minimal reagent consumption. It also allows integrated processing and analysis of complex biological fluids with high efficiency and sensitivity in the healthcare settings, as well as the possibility of rapid and multiplex detection.[37, 55]

1.4.1 Advantages and applications of microfluidic lab-on-a-chip

Microfluidic technology possesses remarkable features for simple, low-cost, and rapid disease diagnosis, and analysis of complex biological fluids with high sensitivity for healthcare application. Numerous microfluidic devices have been developed for biomedical applications. These devices enable on-chip POC diagnosis and real-time monitoring of diseases from a small volume of body fluids. They have the potential to act as a bridge to improve the global healthcare

system with high efficiency and sensitivity, mainly for remote areas with scarce resources, such as the underdeveloped and developing countries, and in emergency situations. Therefore, the LOC technology has great potential to improve global health through the development of POC testing devices.[56, 57] Microfluidic LOC technology possesses several other remarkable features which are discussed below:

(1) Microfluidic LOC is a miniaturized system. It is compact, portable, and consumes much less space with the size of few square centimeters. The device can be easily carried to POC settings such as the underdeveloped and developing countries and in emergency situations.

(2) Minimum volume of samples and reagents are required. The volume required ranges from microliters to picoliters, which has significant importance as sample amount can be limited at times (cancer biopsy, forensic analysis, detection of infectious diseases). It also helps to reduce the cost by decreasing the volume of expensive reagents.

(3) Analysis time of the LOC devices is considerably faster as compared to traditional methods. Fast analysis time is due to several factors including short diffusion distances, high surface-to-volume ratios, increased effective contact areas and concentrations, etc.[58]

(4) Integration of several laboratory functions within a single miniaturized chip is one of the most important features of LOC devices. This provides great flexibility to perform various laboratory functions without the use of sophisticated instruments.

(5) High throughput of the assay remains another remarkable advantage of LOC over conventional techniques. High throughput assay can be achieved in LOC devices due to the massive parallelization and high-speed serial processing.

(6) Microfluidic lab-on-a-chip has a better process control as the device is very small and different processes can be controlled in a better way.

(7) Concentration gradients and controllable diffusion can be easily achieved by the use of gradient generator or different kind of substrates and valves.

(8) Finally, the LOC devices are quite economical as compared to traditional methods as it avoids the use of expensive and sophisticated instruments.

Because of all these significant features, numerous microfluidic devices have been developed for various applications including:

(1) Biomarker detection in disease diagnosis and biochemical analysis (cancers, infectious diseases, and other cardiovascular diseases, single-cell analysis);

(2) Environmental monitoring;

(3) Food safety analysis;

(4) Synthesis of chemicals and nanomaterials;

(5) Synthesis of pharmaceutical drugs and drug carriers;

(6) Drug discovery and controlled drug delivery; and

(7) 3D cell culture, organ-on-a-chip, and organism-on-a-chip.[37, 55, 58-67]

1.5 Substrates for microfluidic platform fabrication

In the early stage of microfluidics, microfluidic devices were predominantly made with methods borrowed from microelectronics field and involved materials such as glass, quartz or silicon. Although glass and silicon have good performance in chemical and thermal resistance, they have expensive and complicated fabrication process, require cleanroom facility, and have low biocompatibility. In addition, silicon is a high-cost material and not feasible for optical detection, which further limits the fabrication and applications of silicon-based microfluidic devices. Silicon and glass are more expensive and less flexible to work with, as compared to polymers (e.g. polydimethylsiloxane (PDMS), poly(methyl methacrylate) (PMMA)).[68-75] Most of

the polymers have good optical properties similar to glass, but their fabrication (e.g. soft lithography) does not have stringent requirements on cleanroom facility, which makes polymer-based microfluidic devices widely used.[76, 77] Within the past few years, paper-based microfluidic devices have debuted as a lower-cost microfluidic platform.[65, 78] The choice of material depends on the research application, detection system, fabrication facility, cost, and other factors such as resistance to different chemicals, thermal conductivity, dielectric strength and sealing properties.

1.5.1 Polydimethylsiloxane (PDMS)

PDMS is among the most commonly used elastomers for microfluidic devices as it is optically transparent, elastic, and cures at low temperature. It can bind to itself and to a range of other materials after being exposed to air plasma. The ease and low cost of fabrication as well as its ability to be cast in high resolution increase its advantages. In contrast to other thermoplastic materials, PDMS is gas permeable, which makes it compatible with cell culture. PDMS is an ideal substrate for applications of microfluidic 3D cell culture and organ-on-a-chip.[79-81] PDMS-based microfluidic devices have been employed for various applications.[82-84] There are different methods available for the fabrication of PDMS devices including soft lithography, casting, injection molding, imprinting, hot embossing, and laser ablation.[62, 76, 85]

Although PDMS is highly suitable for cost-effective microfluidic platforms, there are some limitations of PDMS as well. PDMS swells in organic solvents and low molecular weight organic solutes. It cannot withstand high temperature and has low mechanical resistance.

1.5.2 Poly(methyl methacrylate) (PMMA)

PMMA is another extensively used thermoplastic that serves as an economical alternative to glass and silicon-based microfluidic platforms. PMMA is low-cost, optically transparent, and

is compatible with a variety of chemical and biological reagents. They have moderately high mechanical properties. PMMA is easy to fabricate and economical for mass production and does not require long fabrication and curing time. PMMA devices can be fabricated easily by cutting the pattern using a CO_2 laser cutter followed by bonding with an adhesive or heat to form 3D devices. Multilayered devices can be completely fabricated and made ready for testing in as little as several hours.[87] All these properties make PMMA a widely used substrate for the fabrication of microfluidic devices with a variety of applications.[88-90]

PMMA devices can be fabricated using various methods such as hot embossing or imprinting, laser ablation, injection molding, and soft lithography.[37] Hot embossing and laser ablation are two generally used micromachining techniques.[75, 86] Silicon stamps are the more commonly used embossing tools for the fabrication of these polymeric microfluidic devices. A typical hot embossing setup consists of a force frame, which delivers the embossing force via a spindle and a T-bar to the boss or the embossing master. The microstructures are then transferred from the master to the polymer by stamping the master into the polymer by heating above its glass transition temperature (Tg) under vacuum.[91] Alternatively, polymer devices can be imprinted at room temperature with elevated pressure. The master structure is pressed into the thermoplastic substrate with a force (e.g. 20–30 kN in the case of PMMA) depending on the type and size of the substrate along with the feature to be imprinted.[91] Finally, the master and the substrate are isothermally cooled to a temperature just below Tg and then separated. The resulting plastic microchannel dimensions are the exact mirror image of the silicon stamp when devices are hot embossed.

Laser ablation is also one of the rapid methods for the fabrication of microfluidic devices.[92, 93] Using this technique, the polymer is exposed to a high-intensity laser beam, which

evaporates the material at the focal point by photo-degradation or thermal-degradation or a combination of the two. A pulsed laser is typically used, so that each laser shot will ablate a defined amount of material, depending on the material type and absorption properties, laser intensity, wavelength, and a number of passes made across the channel. This process leads to the rough surface of the laser-ablated microchannels and has a rippled appearance, which depends upon the absorption of the polymer at excimer wavelength. Very high temperature is reached during ablation and particles are ejected from the substrate creating a void, with small particulates on the surface of the substrate material while other decomposition products become gases (carbon dioxide and carbon monoxide). Laser ablation may be achieved in two ways. A polymer substrate can be exposed to a laser through a mask. A mask is usually made from the material that does not have significant absorption at the laser wavelength used. In the mask-less process, which is more commonly used, a polymer substrate is placed on a movable stage and either the focused laser beam or the substrate is moved across in the x and y-direction as defined in the desired pattern to create the microstructure in the polymer substrate.

The major limitation of PMMA is the requirement of surface modification for immobilization of different kinds of sensors and biomolecules.

1.5.3 Paper

Paper-based testing strips for testing pH, diabetes, and pregnancy have been commercially available for decades. Whitesides group introduced paper-based microfluidic devices as a low-cost platform for bioassay and since then paper has been widely used in the field of microfluidics.[94] Paper is a thin sheet of material that is generally produced by pressing together cellulosic or nitrocellulose fibers.[78] The biodegradable paper can transport liquids via capillary effect. Paper, as a low-cost material, has abundant cellulose fibers with three-

dimensional (3D) microstructures. Paper has good stackability, which allows the formation of 3D structures for complex assays. The high surface to volume ratio provided by the macroporous structure in paper improves the immobilization of protein and DNA biomarkers, allowing fast detection.

Fabrication of paper-based devices is simple and does not require the use of clean-room facilities. They can be fabricated both in 2D and 3D for either horizontal or vertical flow without the requirement of the clean room.[95] Fabrication of the paper-based devices can be subdivided into two categories: (i) construction of hydrophobic barriers, and (ii) two-dimensional cutting.

Constructing hydrophobic barriers in the hydrophilic paper matrix is one of the commonly used methods to prepare paper-based analytical devices. In this way, reagents and analytes can be made to flow in a certain path, preventing the mixing and spreading across the surrounding paper surface and achieve multiplex assays, without the issue of cross-contamination. Hydrophobic barriers can be created on the paper through either a physical deposition or a chemical modification method.[96,97] A number of different fabrication methods have been developed to fabricate paper-based devices, such as fast photolithography,[2,94] wax-based fabrication techniques,[96,98] saline UV/O_3 patterning,[99] flexographic printing,[100] and alkenyl ketene dimer (AKD) printing.[97]

Paper-based devices have some limitations such as poor performance in flow control. They are not transparent, so it may cause some problem in optical detection. In addition, repeated washing in paper-based devices may lead to the leakage of reagent through hydrophobic barriers.

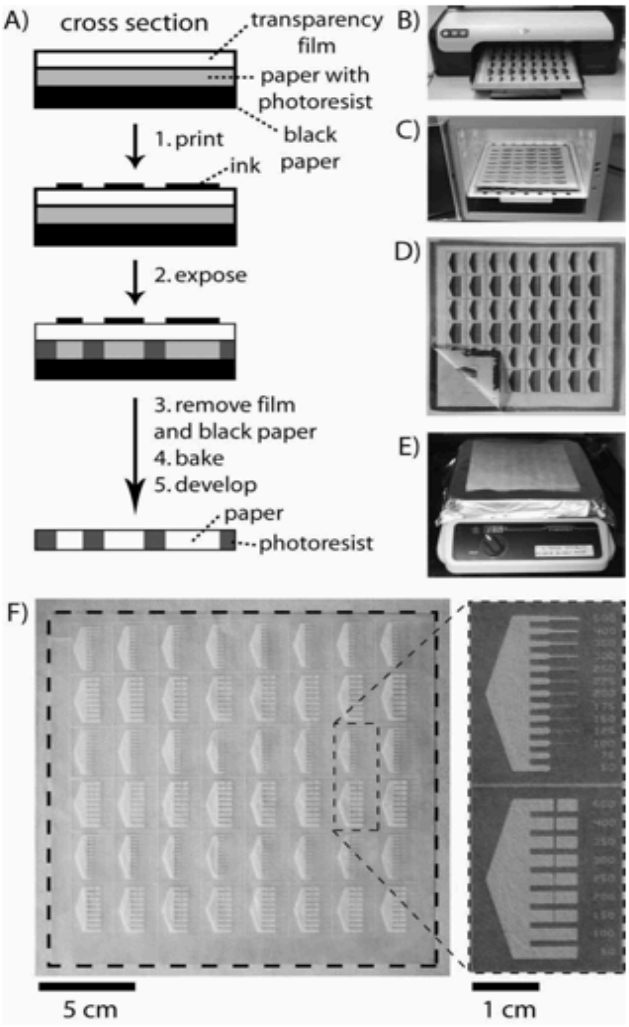

Figure 1.2: Procedure for FLASH fabrication of microfluidic devices in the paper. (A) Schematic of the method. (B) Designs for channels were printed directly onto paper. (C) FLASH paper was exposed to UV light. (D) The photoresist-impregnated paper was removed from the transparency film and black construction paper. (E) The paper was baked on a hotplate. (F) After developing the paper in acetone and 70% isopropyl alcohol, the microfluidic devices are ready for use. The dotted lines indicate the edges of the paper. (Source: Adapted with permission from Martinez *et al*., 2008. Copyright © 2008 RSC).[2]

FLASH (Fast Lithographic Activation of SHeets) or photolithography is an extensively used fabrication technology for constructing hydrophobic barriers in paper-based devices.[2] FLASH requires a UV lamp, a printer, and a hotplate along with a photoresist such as SU-8 and other organic solvents (Figure 1.2). In this technique, a photoresist is first poured onto a piece of

paper, spread evenly and baked on a hotplate at 130 °C for 5–10 min to evaporate propylene glycol monomethyl ether acetate (PGMEA) from the photoresist. Then, the paper is covered with a photomask and exposed to UV light. After incubation in an oven, the chromatography paper is washed in acetone, followed by rinsing with isopropyl alcohol. The paper-based device is ready to use after drying.

Another way to create a paper-based microfluidic device is 2D cutting. Paper channels are cut through computer-controlled X–Y knife plotters or CO_2 laser cutters, and then fixed to suitable plastic cassettes to form hybrid devices.[101] Nitrocellulose, conventional photocopy paper or chromatography paper can be used. Thuo *et al*. described the use of embossing and a "cut-and-stack" method to develop microfluidic devices from a paper.[102] They demonstrated that fluid flow in these devices was similar to open-channel microfluidic devices and cut layer generated 3D systems.

1.5.4 Hybrid microfluidic platforms

Each substrate has its own advantages and disadvantages. PMMA and PDMS are transparent and rapidly delivers reagents to different regions. With very good optical properties and high performance in flow manipulation, they have been widely used in microfluidic bio-applications.[81, 83, 103, 104] However, these polymers require complicated surface modification to immobilize biosensors and other biomolecules such as antibodies and enzymes. On the contrary, paper-based devices can rapidly immobilize biosensors and other biomolecules but do not offer high performance in flow control especially over a long distance. Paper is not transparent leading to difficulties in optical detection, though there are efforts to develop the optically transparent paper.[105, 106] Hybrid devices can take advantages of various substrates while eliminating some limitations of certain substrates. Li group developed the first PDMS/paper hybrid microfluidic

biochip integrated with aptasensors for simple, one-step, and multiplex pathogen detection.[107] Paper in this hybrid device acted as the substrate for facile immobilization of aptamer-functionalized nano-biosensors without complicated surface modification. *Lactobacillus acidophilus* was detected with the LOD of 11.0 cfu/mL within 10 minutes. Two infectious foodborne pathogens (*Staphylococcus aureus* and *Salmonella enterica*) were simultaneously detected with the hybrid device. Recently, Dou *et al*. fabricated another PDMS/paper hybrid microfluidic platform integrated with loop-mediated isothermal amplification for detection of meningitis-causing bacteria (Figure 1.3).[3] It was interesting that they found the hybrid device provided more stable performance than non-hybrid devices over a period of 2 months.

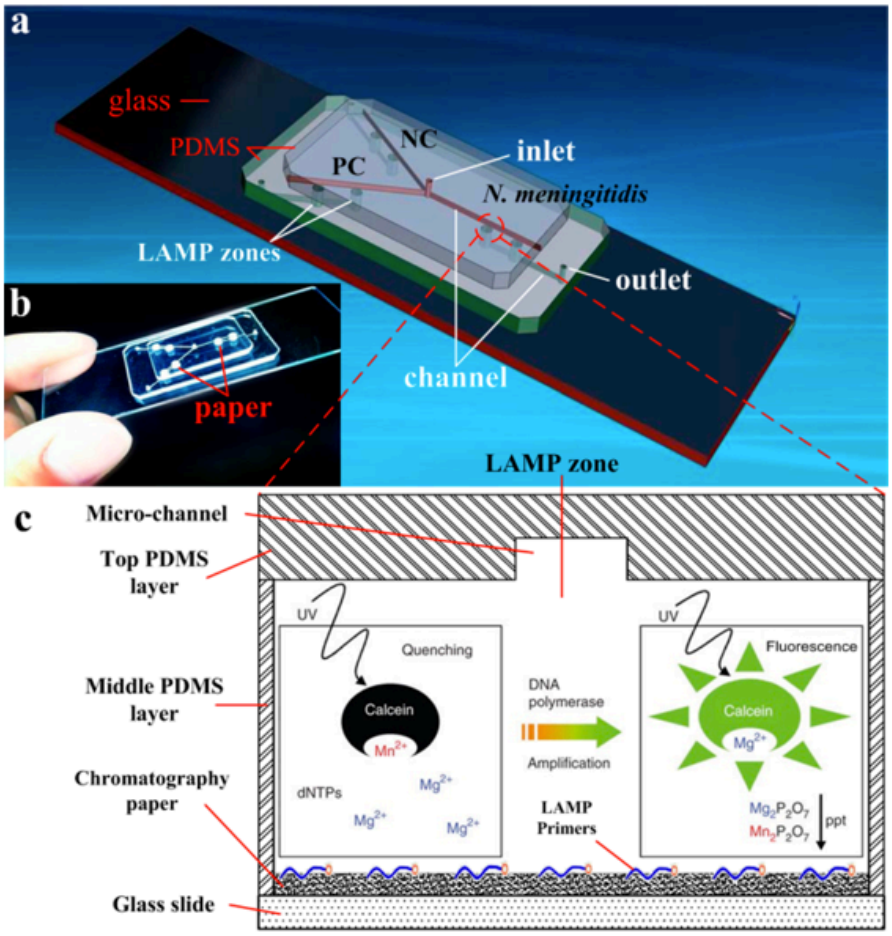

Figure 1.3: Chip layout of the PDMS/paper hybrid microfluidic device. (a) 3D illustration of the schematic of the chip layout. The chip consists of one top PDMS layer, one middle PDMS layer, and one glass slide for reagent delivery, LAMP reaction, and structure support, respectively. A chromatography paper disk is situated inside each LAMP zone to preload LAMP primers. (b) A photograph of the hybrid microfluidic device for infectious disease diagnosis. (c) A cross-section view of the LAMP zone illustrating the principle of the LAMP detection. (Source: Adapted with permission from Dou *et al*., 2014. Copyright © 2014, ACS).[3]

1.6 Immunoassay on microfluidic devices

Although conventional microplates are widely used in hospitals and clinics, they have several limitations as discussed in Section 1.3.2. To address those issues, microplate-format microfluidic devices have been developed for immunoassays. For instance, Kai *et al*. developed a 96-well microfluidic microplate for ELISA with improved sensitivity and reduced sample volumes.[52] The microplate was fabricated with clear polystyrene through injection molding. Each

well was connected to a microfluidic channel on the opposing face of the substrate via a through reservoir at bottom of the well. The ELISA on this microfluidic microplate took less time and consumed less reagents as compared to conventional ELISA, but it still required a fluorescence microplate reader. Sapsford *et al*. developed a miniaturized 96-well microfluidic chip for portable ELISAs with colorimetric detection.[124] The 96-well ELISA chip was micro-machined using clear acrylic and polycarbonate (PC) bound together by double-sided tape. Although the reagent consumption was less than conventional ELISA and a portable detector (electroluminescence semiconductor strip with a charge coupled device (CCD)) was used, overnight incubation and manual fluid handling were required. Similarly, Sun *et al*. fabricated a miniaturized 96-well device for immunological detection, assembling six layers of PMMA core and five PC layers.[125] They performed electrochemiluminescence ELISA of staphylococcal enterotoxin B (SEB) using a CCD detector. The microfluidic device required a complicated functionalization and device assembling steps along with long incubation time to complete the assay. Overall, all these devices require either long incubation time, surface functionalization or complicated detection systems.

1.6.1 Immunoassay on paper-based devices

With the emergence of paper-based devices in recent years, various POC analyses, including paper-based ELISAs have been developed.[94, 126, 127] Paper-based ELISA takes advantage of the high specificity of ELISA and low cost, easy-to-use paper-based devices. Whitesides and his colleagues performed ELISA in a 96-microzone plate fabricated in the paper.[128] Although it was faster and less expensive, sensitivity was lower than conventional ELISA. Similarly, Li *et al*. performed electrochemical ELISA on the paper-based microfluidic device. Electrodes were screen-printed on the surface of the paper to perform the ELISA of IgG achieving a sensitivity

similar to conventional ELISA.[129] Murdock *et al*. used 96-well paper-based ELISA for the assay of human performance biomarker.[130] They used complicated and time-consuming conjugation steps to perform enzyme-free ELISA using gold nanoparticles. Wang *et al*. performed chemiluminescence ELISA of tumor markers on a paper-based device (6 x 3 zones). Chitosan coating and glutaraldehyde cross-linking were required to covalently immobilize antibodies to perform bioassay for tumor markers.[131] Yang *et al*. fabricated quantum dot-based immune-chromatography test strip for the detection of alpha-fetoprotein. It required a time consuming and exhausting preparation of quantum dots (QD) and QD-antibody conjugates.[132] Zhou fabricated paper-based colorimetric bio-sensing platform for the detection of glucose and protein biomarkers. 3-aminopropyltriethoxysilane (APTES) modified filter paper cross-linked with glutaraldehyde was used as the substrate.[133] Gold nanoparticles were then adsorbed on the paper substrate for the absorption of primary antibody. Next, glucose oxidase modified gold nanorod was prepared as detection anti-PSA antibody. The major drawbacks were a long and tiresome modification and conjugation steps. Lei *et al*. performed paper-based immunoassay (8 x 6 zones) for detection of influenza.[134] One of the limitations of the paper-based device is the requirement of highly sensitive dyes. Other limitations in paper-based ELISA include low-performance in flow control and the need of repeated micropipetting for adding reagents and washing all the zones, which is really time-consuming and limits its application for high-throughput detection. In addition, the repeated washing steps in the micro-zones lead to spreading of the reagents over the hydrophobic areas, which is one of the serious problems faced in paper-based devices.

1.6.2 Immunoassay on PMMA devices

Polymers such as PMMA require complicated surface modification procedures to immobilize biosensors and other biomolecules such as antibodies and enzymes. Darain *et al*.

activated the PMMA surface with O_2 plasma and functionalized it with APTES for stable antibody immobilization.[109] The on-chip ELISA was detected using fluorescence microscopy. Zhou *et al*. treated the PMMA under ultrasonic water bath and oxygen plasma before coupling the capture antibody by the use of EDC reagent.[135] Yu *et al*. developed quantum dot-linked immune-diagnostic assay where myeloperoxidase antibodies were covalently linked to PMMA after treating it with polyethylene glycol followed by glutaraldehyde.[136] Liu *et al*. modified the PMMA using PEI for electrochemical detection of a biomarker of neurological disease.[137] Similarly, Liu *et al*. modified PMMA using PEI to determine trace level of α-fetoprotein and hepatocellular carcinoma biomarkers.[114] Yang *et al*. performed sandwich ELISA of Staphylococcal Enterotoxin B by functionalizing antibody with carbon nanotube before immobilizing it to the PMMA.[138] All of these assays require complicated surface modifications including PEI treatment,[111, 114] APTES treatment,[109] and carbon nanotube (CNT) functionalization.[125] In addition, they require expensive instruments like fluorescence microscopy.[109, 111]

1.7 Research objectives

The goal of this research is to develop low-cost hybrid microfluidic diagnostic platforms for rapid and sensitive detection of infectious disease and cancer biomarkers.

We have combined highly sensitive ELISA and low-cost microfluidic platform based on polymer/paper hybrid substrate for rapid and POC detection. We first modified the surface of the PMMA for the low-cost detection of disease biomarkers. Then, we developed paper/polymer hybrid device to get rid of complicated surface modification of PMMA for the detection of infectious diseases including hepatitis B and C virus and cancers including prostate cancer and colorectal cancer. The organization structure of this dissertation can be seen in Figure 1.4.

Chapter 3 introduces a simple method of functionalization of PMMA with Polylysine to be used as the microfluidic substrate for ELISA with high amine density. Chapter 4 introduces an alternate method to covalently bind the protein to carboxylated PMMA surface using carbodiimide chemistry. Immobilization efficiency of proteins on the surface of the modified PMMA was remarkably increased due to the covalent binding of the protein thereby improving the sensitivity of ELISA and decreasing the background noise. The modified microplate can immobilize protein within 20 min with much less reagent consumption and results of the assay can be viewed by the naked eye or scanned through a simple desktop scanner for quantitative analysis within 90 min. Simultaneous detection of IgG, HBsAg, and HBcAg was performed in the surface modified PMMA with LODs in the range of 190-360 pg/mL without any specialized equipment like microplate reader. Surface modified microplates by either method were found to be at least 10-fold more sensitive than commercial ELISA kits.

Although the surface modified PMMA had good sensitivity and can be used in POC settings, the complicated surface modification was still required. To get rid of these time consuming and complicated surface modifications, we developed the hybrid microfluidic microplate. In chapter 5, development of a simple, miniaturized paper/PMMA hybrid microfluidic microplate for low-cost, high throughput, and POC infectious disease diagnosis is discussed. One of the important features of the hybrid device is the funnel-shaped microwells. The novel use of porous paper in the flow-through funnel-shaped microwells facilitates rapid antibody/antigen immobilization avoiding complicated surface modifications. The flow-through microwells also ensure efficient washing, decreasing the background noise. The top reagent delivery channels can simply transfer reagents to multiple microwells thus avoiding repeated manual pipetting to all the microwells and costly robots. IgG and HBsAg were quantitatively

analyzed with good reliability in human serum samples. For the device to be used in the settings of laboratories and hospitals, the hybrid device was further redesigned to make it compatible with traditional microplate readers. Chemiluminescence ELISAs of different infectious disease biomarkers including HBsAg, HBcAg, and HCVcAg were performed and the results could be analyzed using commercial microplate reader. The sensitivity was found to be around 100-fold better as compared to commercial 96-well plate ELISA.

To increase the sensitivity of the colorimetric hybrid device, we developed a reusable, cost-effective, and eco-friendly PMMA/paper hybrid plug-and-play (PnP) device through analyte enrichment, which is discussed in Chapter 6. The PMMA device has multiple slots where a pre-patterned paper substrate can be inserted. The sample flows back and forth through the low-cost 3D paper substrate within the PMMA channels thereby enriching the amount of analyte adsorbed and dramatically decreasing the incubation time from several hours to a few minutes. After the enrichment assay, the paper substrate can be simply plugged out of the device and the device can be reused. The LOD of 200 pg/mL for IgG and 270 pg/mL of HBsAg were observed, which is at least 10 times more sensitive than commercial ELISA kits. In addition, a wide linear range of five and six orders of magnitude was obtained for IgG and HBsAg, respectively.

We further demonstrated the broader application of our hybrid device for detection of cancer biomarkers including PSA and CEA in Chapter 7. A single pre-patterned paper-based substrate can be kept over the pond-shaped structure of the hybrid device. The device has a similar flow-through reservoir as discussed in Chapter 5 but the manual addition of paper-substrate to all the microwells is avoided. We further modify the ELISA assay by adding the capture antibody before adding the sample antigens, thus increasing the sensitivity and reducing the background noise of the assay. LODs of CEA and PSA were found to be 0.32 ng/mL and

0.20 ng/mL, respectively, which were 10-fold more sensitive than the clinical cut off value of 5 ng/mL and 4 ng/mL for CEA and PSA, respectively. Chapter 8 presents the concluding remarks and future directions of the research work.

In summary, the low-cost PMMA and paper/polymer hybrid microfluidic microplates that we developed have great potential for POC diagnosis of a wide range of infectious diseases and cancer biomarkers, especially in low-resource settings such as developing countries where financial and medical resources are extremely limited. In addition, the device can also be used in high-end hospitals and laboratories for various bioassays.

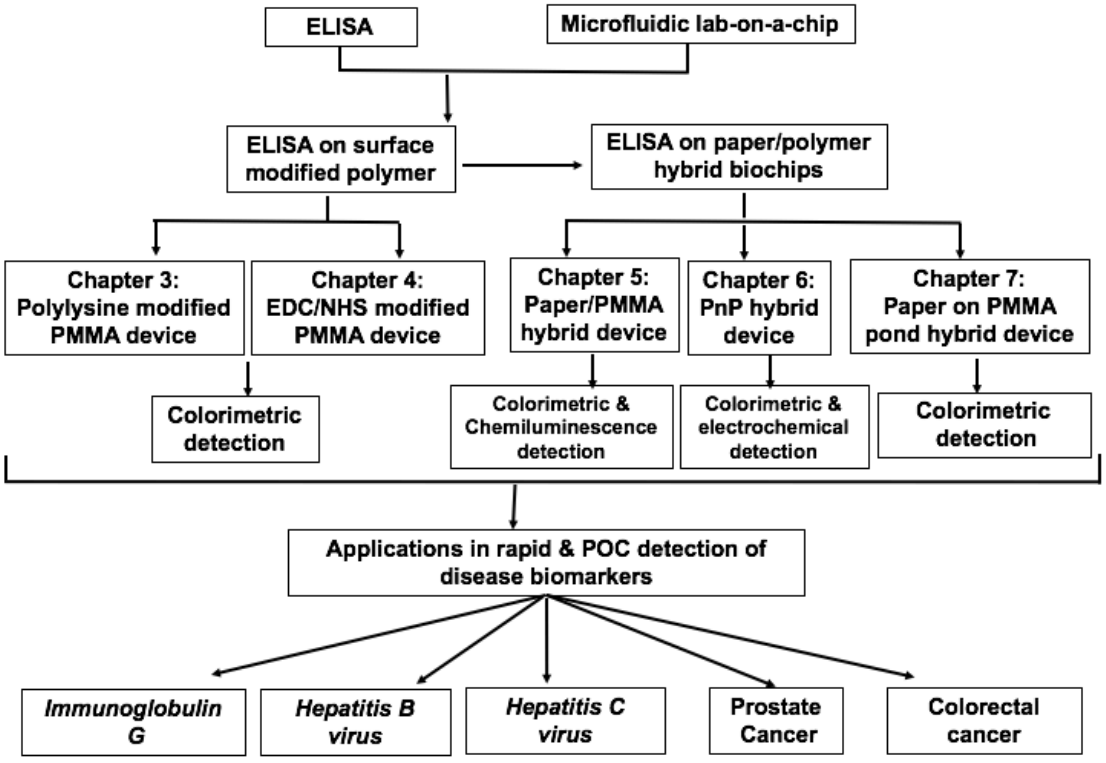

Figure 1.4: The structure of this dissertation.

Chapter 2: Experimental

- This chapter introduces chemicals and materials used in the research projects.
- Fabrication of paper/polymer hybrid microfluidic microplates is described in this chapter.
- The data analysis is demonstrated in this chapter.

2.1 Chemicals and materials

Microfluidic biochip fabrication materials: PMMA was purchased from McMaster-Carr, Los Angeles, CA; Whatman #1 chromatography paper was purchased from Sigma, St. Louis, MO. SU-8, 2010 was purchased from Microchem, Newton, MA.

Surface modification of polymer: Polylysine, sodium hydroxide, and dimethylsulfoxide (DMSO) were purchased from Sigma Aldrich, St. Louis, MO. Glutaraldehyde was purchased from Amresco, Solon, OH. Isopropyl alcohol was purchased from J.T. Baker, Center Valley, PA. *N*-hydroxysulfosuccinimide was purchased from Thermo Scientific, Rockford, IL. 1-ethyl-3-(3-dimethylaminopropyl) carbodiimide hydrochloride was purchased from Advanced ChemTech, Louisville, KY. Sulfuric acid was purchased from Alfa Aesar, Ward Hill, MA.

ELISA: IgG from rabbit serum, Tween 20, albumin from bovine serum, anti-rabbit IgG-alkaline phosphatase, polyclonal anti-carcinoembryonic antigen, monoclonal anti-carcinoembryonic antigen, prostate-specific antigen, serum from normal human male AB plasma, 5-bromo, 4-chloro, 3-indoyl phosphate + Nitroblue tetrazolium (BCIP/NBT) liquid substrate, and Phosphate Buffer Saline (PBS) were purchased from Sigma Aldrich, St. Louis, MO. HBsAg protein (subtype ad) was purchased from Fitzgerald Industries International Inc., Acton, MA. Polyclonal anti-HBsAg was purchased from Novus Biologicals, Littleton, CO. Hepatitis B virus core antigen, anti-hepatitis B virus core antigens, anti-rabbit IgG-HRP, and supersignal ELISA pico chemiluminescent substrate were purchased from Fisher Scientific, Hampton, NH. Cy3-labeled IgG whole molecule was purchased from Jackson Immunoresearch Laboratories Inc., West Grove, PA. Carcinoembryonic antigen, Hepatitis C virus core antigen, anti-hepatitis C virus core antigen, polyclonal anti-PSA, and monoclonal anti-PSA were purchased from Abcam, Cambridge, MA. Ultrapure Milli-Q water (18.2 MΩ.cm) obtained from a Millipore water purification system, Bedford, MA was used in all assays and reagent preparation unless otherwise noted.

2.2 Fabrication of polymer and paper/polymer hybrid microfluidic biochips

2.2.1 Fabrication of PMMA devices

The PMMA devices used in this study were designed by using Adobe Illustrator CS5 and micro-machined using laser cutter (Epilog Zing 16, Golden, CO). In the mask-less laser ablation, the PMMA substrate was placed on a stage and the focused laser beam was moved across in x- and y- directions as defined in the designed pattern. Desired channels and wells were created on the PMMA with the ablation of the PMMA by laser.

2.2.2 Two-level laser fabrication of PMMA devices

Since the power and the speed of the laser cutter can affect the depth of microstructures, in order to achieve the desired depth, we first systematically investigated the relationship between the depth, power, and the speed of the laser cutter, as shown in Fig. 2.1. It can be seen that with the increase of the power for a 30 W CO_2 laser in the raster mode, the structure depth increased correspondingly. Additionally, the laser cutter speed also affects the fabrication depth. The faster the laser's speed, the shallower is the depth of microstructures. Thus, the percentage power and the speed required for cutting PMMA was empirically determined. As seen from Fig. 2.1, the speed of 10% and power of 50% could completely pass through a 2-mm thick PMMA layer creating a reservoir. Similarly, for a 1.5 mm thick PMMA, the speed of 10% and the power of 35% could be used. Based on the data from Fig. 2.1, different structures with desired depth can be created on the PMMA of different thickness.

2.2.3 Fabrication of paper/polymer hybrid microfluidic microplates

Pieces of chromatography paper were also designed using Adobe Illustrator CS5 and cut using a laser cutter. For a paper/polymer hybrid microfluidic microplate, the pieces of chromatography paper can be manually placed inside each microwell, as a 3D surface for ELISA. Alternatively, chromatography paper can also be placed just over the middle layer of the PMMA with microwells, so that the paper pieces directly fall to each microwells in the middle layer during laser cutting, so that there is no need to place the chromatography paper manually to

all the wells. For the PnP hybrid device, paper substrate can be inserted into the slot of the device once it is cut with a laser cutter. Similarly, for a paper in polymer pond device, a single paper substrate can be kept over the pond before binding different layers of the device.

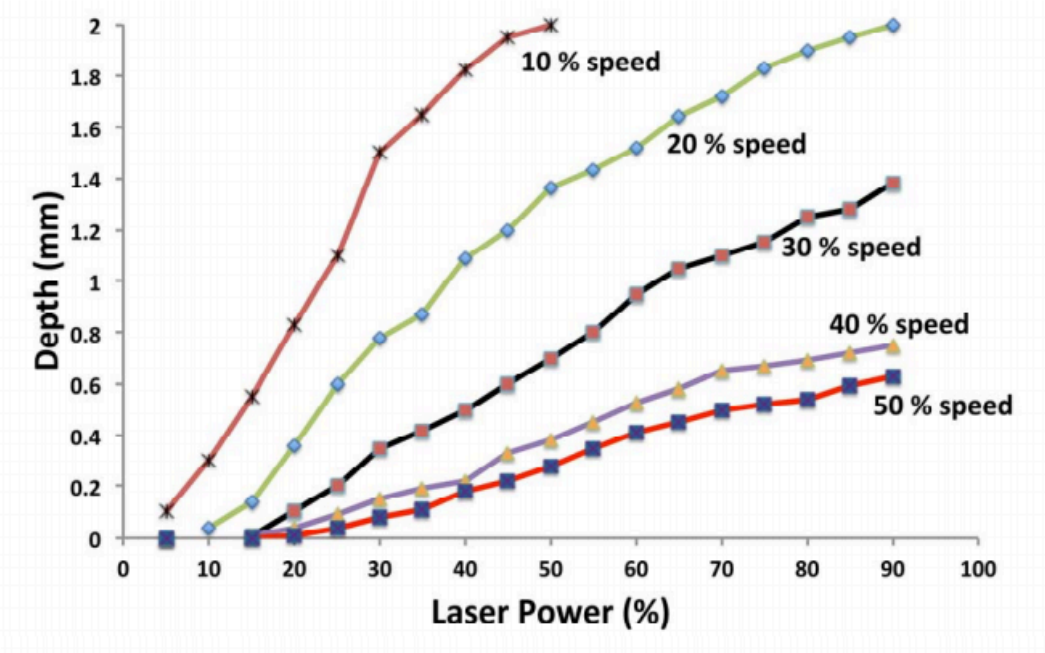

Figure 2.1: Laser ablation of PMMA at different speeds and powers for two-level microfabrication of funnel-shaped microwells. The graph shows the depth of microwells achieved by speed of 10%, 20%, 30%, 40%, and 50%, respectively at different power percentages of a 30 W laser in the raster mode.

2.2.4 Assembly of the paper/polymer hybrid microfluidic microplates

To assemble the hybrid device, different PMMA layers were overlapped together as in the design. The layers were then clamped between two layers of glass slabs and kept in an oven at 115–120 ^{0}C for 35 minutes. The chip could be used once it cooled down to the room temperature. Different PMMA layers could be separated after the assay by applying pressure between the joints so that the device can be reused after cleaning.

2.3 Data analysis

2.3.1 Colorimetric assay

Once the substrate for ELISA was added, the chip was incubated for the required time. The chip was then scanned using a portable flatbed scanner (CanoScan LiDE 700F, Canon). The average brightness of each test zone was obtained by measuring the gray value using the ImageJ software, distributed for free by NIH (http://rsb.info.nih.gov/ij/download.html). The signal of an individual microwell was calculated as the average of the intensity values of respective pixels. RGB images can be converted to the gray scale using the formula, gray = (red + green + blue)/ 3. The display range in ImageJ from minimum to maximum is scaled from 0 to 255. After the average brightness value was measured using ImageJ, it was subtracted from the maximum value (255) to get the corrected brightness value, which was then used for data analysis. The value obtained with a concentration of 0 pg/mL in PBS was defined as the background.

2.3.2 Fluorescence microscope and fluorescence intensities

A highly sensitive Nikon Ti-E fluorescence microscope (Melville, NY) equipped with a motorized stage and a cooled charge-coupled device (CCD) camera was employed for fluorescence detection and confirmation of immobilization of IgG on the surface of the modified PMMA and the paper surface. As Cy3-linked IgG was immobilized on the surface of the PMMA and the paper substrate, a Cy3 optical filter was used for the fluorescence detection. Fluorescence intensities of the images of the devices were then measured using the provided software.

Chapter 3: Simple Polylysine-based Surface Modified Poly(methyl methacrylate) Microfluidic Device for the Detection of Hepatitis B Virus

---

- This chapter introduces a polylysine-based modification of PMMA for covalent immobilization of proteins.
- Modified PMMA microplates can immobilize proteins within 20 min and the results of the assay can be seen by the naked eye without using any specialized instruments.
- A rapid and sensitive quantitative detection of infectious diseases can be achieved within 90 min.
- Immunoassays for the simultaneous detection of IgG, HBsAg, and HBcAg were performed in the surface modified microfluidic devices.

3.1 Introduction

Worldwide, infectious diseases are the leading cause of death and mortality. Unlike other diseases which can result from multiple interacting risk factors, single agent causes most of the infectious diseases; the identification of which leads not only the control measures but treatment measures as well.[12] This underlines the need for accurate surveillance and the development of new strategies for fast, rapid, and sensitive detection of infectious diseases for their control. ELISA is the most widely used laboratory assay for the detection of disease biomarkers but is limited by long incubation periods, consumption of significant volume of samples and reagents, and the requirement of laboratory settings.[52, 144] Low-cost and highly sensitive device for the detection of infectious diseases are needed, especially in resource-limited settings.

As described in Section 1.4, microfluidic devices with features including high surface-to-volume ratio, portability, and integrated processing results in low-cost, minimal reagent consumption, and rapid bioanalysis of complex biological fluids.[37, 62, 146, 147, 152] Different kinds of substrates including PDMS, PMMA, and paper have been used as microfluidic substrates for the detection of infectious diseases as described in Section 1.5.[55, 148, 153] PMMA is a low-cost, rigid, and transparent substrate, which is easier to fabricate and mass-produce than PDMS.[149] It also offers better performance under mechanical stress as compared to PDMS. PMMA substrate has been used to perform ELISA but it shows low sensitivity, as hydrophobic PMMA surface lacks a functional group to immobilize proteins and thus require surface modifications and complex detection techniques.[110]

There is a growing demand to develop easy, fast, sensitive, and preferably inexpensive detection platform for qualitative and quantitative testing in POC settings. Xu *et al*. developed a silicon-based microfluidic device with a complicated micromachining technology to detect HBV using micro-piezoelectric immunoassay.[139] In addition to the requirement of a class-100 clean room, it required impedance analyzer to measure resonant frequency, although the device had the LOD of 0.1 ng/mL. Kamińska *et al*. developed surface-enhanced Raman scattering (SERS)-based microfluidic device for HBV detection, which required complicated fabrication and

modification of the device, and immune-Au nanoflowers.[140] In addition, the polycarbonate-based device required a diode laser, a microscope, and a CCD detector. Akama *et al*. developed a droplet-free digital ELISA for detection of HBsAg.[141] Tyramide substrate reacted with horseradish peroxidase (HRP) labeled with an immune-complex on beads releasing fluorescence signal, which could be counted digitally. The beads were either detected by microscopy or flow cytometry and cannot be used for POC settings. Shen *et al*. developed an electrochemical method for detecting HBsAg using copper-enhanced gold nanoparticle tag and magnetic nanoparticles. It required complicated and time-consuming preparation of antibody-colloid gold conjugates, magnetic Fe_3O_4 nanoparticles, APTES-bound and aldehyde-functionalized magnetic nanoparticles in addition to nearly a 16 hr long assay, as required for conventional ELISA and cannot be used in POC settings.[142] Lee *et al*. devised a microfluidic disc fabricated from PMMA and performed immunoassay of HBsAg and anti-HBs by using carboxylated and aminated polystyrene beads. However, the device was only as sensitive as conventional ELISA.[143] Tsai *et al*. fabricated a thin channel magnetic immunoassay device, which required a centrifuge, syringe pump, and modified functional particles that needed to be counted for the preparation of calibration curve.[6] The thin channel consisted of a cut-out Mylar spacer sandwiched between a plastic and a glass plate. These devices either require specialized instruments and complicated preparation methodologies or are not very sensitive. With the development of nanoparticles and microfluidic devices, portability, integrated processing, and rapid bio-analysis have been more effective and low-cost.[144-147] But to date, the development of a POC microarray platform for multiplex detection, using the miniaturized system, which is as sensitive, effective, and robust as those based on ELISAs and PCR is still a challenge.[37, 55, 148, 149]

Sensitivity and background noise of the biochemical assays is profoundly affected by the total activity and the way of interaction of the specific protein bound to the surface of the assay substrate[109]. In addition, the way of interaction is very sensitive towards their environment and can easily lose their activity as they are brought in close proximity to the solid surfaces[110]. Surface chemistry including treatment with oxygen plasma and strong bases/oxidizers are

necessary for the immobilization of proteins to polymers like PMMA as they lack the functional groups to bind proteins.[112] PMMA surface can be modified by the introduction of carboxyl (-COOH), hydroxyl (-OH), or amine ($-NH_2$) reactive groups, which can be further reacted for the immobilization of the protein.[110]

Functionalization of PMMA with amine groups has been reported but consists of too many steps and yielded a low amine density or involves unstable intermediates and non-environment friendly solvents.[4] Brown *et al*. characterized the surface modification of PMMA microfluidic devices for their adhesion properties.[4] PMMA surface which was modified using air plasma, acid catalyzed hydrolysis, and aminolysis (using ethylenediamine), were used to determine if covalent and or hydrogen bonds between modified PMMA substrate and cover plate increase the adhesion. Llopis *et al*. studied the surface modification of PMMA microfluidic devices for high-resolution separation of single-stranded DNA.[113] They created amine-terminated PMMA surface by a chemical or photochemical process by using ethylenediamine. Methacrylic acid was then covalently linked and used as a scaffold to produce linear polyacrylamides (LPAs). It helped them increase the efficiency of separation of single-stranded DNA electrophoretically. Liu *et al*. modified the base-treated PMMA by immersing PMMA in poly(ethyleneimine) (PEI) followed by treatment with glutaraldehyde.[114] The modified PMMA chip fabricated by hot-embossing machine was used for electrochemical detection of α-fetoprotein (AFP), a hepatocellular carcinoma biomarker but required a syringe pump and an electrochemical workstation. Bai *et al*. studied the surface modification of PMMA to enhance the antibody binding on the polymer-based microfluidic device to perform ELISA. They found that the PEI modified PMMA was 10 times more active in binding antibodies as compared to those without treatment or treated with a small amine-bearing molecule, hexamethylenediamine (HMD).[111] They performed the ELISA of IgG with a similar detection limit as the conventional 96-well plate. PMMA was functionalized for various purposes including ELISA but only provided low amine density resulting in higher LOD.[111] High amine density polylysine has not been used for

the modification of PMMA to covalently bind the antibodies. In addition, complex detection techniques with expensive instruments have been used.

In response to aforementioned challenges, we have developed a polylysine modified microfluidic microplate. Proteins were covalently bound to the surface of the microfluidic microplate to perform a sensitive, rapid, and high-throughput multiplex assay of biomarkers of infectious diseases. 64-microwell microplate with an 8×8 series, designed according to standard 384-well ELISA plates with the same X-axis and Y-axis offset but with reduced diameters and depths was fabricated with a laser cutter so that the working volume could be decreased to 5 μL. Covalent binding of the antibody to surface modified PMMA resulted in significant improvement of sensitivity and decrease in the background noise as compared to traditional microplates. Proteins could be immobilized in the surface modified PMMA within 20 min as compared to overnight incubation in traditional microplates. Results of the ultrasensitive assay with a minimal reagent can be viewed by the naked eye within 90 min or scanned through a desktop scanner for quantitative analysis without the use of any sophisticated instruments. Simultaneous multiplex detection of IgG, HBsAg, and HBcAg was performed with the LODs of 200 pg/mL, 180 pg/mL, and 300 pg/mL, respectively, which are at least 10-fold more sensitive compared to traditional ELISA.[154]

3.2 Experimental

3.2.1 Chemicals and materials

All chemicals and materials are listed in Section 2.1.

3.2.2 Design and fabrication of the microfluidic microplate

The chip used in this study was designed in Adobe Illustrator CS5 and micro-machined using a Laser cutter. The wells in the PMMA layer were designed according to the dimension of standard 384 well plates. As seen from Figure 3.1, the X-axis and Y-axis offset are 4.5 mm (d), which, is the length between the centers of 2 wells. The position of the first well corresponds to A1 of a microtiter plate. A1 row offset (distance from the top edge of the microplate to the center

of wells in 1st row) of the chip is 8.99 mm (a), similar to 384 well microtiter plates. In addition, A1 column offset (distance from the side edge of the microplate to the center of wells in 1st column) of 12.13 mm (b) is also same as a microtiter plate. The diameter of each well was reduced to 3.6 mm (c).

3.2.3 Covalent modification of the PMMA surface

The PMMA microplate was functionalized using two different methods, where aminolysis of the PMMA surface was performed using polylysine followed by activation using glutaraldehyde for the covalent modification of antigen. (Figure 3.1B). In the first method, the PMMA microplate was sonicated for 5 min in 40% by volume of aqueous 2-propanol solution. After the PMMA microplate was dried, it was immersed in 0.2% (v/v) polylysine in DMSO for 20 min at room temperature followed by rinsing in 2-propanol solution. Finally, the aminated PMMA microplate was immersed in a glutaraldehyde solution (1% v/v) at room temperature for 30 min. Glutaraldehyde, which acts as a cross-linker form the Schiff base with the amine group of polylysine. The glutaraldehyde activated PMMA microplate was washed once with PBS and used for the immobilization of antigen/antibody by forming Schiff base at the other end of glutaraldehyde. In the second method, the PMMA microplate was immersed in a 1 N sodium hydroxide (NaOH) solution at 55 ^{0}C for 30 min followed by immersing in 0.2% aqueous polylysine solution at room temperature with pH of 7 for 1 hr. After the aminolysis, PMMA was immersed for 30 min in 1% v/v glutaraldehyde solution at room temperature. The surface modified PMMA was then used for the immobilization of antigen/antibody and further for ELISA procedure after washing it with PBS.

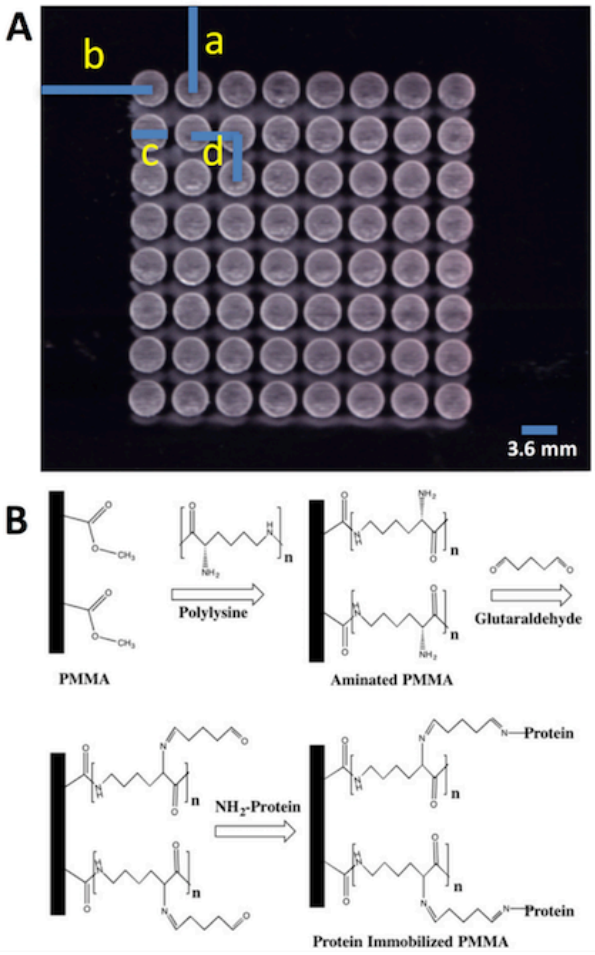

Figure 3.1: Microfluidic platform design and surface modification. (A) Photograph of the actual device with a black background with A1 row offset (a), A1 column offset (b), the diameter of the well (c), and X-axis and Y-axis offsets (d). (B) Schematic of the covalent modification of PMMA using polylysine.

3.2.3 FTIR analysis

FTIR-spectroscopy was used for the structural analysis and verification during the process of surface modification of PMMA. PMMA was first cut into small square pieces of 1 cm × 1 cm by using a laser cutter. Then, the PMMA was laser ablated to obtain wells with a diameter of 3.6 mm. The FTIR spectra were recorded by an FTIR spectrometer, PerkinElmer Spectrum 100. The FTIR spectra were recorded after each modification steps for both the modification procedure to characterize specific functional groups. FTIR spectra were taken for pristine PMMA, polylysine modified PMMA (PMMA + Polylysine), glutaraldehyde cross-linked

PMMA (PMMA + polylysine + glutaraldehyde), and antibody immobilized PMMA (PMMA + polylysine + glutaraldehyde + antibody).

3.2.4 Protein immobilization validation

Unspecific absorption of protein leads to a reduction of functional sites and increase in the background signal. Wells were created in PMMA sheets using a laser cutter. 20 μg/mL of Cy3 IgG were added to the surface modified PMMA (both methods), plasma treated PMMA, and pristine PMMA to see the protein immobilization efficiency. Cy3 IgG was not added to one set of PMMA to record the background fluorescence of PMMA. For plasma treatment of PMMA, the laser ablated PMMA was placed in a plasma cleaner (PDC-32G, Harrick Plasma, NY, USA) for 1 min. PMMA devices were incubated for 20 min with Cy3 IgG, then washed three times with phosphate buffered saline with Tween 20 (PBST) before measuring the fluorescence intensity, which was accomplished using a Nikon Ti-E fluorescence microscope.

3.2.5 ELISA of HBV biomarkers

The surface modified PMMA was used for the ELISA of different biomarkers for infectious diseases including IgG, HBsAg, and HBcAg. For the ELISA of IgG, the rabbit IgG was used as the analyte. 5 μL of IgG between the concentration from 0.1 ng/mL to 100 μg/mL (in 10 mM, pH 8.0 PBS) were then added to each microwells. Each concentration had eight replicas along the same column of the chip. IgG solutions were prepared from the stock solution of 2mg/mL IgG. The chip was incubated at room temperature for 20 min. Following the reaction, 5 μL of Bovine Serum Albumin (4.5 % BSA w/v in PBS + 0.05% Tween 20) was added for 20 min to block the unreacted surface of the PMMA. Next, the chip was thoroughly washed with 5 μL of washing buffer PBST (10 mM, pH 7.4 PBS+ 0.05% Tween 20) to get rid of unbound proteins. After washing, 5 μL of enzyme-linked antibody, i.e., anti-rabbit IgG-Alkaline phosphatase (6 μg/mL) was added and incubated at room temperature for 7 min. Finally, the chip was thoroughly washed with PBST for three times and 5 μL of the substrate (BCIP/NBT) was added. The substrate, which was initially light yellow in color, was converted to insoluble dark

purple NBT diformazan as the product which could be observed visually with the naked eye. Following 10 min of incubation with the substrate, an office scanner was used to scan the chip. Quantitative detection was carried out using the free software, ImageJ by measuring the brightness value of each wells of the chip.

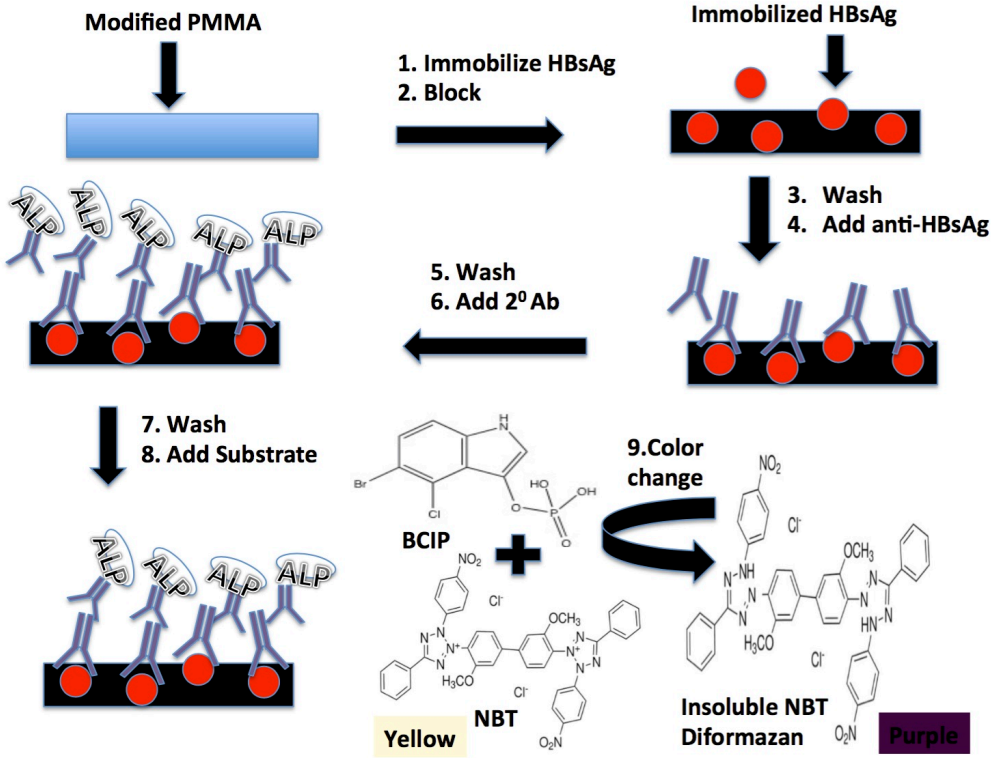

Figure 3.2: Schematic of the approach of immunoassay of HBsAg on the surface modified PMMA microplate, comprising of eight steps: (1) Immobilizing antigen on the surface of modified PMMA, (2) Blocking, (3) Washing, (4) Binding of enzyme conjugated antibody, (5) Washing, (6) Addition of secondary antibody, (7) Washing, (8) Addition of the substrate, and (9) Enzymatic production of insoluble NBT diformazan.

HBsAg and HBcAg were also tested for the detection of HBV and a similar assay procedure as IgG was followed. For the detection of HBsAg, first, the antigen (i.e. HBsAg) was immobilized on the modified surface of the PMMA (Figure 3.2). After the antigen was incubated for 20 min, blocking buffer was added for another 20 min. The incubation was followed by a thorough washing with PBST and addition of anti-HBsAg for another 20 min. Finally, after washing it with PBST, a sandwich-structure immunoassay was formed by the addition of ALP-labeled anti-rabbit IgG. Like the detection of HBsAg, for the detection of HBcAg, anti-HBcAg

was added after the initial immobilization of HBcAg. Finally, ALP-labelled anti-rabbit IgG was added to form a sandwich immunoassay. The chip was scanned 10 min after the addition of the substrate BCIP/NBT in both cases.

3.2.6 Multiplex detection of HBsAg and HBcAg

Here, the device was used for multiplex detection of HBsAg and HBcAg. The first column was negative control with PBS and no antigen. HBsAg was immobilized in the second and third columns, HBcAg was immobilized on the fourth and fifth columns, while both HBsAg and HBcAg were immobilized in the sixth, seventh, and eighth columns. The concentration of capture antigen was 200 ng/mL of HBsAg or 200 ng/mL of HBcAg except for the sixth column where 100 ng/mL of each capture antigen was added. Different combinations of antigens were incubated for 20 min and then blocking buffer was added for another 20 min followed by thorough washing with PBST. After that, anti-HBsAg was added in second, fourth, and seventh columns; anti-HBcAg was added in third, fifth, and eighth columns while both anti-HBsAg and anti-HBcAg were added in first and sixth columns. After the primary antibodies were incubated for 20 min, the ALP-labelled secondary antibody was added and incubated for another 7 min. Finally, the device was scanned using a simple office scanner, 10 min after the addition of the substrate.

3.2.7 Anti-interference test for the detection of HBsAg

Real world samples such as blood serum, urine, and cerebrospinal fluid, contain various complex ingredients consisting of different biomolecules with a wide range of concentrations. A high anti-interference capability is required to screen varieties of disease biomarkers, as these biomolecules may interfere the detection of target proteins. The various columns in the surface modified device were used for anti-interference experiments, where HBsAg was detected with and without various interfering proteins. The first four columns from the left were the negative control without the analyte (HBsAg) and consisted of 1 μg/mL HBcAg, 100 ng/mL CEA, 250 μg/mL BSA, and 10 ng/mL PSA, respectively. Fifth, sixth, and seventh columns had 1 μg/mL

HBcAg, 100 ng/mL CEA + 10 ng/mL PSA, and 250 μg/mL BSA, respectively along with 200 ng/mL of HBsAg. The eighth column had 200 ng/mL of HBsAg. Different combinations of antigens were incubated for 20 min at the room temperature followed by blocking with the blocking buffer for 20 min. After thorough washing with washing buffer, anti-HBsAg was added followed by washing and addition of ALP-labelled secondary antibody for 7 min. Finally, the device was scanned 10 min after the addition of the substrate.

3.3 Results and discussion

3.3.1 FTIR characterization of PMMA surface modification

FTIR characterization was performed after every step of PMMA modification, starting from pristine PMMA to identify different functional groups. As we can see from the FTIR spectrum of the pristine PMMA in Figure 3.3, C–O–C stretching vibration showed a distinct absorption band from 1,150 cm^{-1} to 1,250 cm^{-1}. Similarly, two bands for the α-methyl group vibrations were seen at 1,387 cm^{-1} and 750cm^{-1}. Characteristic absorption vibration of PMMA was represented by the band at 986 cm^{-1} along with the bands at 1,063 cm^{-1} and 841 cm^{-1}. Presence of the acrylate carboxyl group could be confirmed by the band at 1,723 cm^{-1}. Bending vibration of the C–H bonds of the -CH_3 group could be attributed to the band at 1,435 cm^{-1}. Finally, two bands at 2,995 cm^{-1} and 2,951 cm^{-1} could be assigned to the C–H bond stretching vibrations of the –CH_3 and –CH_2- groups, respectively. This spectrum correlated well with the FTIR spectrum of PMMA that has been documented in the literature.[155]

Some major changes could be observed in the spectrum of PMMA after modification using method 1 (Figure 3.3A). The presence of Amide I (1652 cm^{-1}), Amide II (1533 cm^{-1}) and C-N stretch, as well as substantially less intense methyl ester bands after the treatment of PMMA with polylysine, showed that the PMMA was aminated by polylysine. This data suggest PMMA's ester bond was replaced by the amide bond of polylysine as seen in literature for amine-modified PMMA.[155] The aminated PMMA was further treated with glutaraldehyde as seen from C=O (1637 cm^{-1}) and C-N (1442 cm^{-1}) stretch vibration to covalently bind the antibody to

the PMMA surface. We could see strong absorption for Amide I (1646 cm^{-1}) and Amide II (1555 cm^{-1}) after the addition of the antibody, which indicated the covalent binding of the antibody to the modified PMMA surface.

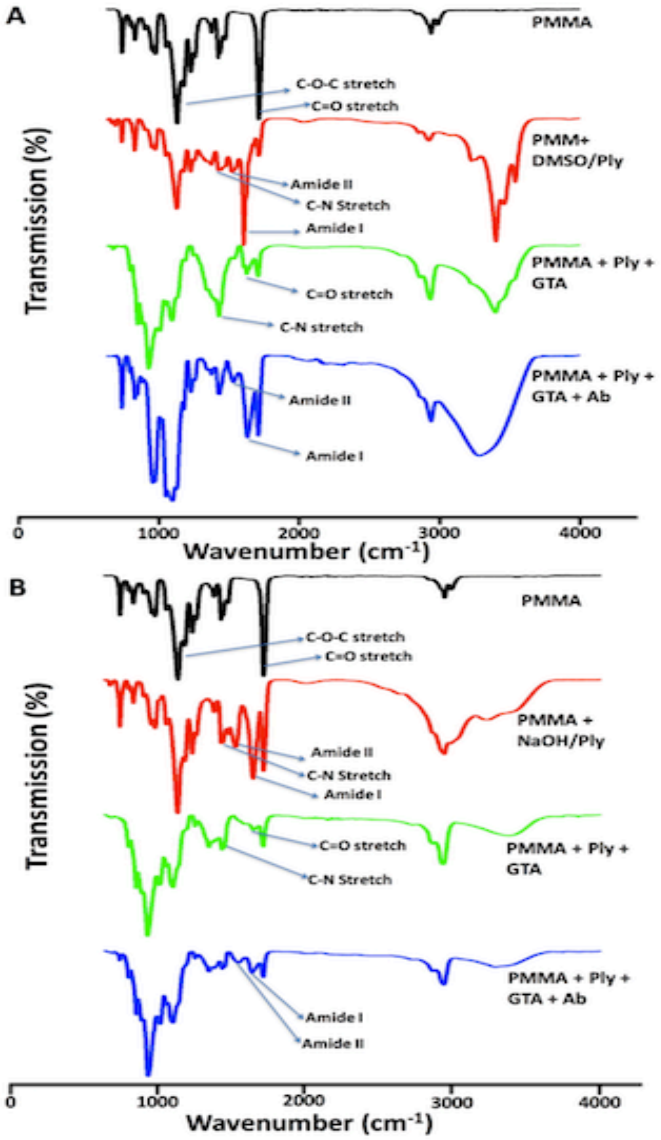

Figure 3.3: Characterization of the polylysine-based surface modification of PMMA. (A) FTIR analysis of the modified PMMA surface (modification method #1). (B) FTIR analysis of modified PMMA surface (modification method #2).

Some major changes were also observed in the spectrum of PMMA after the treatment with NaOH to form hydroxyl groups followed by treatment with polylysine to get aminated PMMA (method# 2, Figure 3.3B). The presence of Amide I (1617 cm^{-1}), Amide II (1534 cm^{-1})

and C-N (1435 cm^{-1}) stretch after the treatment of PMMA with polylysine showed that the PMMA was aminated by Polylysine. Also, we could observe the CH_2 stretching mode of vibration at 2933 cm^{-1} and V1 proton mode band of the peptide at 3239 cm^{-1}. The aminated PMMA was further treated with glutaraldehyde as seen from C=O (1637 cm^{-1}) and C-N (1440 cm^{-1}) stretch vibration to covalently bind the antibody to the PMMA surface. We could observe strong absorption for Amide I (1643 cm^{-1}) and Amide II (1541 cm^{-1}) after the addition of the antibody, which indicated the covalent binding of the antibody to the modified PMMA surface.

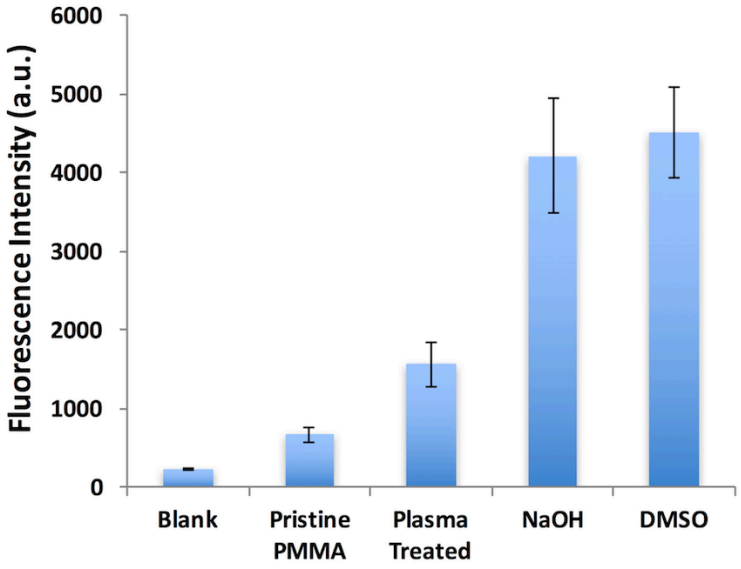

Figure 3.4: Characterization of the polylysine-based surface modification of PMMA by fluorescence microscopy. The bar graph shows the fluorescence intensity of Cy3 immobilized on different surfaces of PMMA.

3.3.2 Confirmation of protein immobilization

Fluorescence microscopy was used to investigate the modification and the differences in immobilization of antibody between the modified PMMA and the pristine PMMA. Figure 3.4 shows that polylysine modified PMMA (both method 1 and 2) gave around seven-fold higher fluorescence intensity as compared to pristine PMMA indicating the increase in efficiency of immobilization of the antibody. Method #1 (Ply/DMSO) had a slightly higher intensity as

compared to method #2 (Ply/NaOH), but the increase in intensity/immobilization was insignificant. We could also observe a three-fold increase in fluorescence intensity of polylysine modified PMMA as compared to plasma treated PMMA. The blank represented the small background fluorescence intensity of PMMA without the addition of Cy3 IgG. The result showed that the immobilization efficiency of protein was significantly increased, confirming the surface modification of the PMMA which may ultimately lead to the increase in the sensitivity of ELISA.

3.3.3 ELISA of biomarkers for HBV

To demonstrate the feasibility of detection of HBV biomarkers, we first performed the colorimetric ELISA for the detection of IgG using the surface modified PMMA microplate. IgG which is the most common antibody in the human blood can be used for diagnosis of autoimmune hepatitis and Neuromyelitis Optica.[156, 157] We performed ELISA of IgG with 10-fold diluted concentrations ranging from 100 μg/mL to 0.1 ng/mL. Each of the microwells just required 5μL of the sample and each concentration had 8 repeats as seen from Figure 3.5. The chip was scanned using a simple office scanner, 10 min after the addition of the substrate. The brightness value of each spot was then measured by ImageJ as described in Section 2.3.1. We could observe that the intensity of the purple color increased from left to right in Figure 3.5A, as the concentration increased from 0.1 ng/mL to 100 μg/mL. The purple color got saturated as the concentration increased higher than 10 μg/mL, leading to the plateau in the calibration curve. Figure 3.5B shows the calibration curve for the detection of IgG by plotting corrected brightness against the concentrations of IgG. The LOD is defined as the concentration value that generates a signal three standard deviation (SD) above the blank value. The fitted curve of IgG in the surface modified PMMA microplate (#1 method) was linear from 10^2 pg/mL to 10^6 pg/mL with a linear regression of $y = 9.72 \log (x) + 98.95$ ($R^2 = 0.98$). The LOD of IgG in the surface modified PMMA microplate (#1 method) was found to be 200 pg/mL.

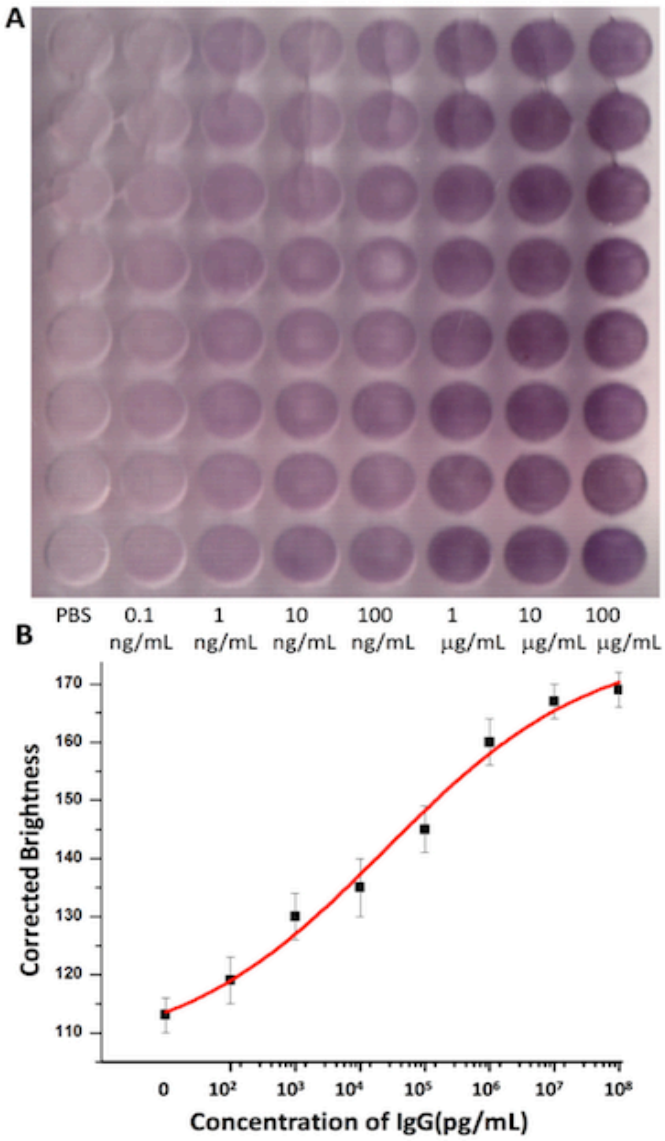

Figure 3.5: Detection of IgG in the surface modified PMMA microplate (#1 method). (A) Scanned image of enzymatic converted substrate in different columns of the chip with concentrations from left to right: blank, 0.1 ng/mL, 1 ng/mL, 10 ng/mL, 100 ng/mL, 1 µg/mL, 10 µg/mL, and 100 µg/mL, respectively. (B) The sigmoidal curve of the corrected brightness of IgG over a concentration range of 10^2 pg/mL to 10^8 pg/mL.

Similar to the detection of IgG by using the surface modified PMMA (#1 method), the calibration curve of IgG in surface modified PMMA microplate (#2 method) was linear over the range of 10^2 pg/mL to 10^7 pg/mL with saturation above 10^7 pg/mL and the linear regression of y = 12.26 log (x) + 42.49 (R^2 = 0.98). The LOD of IgG in the surface modified PMMA microplate (#2 method) was found to be 140 pg/mL (Figure 3.6) which was almost similar to #1 method.

The LOD of IgG was found to be more than 10-fold sensitive as compared to commercial 96-well microplate ELISA (LOD, 1.6 – 6.25 ng/mL) without the use of any specialized instrument like microplate reader.[154] In addition, our device just required 5 μL of sample and 90 min of assay time compared to 50-100 μL of sample and 18 hr of assay time in a traditional microplate. Our surface modified device is also more sensitive as compared to the APTES modified PMMA (12 hr incubation time and LOD of 0.12 μg/mL),[109] the paper-based device (54 f/mol/zone),[128] and our previous hybrid device (LOD, 1.6 ng/mL).[5] Bai *et al*. also used amine bearing poly(ethyleneimine) to modify the PMMA but got LOD only comparable to a 96-well plate and linear dynamic range from 5 to 500 ng/mL even with the use of fluorescence microscope.[111]

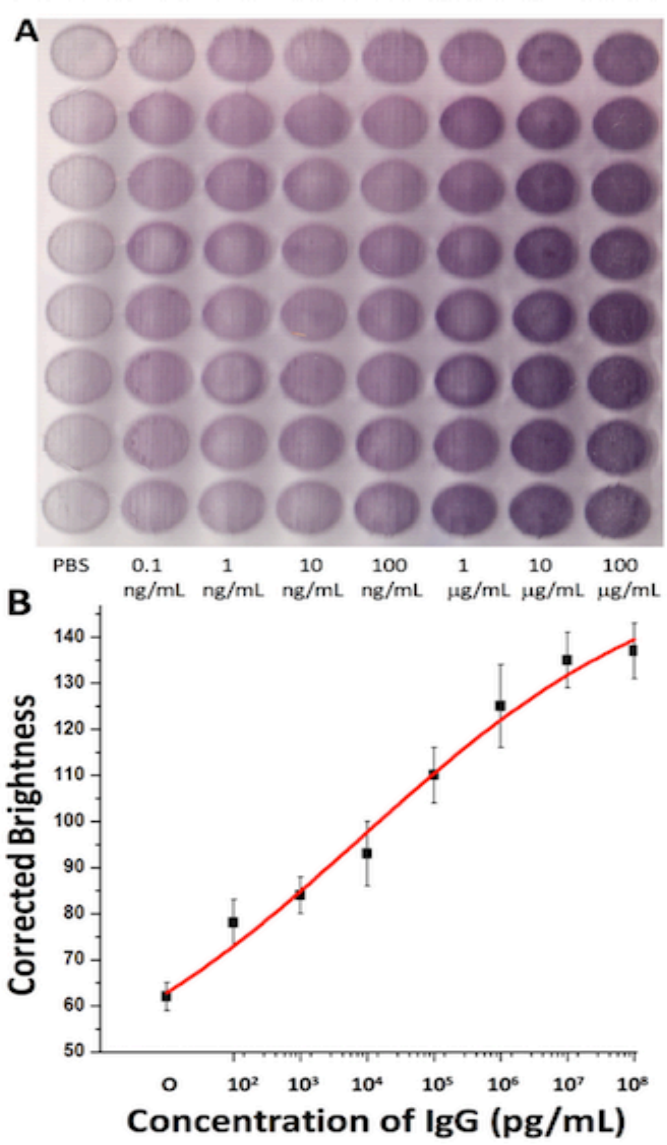

Figure 3.6: Detection of IgG in the surface modified PMMA microplate (#2 method). (A) Scanned image of enzymatic converted substrate in different columns of the chip with concentrations from left to right: blank (PBS), 0.1 ng/mL, 1 ng/mL, 10 ng/mL, 100 ng/mL, 1 µg/mL, 10 µg/mL, and 100 µg/mL, respectively. (B) The sigmoidal curve of the corrected brightness of IgG over a concentration range of 10^2 pg/mL to 10^8 pg/mL.

For the detection of Hepatitis B virus, HBsAg and HBcAg were tested. HBsAg has been mainly used for the diagnosis and remission of hepatitis B.[158, 159] It can be seen from the figure that the purple color intensity increased with the increased concentration of HBsAg (Figure 3.7). As observed in the calibration curve of IgG, the purple color intensity got saturated at higher concentration of HBsAg, starting from 34 µg/mL. The calibration curve of HBsAg on the surface

modified PMMA microplate (#1 method) was linear over the range of 34×10^{1} pg/mL to 34×10^{6} pg/mL with a linear regression of y = 13.13 log (x) + 75.1 (R^2 = 0.98). The LOD of HBsAg on the surface modified PMMA (#1 method) was found to be 180 pg/mL.

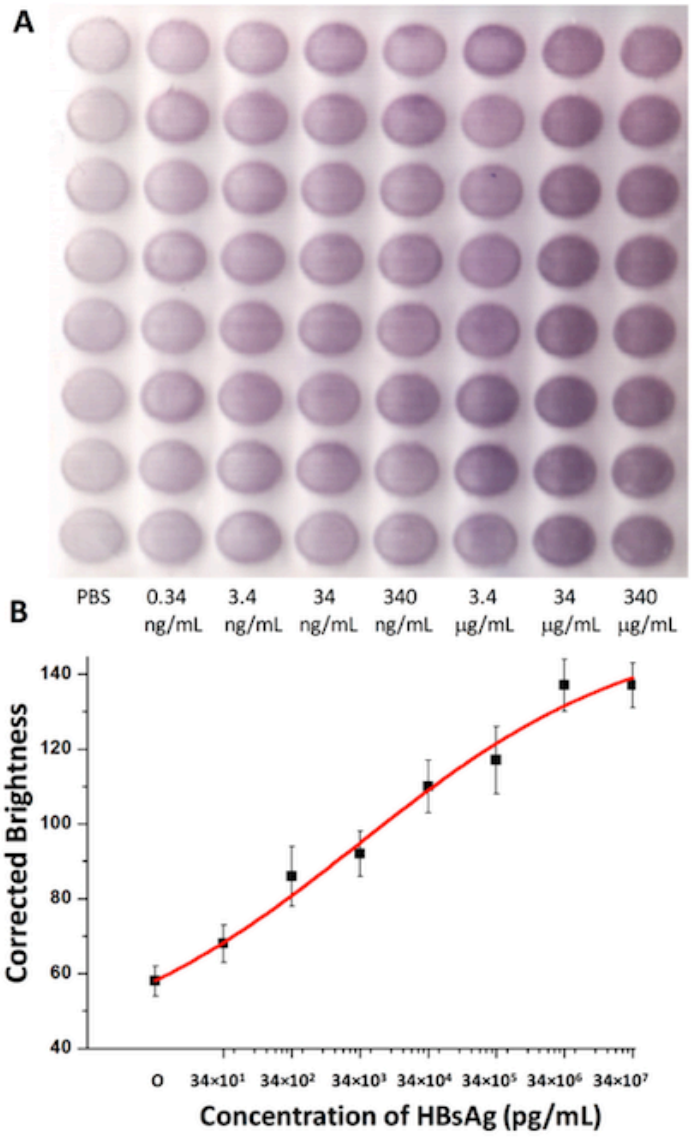

Figure 3.7: Detection of HBsAg in the surface modified PMMA microplate (#1 method). (A) Scanned image of enzymatic converted substrate in different columns of the chip with concentrations, from left to right: blank (PBS), 0.34 ng/mL, 3.4 ng/mL, 34 ng/mL, 340 ng/mL, 3.4 µg/mL, 34 µg/mL, and 340 µg/mL, respectively. (B) The sigmoidal curve of the corrected brightness of ELISA of HBsAg over a concentration range of 34×10^{1} pg/mL to 34×10^{7} pg/mL.

Similarly, the calibration curve of HBsAg on the surface modified PMMA microplate (#2 method) was linear over the range of 34×10^{1} pg/mL to 34×10^{6} pg/mL with saturation at 34

μg/mL. The calibration plot had a linear regression of y = 16.46 log (x) + 74.9 (R^2 = 0.98). The LOD of HBsAg in the surface modified PMMA microplate (#2 method) was found to be 160 pg/mL (Figure 3.8). The LODs obtained from both methods of surface modification was found to be similar. Besides, the LOD of our surface modified device was found to be more sensitive than commercial ELISA kits, HBsAg assay by Yazdani *et al*. (LOD of 0.7 ng/mL), and our previous hybrid device with LOD of 1.3 ng/mL.[5, 160] Our LOD was similar to Xu *et al*. (LOD of 0.1 ng/mL) micro-piezoelectric immunoassay that required experiment in a class-100 clean room and an impedance analyzer.[139]

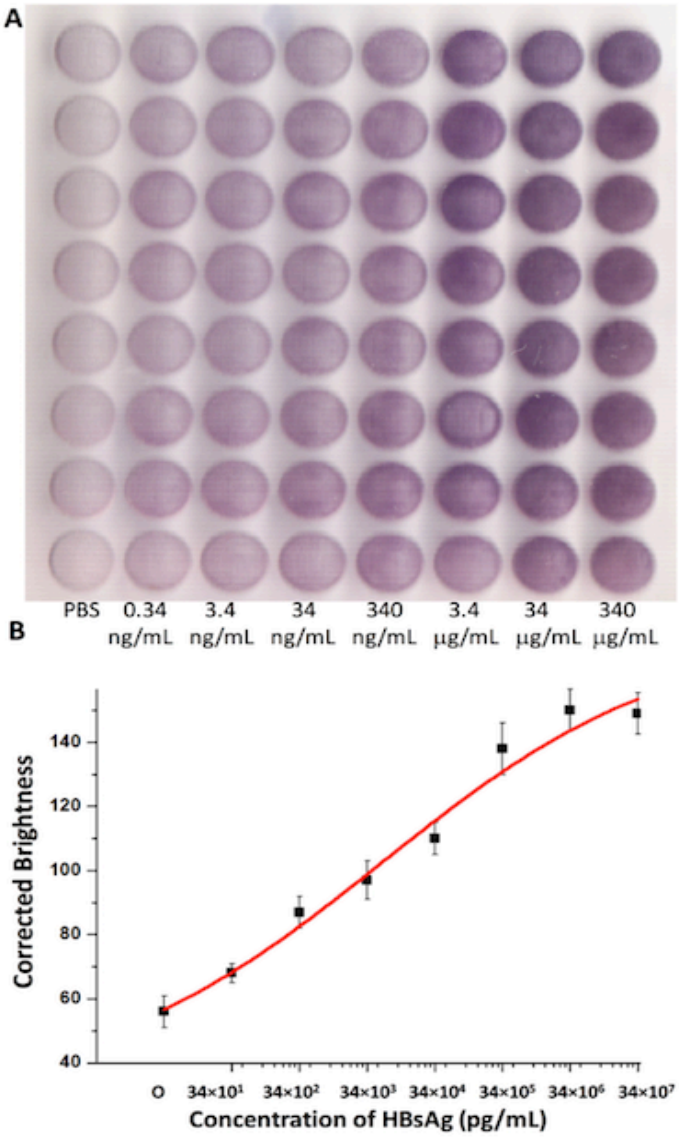

Figure 3.8: Detection of HBsAg in the surface modified PMMA microplate (#2 method). (A) Scanned image of enzymatic converted substrate in different columns of the chip with concentrations, from left to right: blank (PBS), 0.34 ng/mL, 3.4 ng/mL, 34 ng/mL, 340 ng/mL, 3.4 µg/mL, 34 µg/mL, and 340 µg/mL, respectively. (B) The sigmoidal curve of the corrected brightness of ELISA of HBsAg over a concentration range of 34×10^{1} pg/mL to 34×10^{7} pg/mL.

ELISA of HBcAg and all other subsequent ELISA were performed in the surface modified PMMA (#1 method) because the LOD for both the modification methods were similar but modification method #1 was more time efficient (1 hr) compared to the modification method #2 (2 hr). For ELISA of HBcAg, different concentrations of HBcAg between 0.1 ng/mL to 10 µg/mL were evaluated. As we can observe from Figure 3.9, the color intensity increased slightly

at lower concentration up to 1 ng/mL after which the intensity increased rapidly until 1 µg/mL, after which the intensity increased slightly. The calibration curve of HBcAg in surface modified PMMA microplate (#1 method) was linear over the range of 10^3 pg/mL to 10^7 pg/mL with a linear regression of y = 14.7 log (x) + 15.5 (R^2 = 0.98). The LOD of HBcAg on the surface modified PMMA microplate was found to be 300 pg/mL (Figure 3.9) which was more sensitive than commercial ELISA kits.[154]

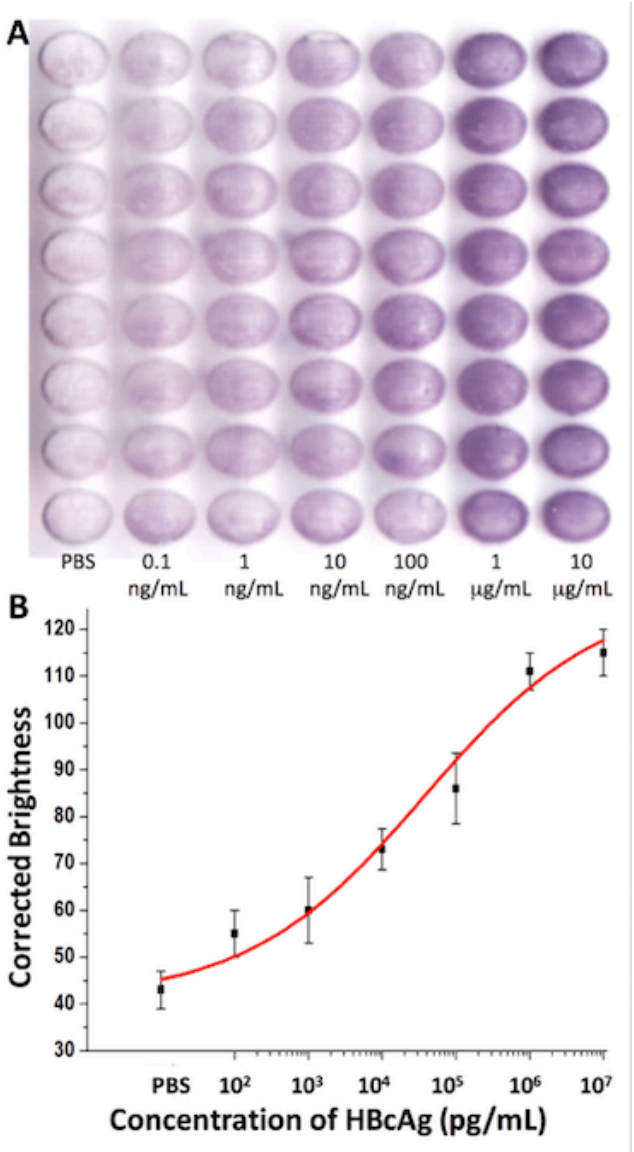

Figure 3.9: Detection of HBcAg in the surface modified PMMA microplate. (A) Scanned image of enzymatic converted substrate in different columns of the chip with concentrations from left to right: blank, 0.1 ng/mL, 1 ng/mL, 10 ng/mL, 100 ng/mL, 1 µg/mL, and 10 µg/mL, respectively. (B) The sigmoidal curve of the corrected brightness of HBcAg over a concentration range of 10^2 pg/mL to 10^7 pg/mL.

3.3.4 Multiplex detection of HBsAg and HBcAg

To demonstrate that the surface modified PMMA microplate has an efficient multiplex biomarker sensing capability, the surface modified PMMA microplate was used for simultaneous colorimetric detection of biomarkers for HBV (HBsAg and HBcAg). As shown in Figure 3.10, the first column was negative control without any antigen, hence no color was developed. Second and third columns were for the detection of HBsAg while fourth and fifth columns were for the detection of HBcAg. Third and fourth columns didn't develop color, as they didn't have the respective antibody against the antigen but second and fifth columns developed color as they had their respective antibody. This also acted as specificity test, as HBsAg could only bind to anti-HBsAg (2^{nd} column) and not anti-HBcAg (3^{rd} column). Sixth, seventh and eight columns had both antigens i.e. HBsAg and HBcAg. All of them developed color as they had their respective antibody or the mixture of both antibodies. Figure 3.10 shows the multiplex detection of biomarkers including HBsAg and HBcAg, as well as the specificity test of different biomarkers in the surface modified PMMA microplate.

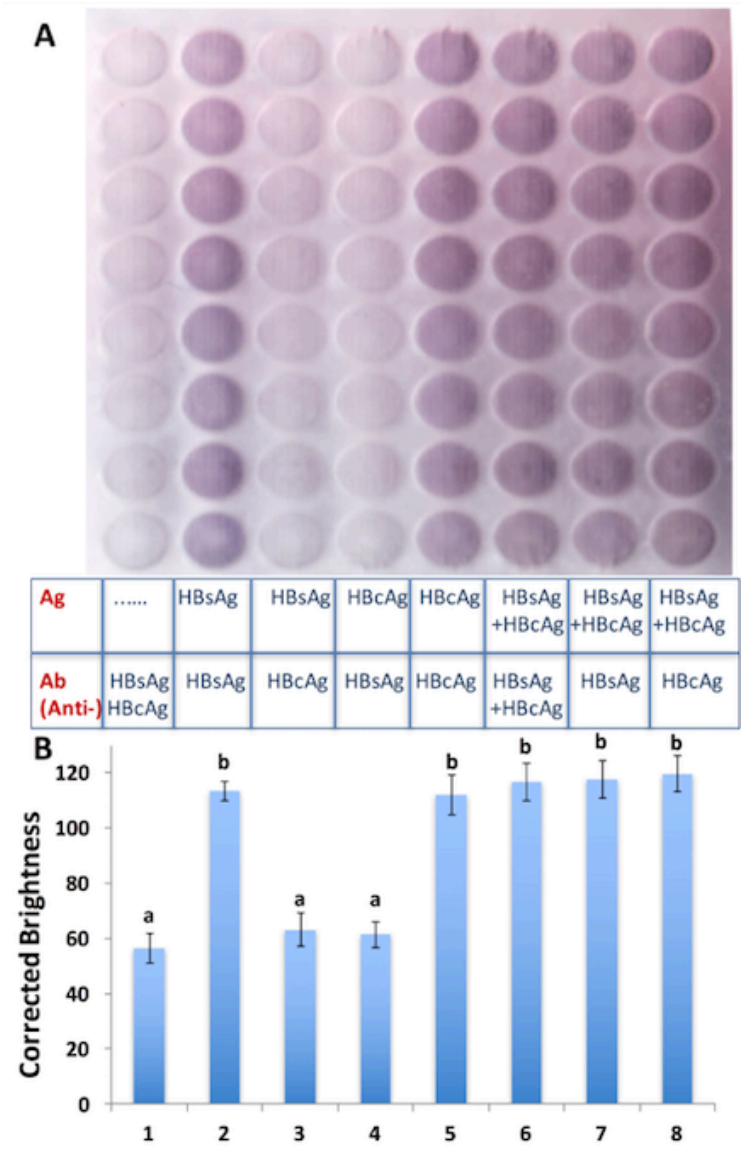

Figure 3.10: Multiplex assay of HBsAg and HBcAg in the surface modified PMMA microplate. Scanned image of the enzyme-catalyzed substrate (A) and bar plot of the corrected brightness of the scanned image (B). From left to right: immobilized probe, none (1), HBsAg (2) and (3), HBcAg (4) and (5), and HBsAg + HBcAg (6), (7), and (8), respectively. Test: From left to right: solution containing, anti-HBsAg and anti-HBcAg (1) and (6), HBsAg (2), (4), and (7), and HBcAg (3), (5), and (8). "a" and "b" shows that the data are significantly different from each other at $p = 0.05$.

3.3.5 Anti-interference test for the detection of HBsAg

The detection assay needs to have a high anti-interference capability to screen various infectious diseases as the serum contains complex ingredients consisting of different proteins with a wide range of concentrations that may interfere the detection of target proteins. So, anti-

interference experiments were performed in various columns of the modified PMMA. The experiment shows the detection of 200 ng/mL of HBsAg with and without various concentrations of interfering proteins (1 μg/mL HBcAg, 100 ng/mL CEA, 250 μg/mL BSA, and 10 ng/mL PSA). As shown in the Figure 3.11, first four columns didn't contain HBsAg, while the last four columns contained 200 ng/mL of HBsAg with various concentrations of interfering proteins. In the absence of HBsAg, there was no development of color in first 4 columns of the device from the left. Furthermore, the color intensity for the detection of 200 ng/mL of HBsAg in the presence of different interfering proteins (column 5, 6, and 7) was similar to the detection of 200 ng/mL of HBsAg without the interfering proteins (column 8). It demonstrates that even 1,250 times concentrated interfering proteins could not influence the specific detection of HBsAg in the surface modified PMMA microplate.

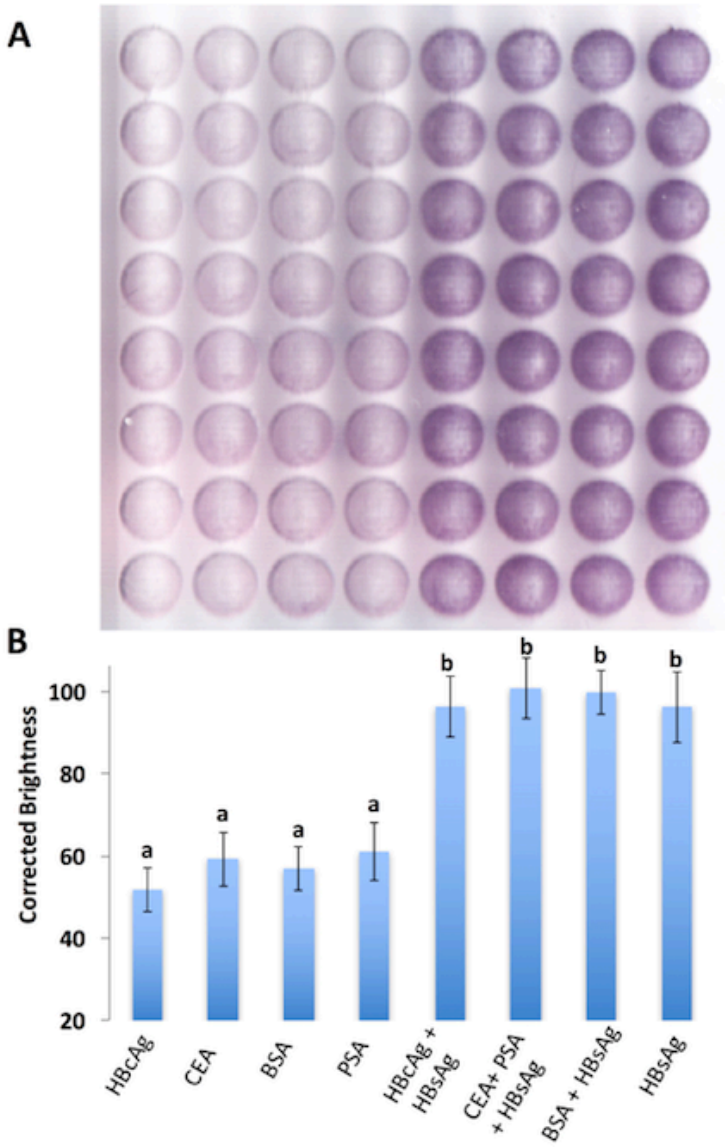

Figure 3.11: Anti-interference test for the detection of HBsAg in the surface modified PMMA microplate. The scanned image of the chip after the assay (A) and the corrected brightness of the scanned image of ELISA in the chip (B). Left four columns: Detection of 0 ng/mL of HBsAg in 1μg/mL of HBcAg (1), 100 ng/mL CEA (2), 250 μg/mL BSA (3), and 10 ng/mL PSA (4), respectively. Right four columns: Detection of 200 ng/mL of HBsAg in 1μg/mL HBcAg (5), 100 ng/mL CEA + 10 ng/mL PSA (6), 250 μg/mL BSA (7), and PBS (8), respectively. "a" and "b" shows that the data are significantly different from each other at $p = 0.05$.

3.4 Summary

In summary, we have developed a novel polylysine-based surface modification method to functionalize PMMA microplate for enhanced covalent binding of the protein to perform an ultrasensitive immunoassay for various biomarkers. Amine dense polylysine was used to

introduce amine groups onto PMMA surface while the glutaraldehyde acted as a cross-linker ultimately increasing the immobilization efficiency of the protein within a short period of time (20 min compared to overnight incubation in traditional methods). The surface modified PMMA was able to improve the sensitivity of the assay without using the complex detection system. LODs of 200 pg/mL, 180 pg/mL, and 300 pg/mL were obtained for IgG, HBsAg, and HBcAg, respectively, which were at least 10-fold more sensitive than traditional microplate readers. In addition, a wide linear range of detection, dramatically low reagent consumption, and a short assay time of 90 min was achieved. The basic system used here can perform 8 × 8 or 7 × 8 assays but the design can simply be modified to perform as many experiments and repeats as desired. In future, the study may lead to a simple, ultrasensitive, and POC device for the simultaneous detection of low concentration biomarkers in a very low sample volume of different body fluids such as saliva, tear, urine or serum. The device may find broad applications in biochemical assays and clinical diagnosis, especially in low-resource settings and developing nations.

Chapter 4: Detection of Biomarkers for Hepatitis B Virus in Surface Modified PMMA Microplates with Carbodiimide Chemistry

---

- This chapter introduces carbodiimide chemistry-based modification of PMMA for covalent immobilization of proteins.
- Surface modified PMMA microplate can immobilize proteins within 20 min and results of the assay can be seen by the naked eye without using any specialized instruments.
- A rapid and sensitive quantitative detection of infectious diseases can be achieved within 90 min.
- Immunoassay for the detection of HBV was performed in the surface modified PMMA microplate with the LODs of 360 pg/mL and 380 pg/mL for HBsAg and HBcAg, respectively.

4.1 Introduction

One of the most initial plans for the treatment of HBV is the screening or the diagnosis of the virus and the antiviral treatment of the infected people before it develops into an advanced liver disease or cirrhosis. According to Toy *et al.,* it is economically beneficial to prevent or delay progression by antiviral treatment and cost-effective diagnosis for CHB related liver diseases owing to the increased cost of the disease management.[161] In addition, United States Preventive Task Force recommends that screening is beneficial for the population at high risk for HBV infection as they found convincing evidence that early antiviral treatments are effective in improving clinical outcomes of HBV infected patients.[162] The control of infection due to HBV has been a burdensome task, especially in under-developed countries due to limited access to diagnostics and antiviral treatment resulting from high costs and deficient infrastructures in healthcare systems.[163] The currently available diagnostic technologies are not suitable for POC settings as they are tiresome, consume a large volume of samples, require overnight incubation and expensive resources. There is a growing demand to develop easy, fast, sensitive and preferably inexpensive HBV detection platform for qualitative and quantitative testing in POC settings.[144-147] But to date, the development of a POC microarray platform for multiplex detection using the miniaturized system, which is as sensitive, effective, and robust as those based on ELISAs and PCR is still a challenge.[37, 55, 148, 149]

Varieties of challenges need to be mastered to develop highly sensitive and specific POC device for viral analysis in blood samples. Viral biomarkers' concentration is extremely low at early stages and to improve signal-to-noise ratio, enrichment may be needed[164] or the device substrate may need to be modified to increase the sensitivity. Acid/base catalysis or plasma/UV treatment followed by carbodiimide conjugation can also be used to immobilize proteins on the PMMA surface. Brown *et al*. performed acid catalysis using sulfuric acid and other surface modifications for bonding and characterization of PMMA. Nugen *et al*. developed a PMMA

biosensor for electrochemical detection of nucleic acids. PMMA surface was treated with UV to get carboxylic acid functional groups, which were then conjugated, to cystamine using carbodiimide chemistry.[115] Plasma treatment provides modification with less surface roughening and degradation and does not involve toxic solvents to generate reactive functional groups. Surface aging of the polymer after the plasma treatment is a major drawback as the resultant functional groups are not stable and results are difficult to repeat.[116] Carbodiimide chemistry has been widely used for the conjugation of proteins to various substrates including quantum dots,[117] nanoparticles,[118] carbon nanotubes,[119] poly(l-lactide-co-glycolide) (PLGA) nanospheres,[120] and other biomacromolecules.[121, 122] Khnouf *et al*. found that carbodiimide chemistry resulted in more than twice the bonding efficiency of the protein to the PDMS microchannel as compared to passive binding.[123] Although carbodiimide chemistry has been widely used for the immobilization of protein to varieties of the substrate, it has not been reported for the covalent binding of antigen/antibody onto the acid/base catalyzed PMMA surfaces.

Therefore, we have developed a simple 64-microwell surface modified PMMA microfluidic microplate where the protein is covalently bound to the modified surface for rapid, sensitive and high-throughput multiplex detection of biomarkers of HBV. 8 × 8 series of microwells designed according to standard 384 well plates were created on the PMMA surface by laser ablation. The X-axis and Y-axis offset were kept like the standard 384-well plate while the diameter and the depth of the wells were reduced. We performed the acid catalysis of the PMMA to obtain carboxyl functional groups followed by carbodiimide chemistry for the cross-linking of the protein onto the carboxylated PMMA surface. The modification method yielded significantly better results for immunoassay as compared to the plasma treated and pristine PMMA. Covalent binding of proteins not only enhanced the binding efficiency of protein but also improved the immunoassay sensitivity and decreased the background noise. In addition,

rapid and ultrasensitive detection of the disease biomarkers could be completed within 90 min in this microplate as compared to more than 16 hr in traditional 96-well microplates. The assay does not require a large volume of expensive reagents and sophisticated instruments as results can be seen with the naked eye. A simple desktop scanner can be used to scan the device for quantitative analysis. Multiplex detection of IgG, HBsAg, and HBcAg was performed as a proof-of-concept and LODs of 190 pg/mL, 360 pg/mL, and 380 pg/mL were obtained for IgG, HBsAg, and HBcAg, respectively, which were more sensitive than commercial ELISA kits.[154]

4.2 Experimental

4.2.1 Chemicals and materials

All chemicals and materials are listed in Section 2.1.

4.2.2 Design and fabrication of microfluidic microplate

The chip (Figure 4.1) used in this study was designed in Adobe Illustrator CS5. The device was then fabricated using a Laser cutter. The laser cutter moved in x- and y-direction as defined in the pattern to erode the material creating the microwells according to the dimension of the standard 384-well plate as discussed in Section 3.2.2. As seen from Figure 4.1A, both the X-axis and Y-axis offset are 4.5 mm (d). A1 row offset of the chip is 8.99 mm (a) and A1 column offset of the chip is 12.13 mm (b) similar to the 384-well microtiter plate. The diameter of each well of the chip is 3.6 mm (c) which is smaller than the diameter of 384-well microtiter plate.

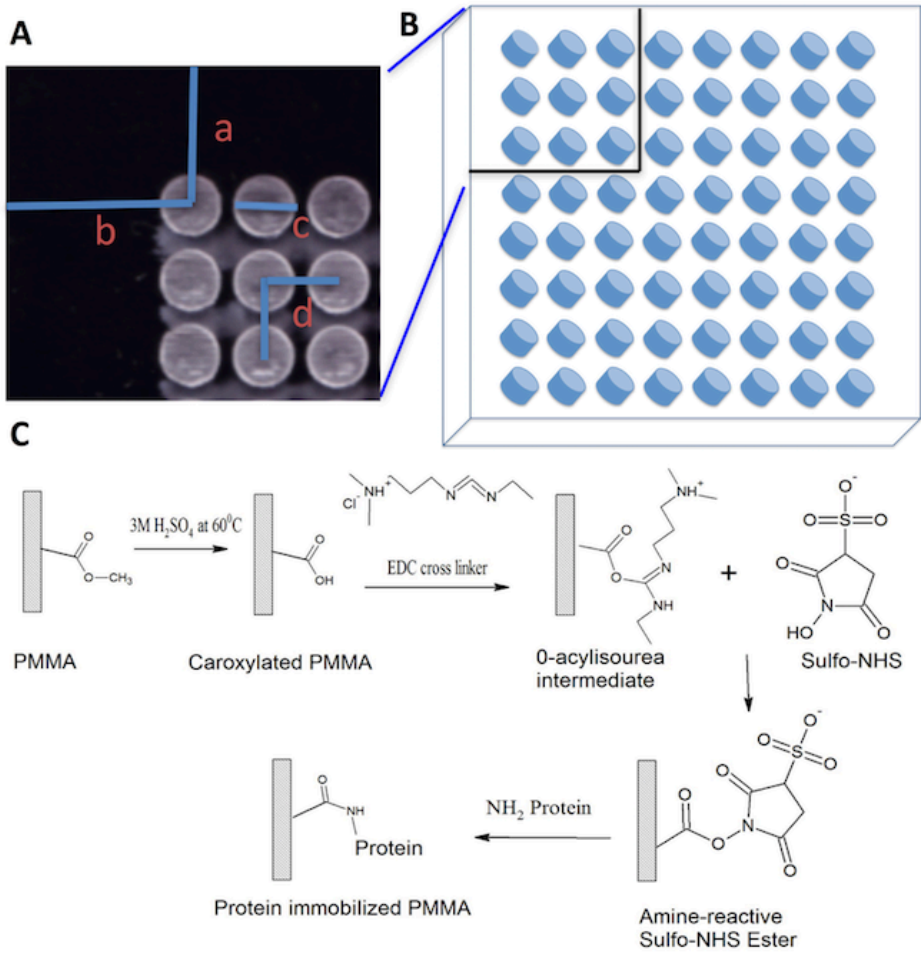

Figure 4.1: Surface-modified PMMA microplates. (A) Photograph of the actual device showing different dimensions with A1 row offset (a), A1 column offset (b), the diameter of the well (c), and X-axis and Y-axis offsets (d). (B) 3D image of PMMA microplate with 8 × 8 wells. (C) Schematic of the covalent modification of PMMA using carbodiimide chemistry.

4.2.3 Surface modification of the PMMA microplate to covalently link antibodies

The surface of PMMA can be functionalized by different methods to increase the immobilization efficiency of different biomolecules including proteins and DNA without a change in its transparency and original mechanical properties. Base and acid hydrolysis can be used to generate carboxylic acid functional groups.[4, 116] Here, for the generation of the carboxylic acid functional groups, PMMA was first sonicated for 5 minutes in 40% aqueous 2-propanol solution. PMMA was dried and then submerged in 3M sulfuric acid at 60 ^{0}C for 20 minutes. After that, PMMA was rinsed first with water, then with 2-propanol and dried (Figure 4.1). Carbodiimide compounds have been used to activate carboxylic acid to directly conjugate to the

primary amines of different biomolecules for various purposes including analysis by high-performance liquid chromatography or fluorescent labeling. In this method, 1-ethyl-3-(3-dimethylaminopropyl)carbodiimide hydrochloride (EDC) was used to obtain an intermediate O-acylisourea which is quite unstable in aqueous solution. Sulfo- *N*-hydroxysuccinimide (Sulfo-NHS) was added to improve efficiency and create dry-stable (amine-reactive) intermediate. First of all, carboxylated PMMA was taken and EDC/NHS solution (0.35 M EDC + 0.1 M NHS) was added and incubated for 20 minutes (Figure 4.1C). After 20 min, the PMMA was washed with PBS. Protein was then added to the EDC/NHS modified PMMA microplate and incubated for 20 min so that there is a covalent amide bonding between the protein and the modified PMMA surface.

4.2.4 Characterization of the surface modification

The structure of PMMA after each step of surface modification and protein immobilization was analyzed by FTIR-spectroscopy to confirm the formation of certain functional groups on the surface of PMMA. First of all, PMMA was cut into small square pieces of 1 cm × 1 cm by using the laser cutter followed by ablation of well with a diameter of 3.6 mm. The FTIR spectra were recorded after each modification steps, viz. pristine PMMA (without any modification), acid-catalyzed hydrolysis of PMMA (PMMA + H_2SO_4), carbodiimide cross-linking (PMMA + H_2SO_4 + EDC/NHS), and finally protein immobilization (PMMA + H_2SO_4 + EDC/NHS + IgG antibody).

4.2.5 Confirmation of immobilization of proteins

Surface modification for the covalent binding of the protein to the modified surface thus increasing the amount of immobilized antibody was confirmed using a fluorescence microscopy. Once the PMMA was modified using EDC/NHS, 20 μg/mL of Cy3 IgG was added to the PMMA surface and incubated for 20 minutes. Similarly, 20 μg/mL of Cy3 IgG was added to pristine PMMA and plasma treated PMMA for 20 minutes. PMMA was then washed with PBST for three times. Fluorescence intensity was measured before and after washing with PBST.

4.2.6 Detection of biomarkers of HBV

The surface modified PMMA microplate was first used for the detection of IgG followed by detection of HBV using HBsAg and HBcAg. To perform the ELISA of IgG, serially diluted IgG ranging from 100 μg/mL to 0.1 ng/mL were prepared from a stock solution of 2mg/mL IgG. Different concentrations of IgG were pipetted to the chip (5 μL/well) having eight replicates along each column. After the chip was incubated with primary antibody, the assay procedure similar to detection of IgG as discussed in Section 3.2.5 was followed.

For the detection of HBV, similar assay procedures were followed and two biomarkers HBsAg and HBcAg were analyzed. To detect HBsAg, the antigen i.e., HBsAg was immobilized on the surface modified PMMA for 20 min followed by the addition of blocking buffer and anti-HBsAg, respectively. Finally, ALP-labelled anti-rabbit IgG was added followed by the addition of BCIP/NBT. Similarly, for the detection of HBcAg, anti-HBcAg was added after the immobilization of HBcAg. ALP-labeled anti-rabbit IgG was added followed by the addition of the substrate. The microplate was scanned by a desktop scanner 10 min after the addition of the colorimetric substrate.

4.2.7 Multiplex immunoassay for detection of HBsAg and HBcAg

The surface modified PMMA can be used for simultaneous colorimetric detection of eight different biomarkers with eight replicas in eight columns of the microplate or simply be modified into 96- or 384-wells microplate. Herein, the device was used for simultaneous multiplex detection and specificity test of HBsAg and HBcAg as discussed in Section 3.2.6.

4.2.8 Evaluation of cross-reactivity

A detection assay needs to have a high anti-interference capability while having a minimum or no cross-talk and cross-reactivity to screen various infectious diseases as the biological samples contain complex ingredients of proteins with a wide range of concentrations. So, the anti-interference experiment was performed to evaluate the cross-talk and cross-reactivity

in the various columns of the modified PMMA microplate as discussed in Section 3.2.7. The microplate was scanned 10 min after the addition of the substrate.

4.3 Results and discussion

4.3.1 Characterization of surface modification

FTIR was used to characterize the modification of the PMMA microplate after each step. FTIR spectra of the pristine PMMA was analyzed first. As we can see from the FTIR spectrum of the PMMA in Figure 4.2, there were distinct absorption bands for different functional groups of PMMA as discussed in Section 3.3.1. The spectrum of the PMMA corresponded very well with the documented one in the literature for the FTIR spectrum of the PMMA.[155, 165]

We could observe some major changes in the FTIR spectrum of PMMA once its surface was modified (Figure 4.2A). The first step in the modification involved the acid catalysis of PMMA with H_2SO_4 to create a carboxyl functional group on the surface of the PMMA. The split C=O stretch vibration for the acrylated (1724 cm^{-1}) and non-acrylated (1699 cm^{-1}) carboxyl group indicated the formation of carboxyl functional groups at the surface of the PMMA. EDC/NHS method was then used to treat the carboxylated PMMA to obtain the amine-reactive sulfo-NHS ester, indicated by the S=O (1347 cm^{-1}) asymmetric stretch, S-O (853 cm^{-1}) stretch and S=O (1152 cm^{-1}) symmetric stretch. Strong absorption for Amide I (1558 cm^{-1}) and Amide II (1646 cm^{-1}) was observed after the addition of the antibody, which indicated the covalent binding of the antibody to the modified PMMA surface by the formation of an amide bond.

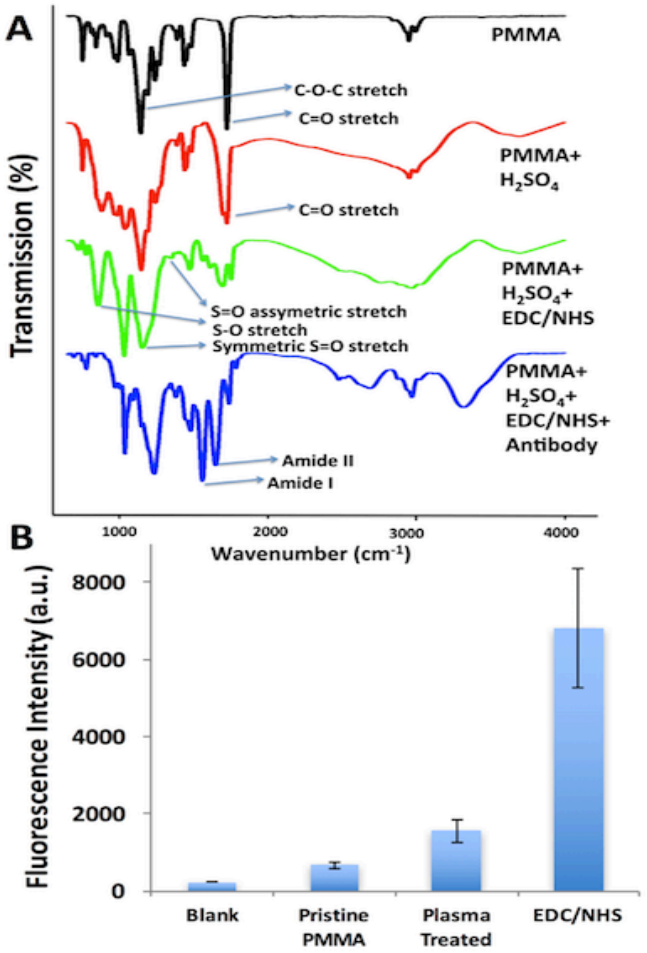

Figure 4.2: Characterization of the surface modified PMMA microplate. (A) FTIR analysis of surface modified PMMA. (B) Fluorescence intensity of Cy3 IgG immobilized on the surface of the pristine and surface modified PMMA.

4.3.2 Cross-linking of proteins to the surface modified PMMA microplate

The main aim of surface modification of PMMA was to increase the immobilization efficiency of the protein to the surface of PMMA, which could ultimately lead to increase in the sensitivity of the ELISA and decrease the background signal. To access the modification of the PMMA microplate and observe the differences in immobilization of antibody between the pristine and surface modified PMMA, a fluorescence microscopy was used. It can be seen from Figure 4.2B that EDC/NHS modified PMMA showed the highest fluorescence intensity, which was at least 10-fold higher than the pristine PMMA indicating the increase in efficiency of immobilization of the antibody. We could also observe a 5-fold increase in fluorescence intensity

of EDC/NHS modified PMMA as compared to the plasma treated PMMA. The blank represented the small background fluorescence intensity of PMMA without the addition of Cy3 IgG. Figure 4.2B showed that the proposed modification and cross-linking of protein onto the modified PMMA surface was quite stable within 20 min of incubation as the immobilization efficiency is remarkably enhanced as shown by the enhancement of fluorescence intensity of surface modified PMMA as compared to the pristine and plasma treated PMMA.

4.3.3 Detection of HBV using surface modified PMMA

Herein, the surface modified PMMA microplate was used for detection of IgG followed by the detection of biomarkers for HBV. Figure 4.3 shows the standard fitted curve of 10-fold diluted IgG sample from 100 μg/mL to 0.1 ng/mL and one negative control with PBS performed in the surface modified PMMA microplate. We could observe from Figure 4.3A that there was the minimum development of color for the negative control as there was no IgG. The purple color intensity for detection of IgG increased from lower concentration (0.1 ng/mL) to higher concentration (10 μg/mL) and got saturated after 10 μg/mL, as there was no significant increase in the intensity of purple color with higher concentrations. Figure 4.3B shows the calibration curve for the detection of IgG as corrected brightness versus the concentration of IgG. The calibration curve of IgG in the surface modified PMMA microplate was found to be linear over the range of 10^2 pg/mL to 10^8 pg/mL with a linear regression of $y = 17.86 \log (x) + 9.57$ ($R^2 = 0.98$). The LOD of IgG in the surface modified PMMA microplate was found to be 190 pg/mL. The surface modified PMMA microplate required just 90 min of assay time, 5 μL of sample, and a simple desktop scanner to read the result as compared to 18 hr of assay time, 50-100 μL of sample, and specialized instrument like microplate reader in the conventional commercially used microplate. The LOD of IgG was still found to be more than 10-fold sensitive as compared to the commercial 96-well microplate ELISA (LOD, 1.6–6.25 ng/mL)[154] because of surface modification of PMMA and higher efficiency of protein immobilization in our microplate. The surface modified device was also found to be more sensitive as compared to APTES modified

PMMA (LOD of 0.12 μg/mL),[109] poly(ethyleneimine) modified PMMA (comparable to a 96-well plate and linear dynamic range from 5 to 500 ng/mL even with the use of fluorescence microscope),[111] superparamagnetic beads for molecular analysis (LOD of 10 ng/mL),[166] paper-based device (54 fmol/zone),[128] and PMMA/paper hybrid device (LOD, 1.6 ng/mL).[5]

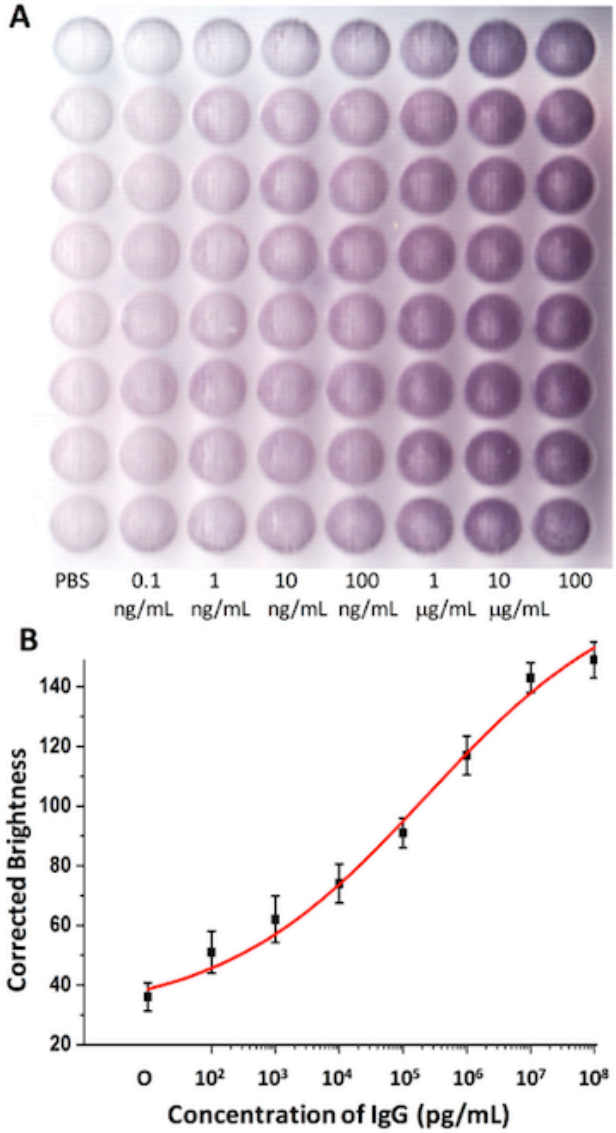

Figure 4.3: Detection of IgG in the surface modified PMMA microplate. (A) Scanned image of enzymatic converted substrate in different columns of the chip with concentrations from left to right: blank, 0.1 ng/mL, 1 ng/mL, 10 ng/mL, 100 ng/mL, 1 μg/mL, 10 μg/mL, and 100 μg/mL, respectively. (B) The sigmoidal curve of the corrected brightness of IgG over a concentration range of 10^2 pg/mL to 10^8 pg/mL.

Two different biomarkers, HBsAg and HBcAg were used for the detection of HBV. For the detection of HBsAg, 10-fold diluted samples of HBsAg ranging from 340 μg/mL to 0.34 ng/mL were prepared by diluting a stock solution of 3.4 mg/mL of HBsAg. Antigens were immobilized in 8 × 8 microarrays of the microplate with eight replicas of each concentration as performed in IgG. Figure 4.4 shows that the purple color intensity increased from left to right as the concentration of HBsAg increased from 0.34 ng/mL to 34 μg/mL. As we could observe from the fitted curve in Figure 4.4 the corrected brightness for the detection of HBsAg reached a plateau after 34 μg/mL and there was no more increase in purple color intensity value when the concentration was increased further. The calibration curve of HBsAg (corrected brightness vs concentration of HBsAg) in the surface modified PMMA microplate was linear over the range of 34×10^{1} pg/mL to 34×10^{6} pg/mL with a linear regression of $y = 11.05 \log (x) + 91.76$ ($R^2 = 0.98$). The LOD of HBsAg in the surface modified PMMA microplate was found to be 360 pg/mL.

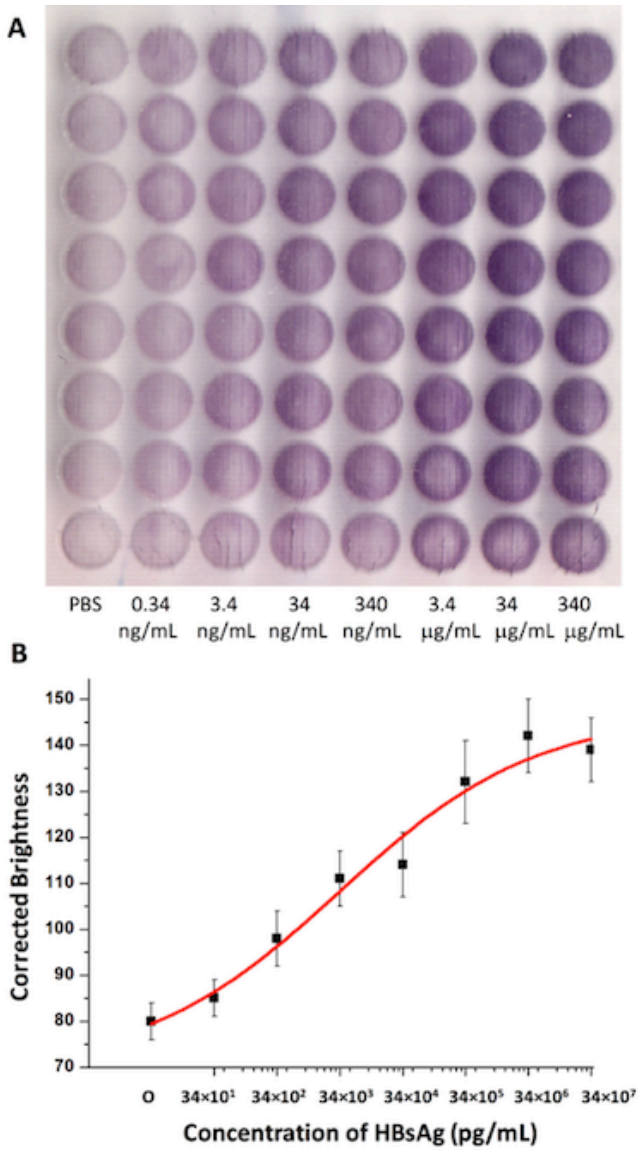

Figure 4.4: Detection of HBsAg in the surface modified PMMA microplate. (A) Scanned image of enzymatic converted substrate in different columns of the chip with concentrations, from left to right: blank, 0.34 ng/mL, 3.4 ng/mL, 34 ng/mL, 340 ng/mL, 3.4 µg/mL, 34 µg/mL, and 340 µg/mL, respectively. (B) The sigmoidal curve of the corrected brightness of ELISA of HBsAg over a concentration range of 34×10^{1} pg/mL to 34×10^{7} pg/mL.

Like the detection of IgG and HBsAg, the detection for HBcAg was performed in the surface modified PMMA microplate but with 8×7 arrays microplate for the 10-fold diluted concentrations of HBcAg from 10 µg/mL to 0.1 ng/mL. Rapid increase in color intensity was observed with the increased concentration of the analyte (HBcAg) after initial slight increase from PBS to 0.1 ng/mL. In case of HBcAg, saturation of color intensity was not observed, as the

highest concentration measured was 10 μg/mL (Figure 4.5). The calibration curve of HBcAg in the surface modified PMMA microplate was found to be linear over the range of 10^2 pg/mL to 10^7 pg/mL with a linear regression of y = 14.07 log (x) + 29.64 (R^2 = 0.98). The LOD of HBcAg in the surface modified PMMA microplate was found to be 380 pg/mL. The LOD of the surface modified PMMA microplate was found to be more sensitive than commercial ELISA kits,[154] HBsAg assay by Yazdani *et al*. (LOD of 0.7 ng/mL),[160] fully automated lab-on-a-disc (LOD 0.51 ng/mL),[143] and paper/PMMA hybrid microfluidic device (LOD of 1.3 ng/mL).[5] In addition, the LOD of the surface modified PMMA microplate was found to be similar to Xu *et al*. (LOD of 0.1 ng/mL) which required experiment in a class-100 clean room.[139]

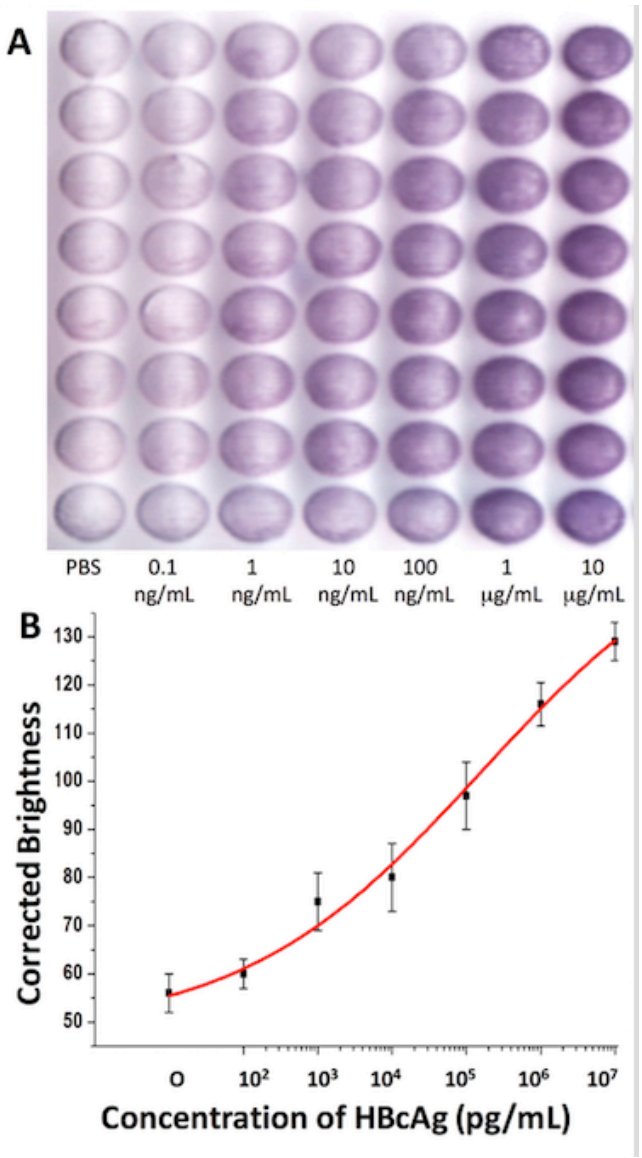

Figure 4.5: Detection of HBcAg in the surface modified PMMA microplate. (A) Scanned image of enzymatic converted substrate in different columns of the chip with concentrations from left to right: blank, 0.1 ng/mL, 1 ng/mL, 10 ng/mL, 100 ng/mL, 1 µg/mL, and 10 µg/mL, respectively. (B) The sigmoidal curve of the corrected brightness of HBcAg over a concentration range of 10^2 pg/mL to 10^7 pg/mL.

4.3.4 Multiplex immunoassay in EDC/NHS surface modified PMMA microplate

Simultaneous detection of HBsAg and HBcAg was performed in the carbodiimide-based surface modified PMMA microplate to demonstrate that the device has an efficient multiplex biomarker sensing capability. Figure 4.6 shows the multiplex detection of HBsAg and HBcAg in the surface modified PMMA microplate. The first, third, and fourth columns did not produce

color as they didn't have the capture antigen for the respective antibody. All other columns produced color as they had the capture antigen or the combination of capture antigens for the respective antibody. Figure 4.6 showed the proficiency of the surface modified PMMA microplate to perform multiplex detection of biomarkers including HBsAg and HBcAg as well as the specificity for the detection of different biomarkers.

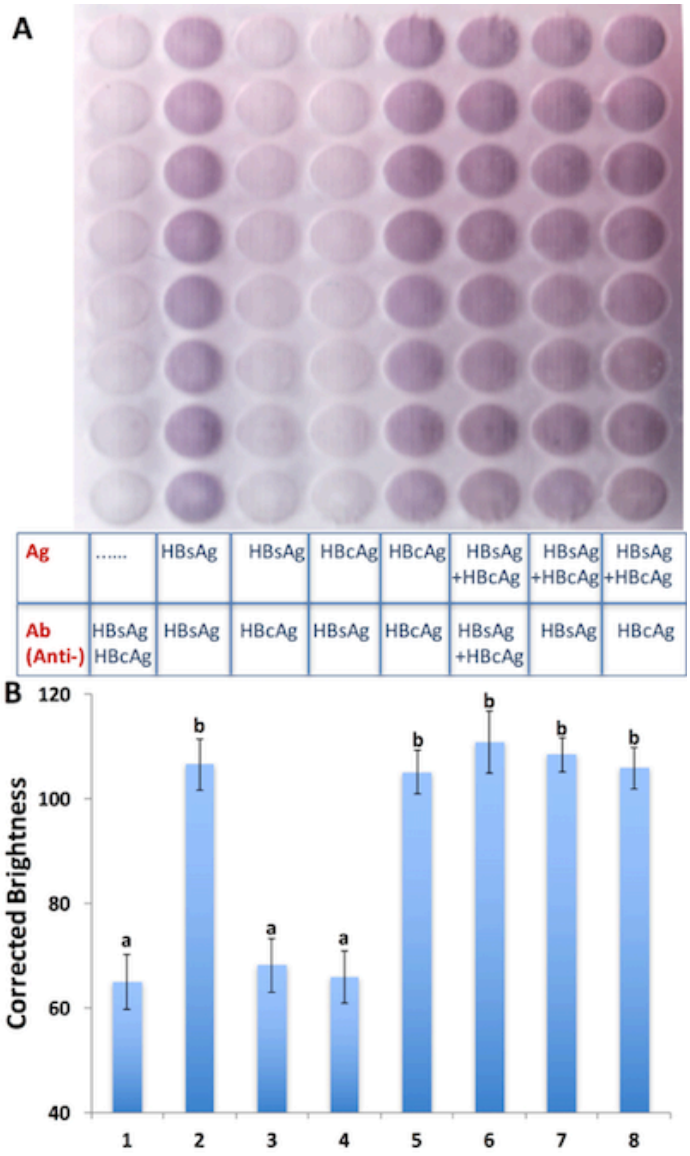

Figure 4.6: Multiplex detection of HBsAg and HBcAg in the surface modified PMMA microplate. Scanned image of the enzyme-catalyzed substrate, (A) and bar plot of the corrected brightness of the scanned image (B). From left to right: immobilized probe, none (1), HBsAg (2) and (3), HBcAg (4) and (5), and HBsAg + HBcAg (6), (7), and (8), respectively. Test: From left to right, solution containing, anti-HBsAg and anti-HBcAg (1) and (6), HBsAg (2), (4), and (7),

and HBcAg (3), (5), and (8). “a” and “b” shows that the data are significantly different from each other at $p = 0.05$.

4.3.5 Cross-reactivity test in the surface modified PMMA microplate

Evaluation of cross-talk or cross-reactivity remains one of the most important factors for the development of potential multiplex detection platform. So, anti-interference test of the model analyte, HBsAg was performed in the various columns of the surface modified PMMA microplate. The test as shown in Figure 4.7 shows the anti-interference test for the detection of HBsAg with and without various concentrations of interfering proteins. As shown in Figure 4.7, the first four columns didn’t contain HBsAg and only contained interfering proteins so there was no development of color. Moreover, the purple color intensity for the detection of 200 ng/mL of HBsAg without the interfering protein (eighth column) was found to be similar to the detection of 200 ng/mL of HBsAg in the presence of different interfering proteins (fifth, sixth, and seventh column). The anti-interference test results showed that different interfering proteins with concentration ranging from 10 ng/mL to 250 μg/mL could not interfere with the specific detection of HBsAg.

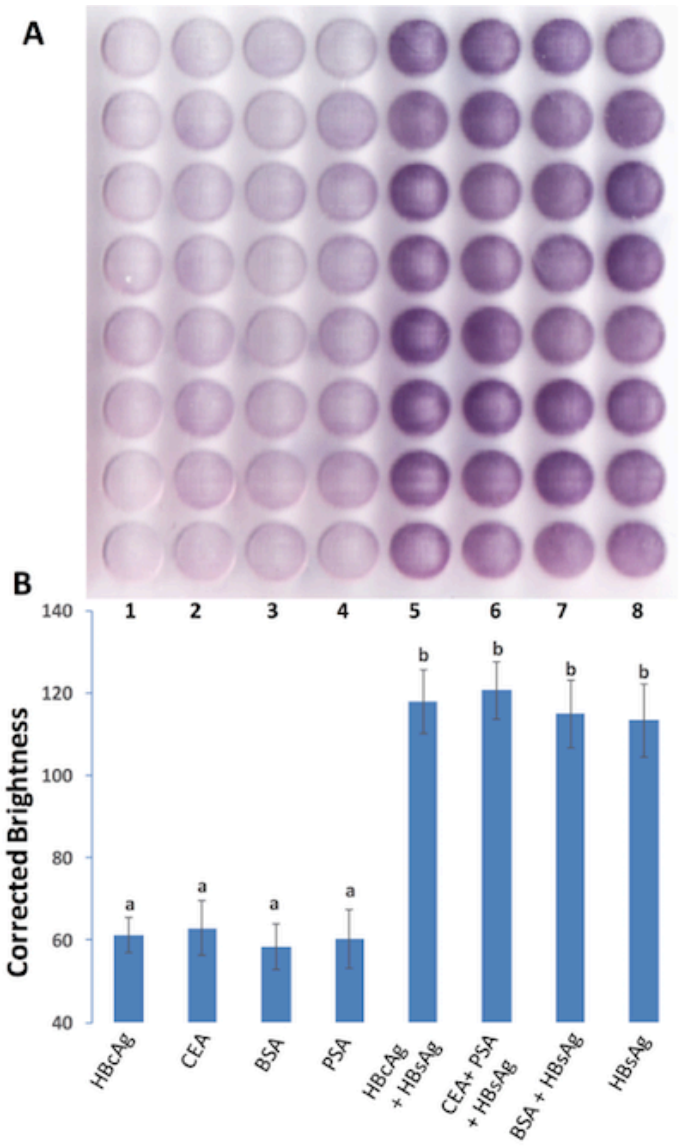

Figure 4.7: Anti-interference test for the detection of HBsAg in the surface modified PMMA microplate. The scanned image of the chip (A) and the corrected brightness of the scanned image of ELISA (B) for the detection of HBsAg. From left to right: detection of 0 ng/mL of HBsAg in the solution containing 1µg/mL HBcAg (1), 100 ng/mL CEA (2), 250 µg/mL BSA (3), and 10 ng/mL PSA (4), respectively and 200 ng/mL of HBsAg in 1µg/mL HBcAg (5), 100 ng/mL CEA + 10 ng/mL PSA (6), 250 µg/mL BSA (7), and PBS (8), respectively. "a" and "b" shows that the data are significantly different from each other at $p = 0.05$.

4.4 Summary

We have developed a novel carbodiimide method to cross-link proteins onto the surface of carboxylated PMMA microplate to improve the covalent binding of the antibody including IgG, HBsAg, and HBcAg to perform a highly sensitive ELISA for the detection of various

biomarkers. The use of EDC/NHS to cross-link the protein led to highly efficient immobilization of antibody to the surface of PMMA microplate so that protein immobilization could be accomplished within 20 min and the whole assay could be completed within 90 min. As a proof-of-concept, simultaneous detection of IgG, HBsAg, and HBcAg was achieved with the LODs of 190 pg/mL for IgG, 360 pg/mL for HBsAg, and 380 pg/mL for HBcAg. The sensitivity of ELISA was improved significantly without the use of any sophisticated instrument like a microplate reader. A wide linear range of detection and 10-fold more sensitive detection limit was achieved just with a simple desktop scanner. The results could be viewed with the naked eye or smartphone can be used for quantitative detection. In addition, the reagent consumption is minimum (5 μL/well) which can save the expensive reagent and limited amount of sample in many cases. The basic design of the PMMA microplate used in the study had 8 × 8 or 7 × 8 assays-wells but the design can simply be modified to perform as many experiments and repeats as desired and can simply be modified into 96- or 384-wells. The surface modified PMMA microplate could find massive attention as a simple, high throughput, and POC detection system in resource-limited settings where expensive diagnostic equipment like spectrophotometer is not available. In future, the PMMA microplate with high protein immobilization efficiency may find broad application as an ultrasensitive and multiplex biochemical assay or a clinical diagnosis platform.

Two different methods were used for the modification of PMMA microplate. In the first method, PMMA was functionalized with amine groups using polylysine followed by glutaraldehyde for the cross-linking of the proteins to the modified PMMA surface. In the second method, PMMA was acid hydrolyzed to obtain carboxyl functional groups followed by carbodiimide chemistry (EDC/NHS) to link proteins to carboxylated PMMA. The modification time for the polylysine-based method was 1hr using DMSO/polylysine and 2hr using NaOH/Polylysine but only 45 min for the carbodiimide-based method. LODs for different biomarkers was found to be similar to both the methods, however, modification time was less in the carbodiimide-based method.

Chapter 5: A Polymer/paper Hybrid Microfluidic Platform for Rapid Quantitative Detection of Multiple Disease Biomarkers

---

- Parts of this chapter were published in *Scientific Reports* as a research article in 2016 (**Sanjay, S. T.,** Dou, M., Sun, J., & Li, X. (2016). *Scientific reports*, *6*, 30474).
- This chapter introduces a versatile polymer/paper hybrid microfluidic platform for detection of multiple disease biomarkers.
- Novel use of porous paper in flow-through microwells facilitates rapid protein immobilization and efficient washing, avoiding complicated surface modifications.
- The top reagent delivery channels can simply transfer reagents to multiple microwells thus avoiding repeated manual pipetting and costly robots.
- For the device to be used in the settings of laboratories and hospitals, the hybrid device was redesigned to make it compatible with traditional microplate readers as well.
- For the chemiluminescence assay, the LODs of 20 pg/mL for IgG, 50 pg/mL for HBsAg, and 10 pg/mL for HCVcAg were achieved.

5.1 Introduction

Acute infectious diseases caused by various pathogenic microorganisms are usually diagnosed by exhausting immunoassay tests like ELISA, immunofluorescence, western blotting, and immunodiffusion along with PCR, flow cytometry and a wide range of other techniques.[167-169] Although there is a considerable progress in science and technology, rapid and sensitive POC detection of diseases or biological agents in low-resource settings (e.g. high-poverty regions) is still a challenge.[170]

As discussed in Section 1.4, microfluidic LOC devices possess astonishing features for low-cost, simple, and rapid bioanalysis. These highly portable microfluidic devices with integrated processing can analyze complex biological fluids including serum, urine,[171] cells, and cell lysates for various applications, such as detection of diseases,[37, 172, 173] single cell analysis,[174-176] 3D cell culture for tissue-based bioassays,[61] forensic analysis,[59] and a wide range of other fields.[62, 177-180]

To address issues from conventional microplates, a few microplate-format microfluidic devices have been developed for immunoassays as discussed in Section 1.7.[52, 124, 125] Overall, all these devices require either long incubation time, surface functionalization or complicated detection systems. With the emergence of paper-based devices in recent years, various POC analyses, including paper-based ELISAs have been developed.[94, 126, 127] The limitations in paper-based ELISA include low-performance in flow control and the need of repeated micropipetting for adding reagents and washing all the zones, which is time-consuming and limits its application for high-throughput detection, especially in low-resource settings as discussed in Section 1.7.1.

Along with paper, some polymers such as PMMA have also been widely used for the fabrication of microfluidic devices. Each substrate has its own advantages and disadvantages. PMMA is transparent, rigid and rapidly delivers reagents to different regions. However, polymers such as PMMA require complicated surface modification procedures to immobilize biosensors and other biomolecules such as antibodies and enzymes. On the contrary, paper-based devices can rapidly immobilize biosensors and other biomolecules but do not offer high

performance in flow control especially over a fairly long distance. Hybrid devices can take advantages of various substrates while eliminating some limitations of certain substrates as discussed in Section 1.5.4. These types of hybrid devices have been used for various applications including infectious diseases diagnosis.[181-183]

Herein, we have developed a simple miniaturized 56-microwell paper/PMMA hybrid microfluidic ELISA microplate for rapid and high-throughput detection of infectious diseases. A series of novel funnel-shaped PMMA microwells have been created by laser ablation of PMMA, wherein a paper substrate can be placed to complete ELISA within an hour. The introduction of 3D micro-porous paper with the high surface-to-volume ratio in microwells of this hybrid microplate facilitated rapid immobilization of antibody/antigen and also avoided complicated surface modifications. The top reagent delivery channels along with the vertical flow-through microwells in the middle PMMA layer can simply transfer reagents to multiple microwells, thus avoiding repeated manual pipetting and washing steps into each well in conventional ELISA or the use of costly robots. All the reagents/analytes pass through the 3D matrix of the paper surface from the funnel-shaped microwells. This design not only provides efficient washing but also increases the opportunities for analytes to be rapidly and efficiently captured, thus resulting in higher detection sensitivity. ELISA of IgG and HBsAg were performed in the hybrid device and LODs comparable to commercial ELISA kits were obtained by using an office scanner, without the use of any specialized instruments like a microplate reader.

5.2 Experimental

5.2.1 Chemicals and materials

All chemicals and materials are listed in Section 2.1.

5.2.2 Design and fabrication of microfluidic platform

The chip used in this study was designed by using Adobe Illustrator CS5 and micro-machined using the laser cutter. Since the funnel-shaped microwells involve different depths, multi-level fabrication is needed. Although photolithography is one of the most widely used

fabrication techniques to fabricate microfluidic devices, it is difficult, expensive and complicated to create a microfluidic device with different depths.[94, 184, 185] On the contrary, laser ablation is a rapid prototyping method for the fabrication of microfluidic devices. By applying different intensities, microstructures with different depths can be readily fabricated. Therefore, we developed a simple laser ablation method to create the funnel-shaped microwells, which can be completed within minutes, without using any photomask. As shown in Figure 5.1a, the microfluidic device consists of three different layers. The topmost layer, the fluid delivery layer, is used to deliver all the assay reagents and also forms the cover for the microwells in the assay plate (middle layer). Each of the channels connected to different inlet reservoirs of upper layer delivers reagents to 7 microwells in the middle layer. Pieces of chromatography paper were placed inside each microwell. The middle layer contains funnel-shaped (Figure 5.1c) microwells with an upper diameter of 2 mm and a lower diameter of 0.3 mm, wherein a paper disk can be placed, as shown in the cross-section view of the device from Figure 5.1b. The 0.3 mm diameter-lower microwells are placed just below the upper microwells of the middle layer and helps to hold the paper in place and minimize the chances of backflow of the reagents. Just underneath the bottom of the assay microwells, is attached the outlet system. The outlet channels are connected to a single outlet microwell, which acts as an outlet reservoir once a negative pressure is applied. Arrows in Figure 5.1b shows the direction of the flow of reagents.

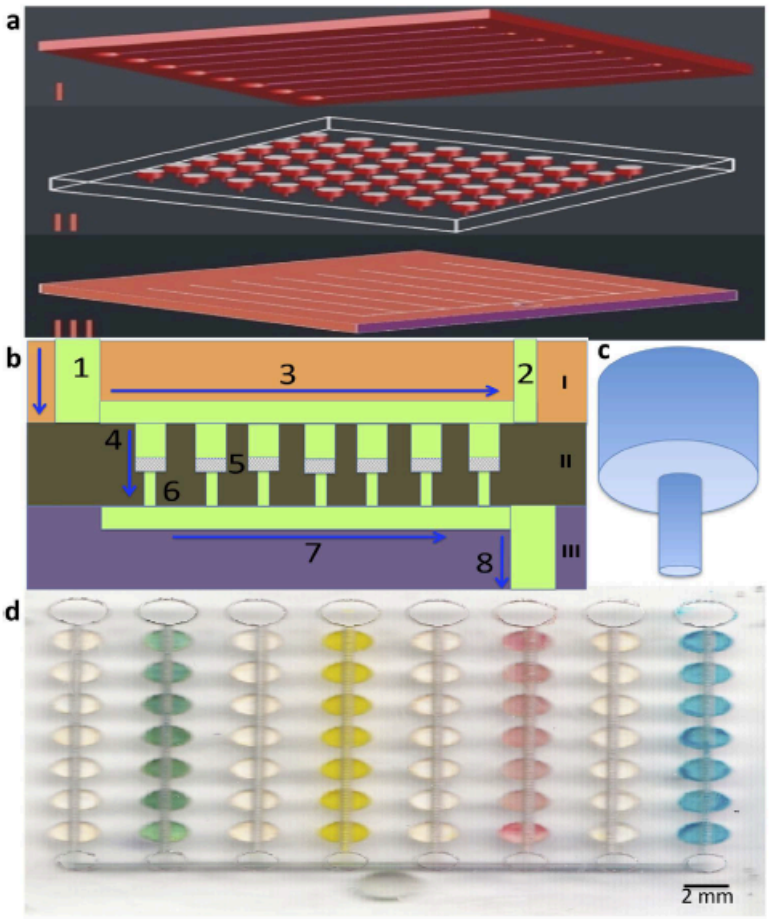

Figure 5.1: Chip design of the PMMA/paper hybrid microfluidic microplate. (a) 3D schematic of the exploded view of the hybrid device. (b) Cross-section view of the chip. The chip consists of three PMMA layers. The top layer (I) for fluid delivery consists of inlet reservoir '1' and fluid distribution channel '3'. The middle layer (II) for incubation consists of 56 unique funnel-shaped microwells, with upper microwell '4' and lower microwell '6', with paper disks '5' placed in between. The lowermost layer (III) for fluid removal consists of an outlet channel '7', which leads to a common outlet reservoir '8'. (c) 3D exploded view of the funnel-shaped microwell. (d) Photograph of the actual assembled device with water and different colored dyes in alternate columns.

5.2.2 Colorimetric detection of IgG and HBsAg using the hybrid device

The hybrid device can be used for a wide range of bioassays. Figure 5.2 illustrates the main steps for the IgG detection by on-chip ELISA using the hybrid device. The primary antibody IgG (0.1 ng/mL-100 μg/mL in 10 mM, pH 8.0 PBS) was introduced to the chip from different inlet reservoirs in the first layer of the chip. After the chip was incubated with the primary antibody for 10 minutes, the unreacted paper surface was blocked with a blocking buffer

for another 10 minutes. After washing with PBST, anti-rabbit IgG-alkaline phosphatase (6 μg/mL) was added for another 7 min. Then, the final wash was done with the washing buffer for three times. Finally, the substrate (BCIP/NBT) was added. After a 10-minute incubation, different layers of the chip were separated, and the middle layer was scanned with a scanner after another 15 minutes.

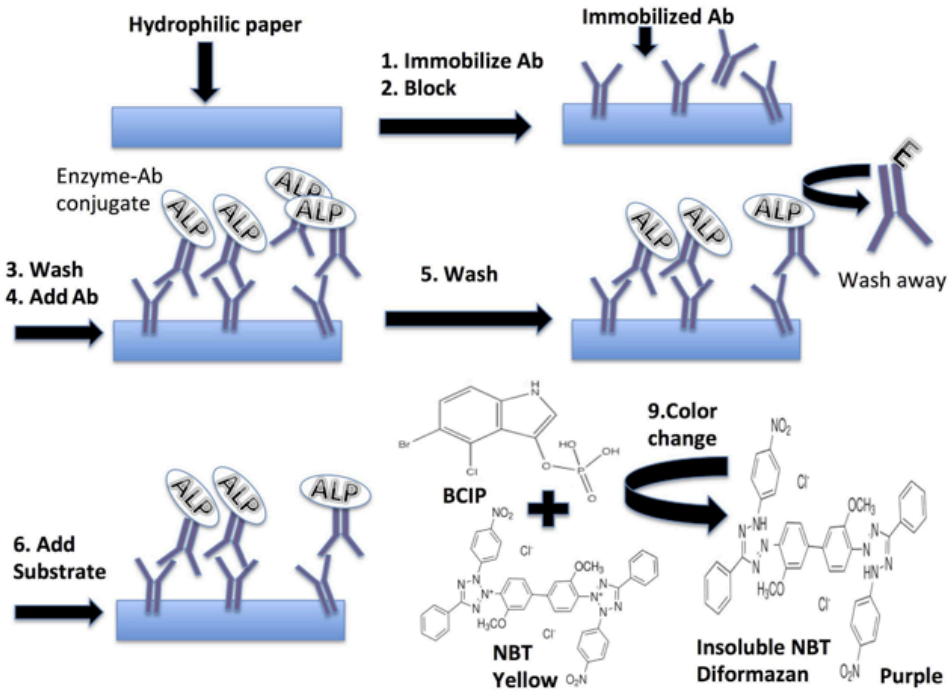

Figure 5.2: Schematic illustration of the approach of immunoassay on the hybrid device, comprising six steps: (1) Immobilizing antibody on paper, (2) Blocking, (3) Washing, (4) Binding of enzyme conjugated antibody, (5) Washing, and (6) Enzymatic production of insoluble NBT diformazan.

Regarding HBsAg detection, a similar assay procedure was followed. The main difference was that the first step was to immobilize the antigen, i.e., HBsAg, followed by addition of anti-HBsAg, and finally forming a sandwich-structure immunoassay by the addition of ALP-labelled anti-rabbit IgG.

5.2.3 Rapid detection of HBsAg in human serum

To validate the reliability of the developed hybrid microfluidic microplate and to test its feasibility for real human sample detection, HBsAg was spiked in normal human serum. 10 μL of varying concentrations of HBsAg were spiked into 1.0 mL human serum which was pre-diluted 3 folds using PBS to get the final concentrations of 3.4 ng/mL, 34 ng/mL, 0.34 μg/mL, and 3.4 μg/mL, respectively. After mixing thoroughly, the spiked samples were used for the rapid detection of HBsAg, following steps similar to the detection of standard HBsAg prepared in PBS buffer and spike recoveries were calculated.

5.2.4 Rapid detection of HBcAg and HCVcAg

Herein, for the detection of HBV, first, different concentrations of HBcAg (1 ng/mL-100 μg/mL) were pipetted to the chip through the inlet microwells in the top reagent delivery layer. After blocking the device with blocking buffer for 10 min, anti-HBcAg was added followed by washing with PBST and addition of the ALP-linked secondary antibody for 7 min. Finally, BCIP/NBT substrate was added after washing the chip three times with PBST. The chip was incubated for 10 min and scanned by a common desktop scanner. The brightness value of the scanned chip was then measured by the software ImageJ.

Regarding the detection of HCV, a similar assay protocol as HBcAg was followed. First, HCVcAg was immobilized on the paper substrate of the hybrid device followed by the addition of blocking buffer and anti-HCVcAg. Finally, ALP-labelled anti-rabbit IgG was added followed by the addition of the substrate. Washing was required after each step similar to the detection of HBcAg.

5.2.5 Colorimetric multiplex detection of HBsAg and HBcAg

To demonstrate the feasibility of multiplex detection in the hybrid microfluidic microplate, two biomarkers for HBV were used as model analytes. Colorimetric detection of HBsAg and HBcAg was performed in the device as described in Section 3.2.6. Different combination of capture antigens was added to the device followed by the addition of the

blocking buffer and the primary antibody. After the addition of primary antibody, the ALP-linked secondary antibody was added. Finally, 10 min after the addition of BCIP/NBT substrate, the chip was scanned with the scanner.

5.2.6 Colorimetric anti-interference test

To establish a device as an efficient infectious diseases detection platform, the detection assay in the device needs to show a high anti-interference capability. So, the anti-interference assay was performed in different columns of the hybrid microfluidic microplate to detect HBsAg. Different kinds of capture antigens were immobilized on the paper surface as described in Section 3.2.7. After the addition of the capture antigen, blocking buffer was added in all the columns followed by the addition of anti-HBsAg. Finally, the secondary antibody linked with alkaline phosphatase and the substrate was added before scanning the device with a scanner.

5.2.7 Rapid chemiluminescent detection of infectious diseases

Chemiluminescence detection of IgG in the hybrid microfluidic microplate was carried out similar to the colorimetric detection of IgG in the device. The major difference in the assay protocol was the use of the HRP-linked secondary antibody in chemiluminescence assay instead of ALP-linked secondary antibody in the colorimetric assay. Similarly, the substrate used in the assay was Supersignal® ELISA Pico chemiluminescent substrate (peroxide + luminol + enhancer) instead of BCIP/NBT. Finally, after the completion of the assay, the device was read using a microplate reader instead of a desktop scanner. Briefly, IgG was pipetted to the inlet microwells of the hybrid chip. The device was incubated for 10 min and the unreacted paper surface was blocked with blocking buffer for another 10 minutes. After washing with the washing buffer, HRP-linked secondary antibody (0.4 μg/mL) was added. It was then incubated for another 7 min followed by washing for three times. Finally, the substrate for the HRP was added. After incubating the substrate for 2 min, the chemiluminescent intensity was read at 425 nm by a spectrophotometer.

Regarding the chemiluminescence detection of HBsAg, a similar assay protocol as IgG was followed. First, HBsAg was immobilized on the paper substrate of the hybrid microfluidic microplate followed by the addition of the blocking buffer and anti-HBsAg. Finally, HRP-labelled anti-rabbit IgG was added followed by the addition of the chemiluminescent substrate. Similarly, detection of HBcAg and HCVcAg were performed with their respective antibodies.

5.2.8 Chemiluminescence multiplex detection of HBsAg and HBcAg

To demonstrate the feasibility of multiplex chemiluminescent detection in the hybrid microfluidic microplate, similar to the colorimetric detection, the assay of HBsAg and HBcAg were performed in the hybrid device. The assay procedure was similar to that of colorimetric multiplex detection; the only difference being the addition of HRP-linked secondary antibody instead of an ALP-linked secondary antibody. After the completion of the assay, the chemiluminescent substrate was added and the device was scanned after 2 min with a spectrophotometer at 425 nm.

5.2.9 Chemiluminescence anti-interference test

To demonstrate that the chemiluminescent detection assay in the hybrid device has a high anti-interference capability, the anti-interference assay was performed in various columns of the hybrid device, similar to the colorimetric assay as described in Section 5.2.6. Instead of ALP-linked secondary antibody, HRP linked-secondary antibody was added. The device was scanned by a spectrophotometer, 2 min after the addition of the chemiluminescent substrate.

5.2.10 Rapid chemiluminescent detection of HBsAg & HCVcAg in human serum

All the previous assays in this chapter were performed in the hybrid microfluidic microplate with pure protein in PBS. However, for the validation of the reliability of the proposed chemiluminescence assay, the detection of the biomarkers was performed in normal human serum samples. The feasibility of the assay was tested by spiking different concentrations of HBsAg and HCVcAg in normal human serum samples as the biomarkers for HBV and HCV, respectively. The human serum samples were diluted 3 folds using PBS. 10 μL of different

concentrations of HBsAg were spiked in 990 μL of the diluted human serum to get the final concentrations of 3.4 ng/mL, 34 ng/mL, 0.34 μg/mL, 3.4 μg/mL, and 34 μg/mL, respectively. Similarly, 10 μL of different concentrations of HCVcAg were spiked in 990 μL of the diluted human serum to get the final concentrations of 0.1 ng/mL, 1 ng/mL, 10 ng/mL, 100 ng/mL, and 1μg/mL, respectively. The hybrid microfluidic microplate was used for the rapid chemiluminescence detection following similar procedure and incubation time as mentioned in Section 5.2.7. After the assay, chemiluminescence intensity was measured and the spiked recoveries were calculated for each samples.

5.3 Results and discussion

5.3.1 Cross-contamination test

After the assembly of the hybrid microfluidic microplate, cross-contamination test was performed, as microwells were connected through channels at the bottom layer. For the cross-contaminations test, fluorescein isothiocyanate (FITC) was added to alternate columns of the device, while Milli Q water was added in the adjacent columns. As seen from the fluorescent image (Figure 5.3), the high fluorescent intensity was only observed in the alternate column (a, c, e, and g) where FITC was added; there was no fluorescence in adjacent columns (b, d, f, and h). The result shows that there was no cross contamination or leakage within different columns. To confirm this, different colored dyes were similarly passed into the alternate columns, with water in the adjacent columns. Similar results were obtained with colors showing up only in the alternate columns and clear background in the adjacent columns (Figure 5.1d). This further confirmed that there was no cross-contamination between the adjacent columns.

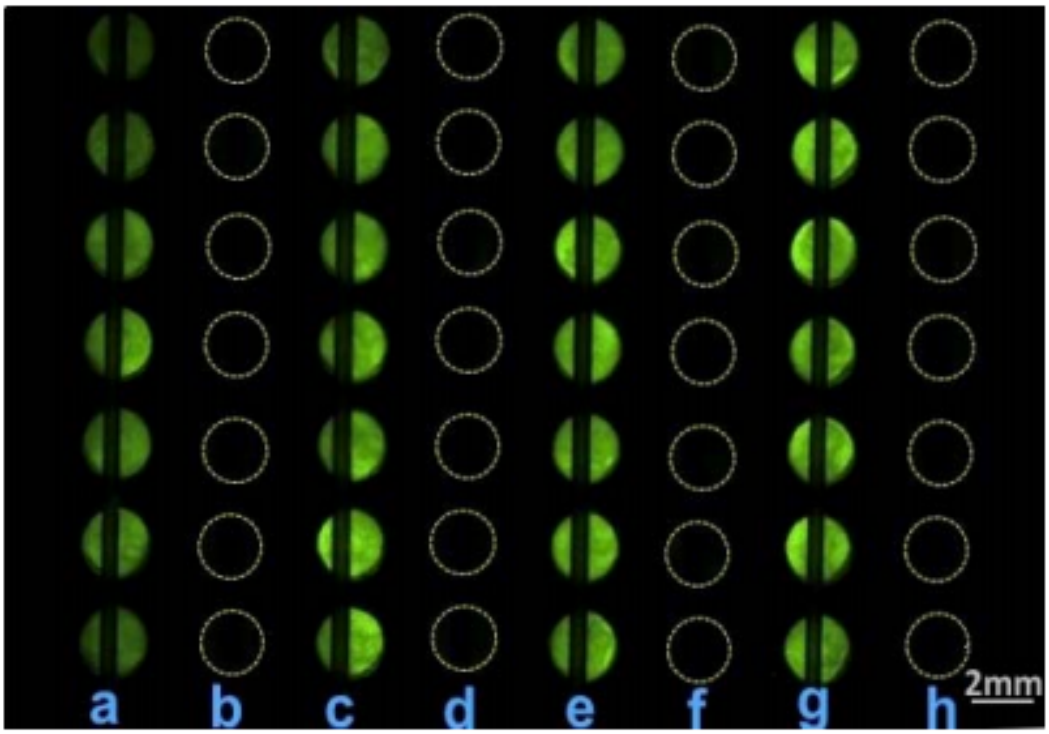

Figure 5.3: Cross contamination/leakage test for the hybrid chip. Fluorescence was observed in columns a, c, e, and g where FITC was added, but not in columns b, d, f, and h, where Milli-Q water was added.

5.3.2 Rapid immobilization of protein

Because of the novel introduction of paper in this hybrid microfluidic microplate, antigen/antibody can be quickly immobilized within 10 minutes as compared to overnight incubation in conventional microplates.[128] Cy3-labeled IgG was used to assess rapid immobilization of antibody on the paper surface. Different concentrations of Cy3-labeled IgG (100, 50, 25, and 12.5 μg/mL) were introduced into alternate columns of the device, and PBS in the adjacent columns for 10 minutes. After washing, from Figure 5.4a, we can see the decreasing intensity of fluorescence in the alternate columns (from left to right), with the decrease in concentration of IgG. There was no fluorescence in the adjacent columns where PBS was added. The assay confirms the rapid immobilization of proteins within 10 min.

Yet, in another experiment, the blocking buffer (4% BSA + 0.05% Tween 20) was added to one column and PBS to another to test the effectiveness of the blocking buffer. After 10

minutes, Cy3-labeled IgG was added to both and incubated for 10 more minutes followed by washing three times with PBST. Figure 5.4b shows that blocking buffer can be used to effectively block the paper surface. Minimal fluorescence can be seen in the column where blocking buffer was added before the addition of Cy3-labeled IgG.

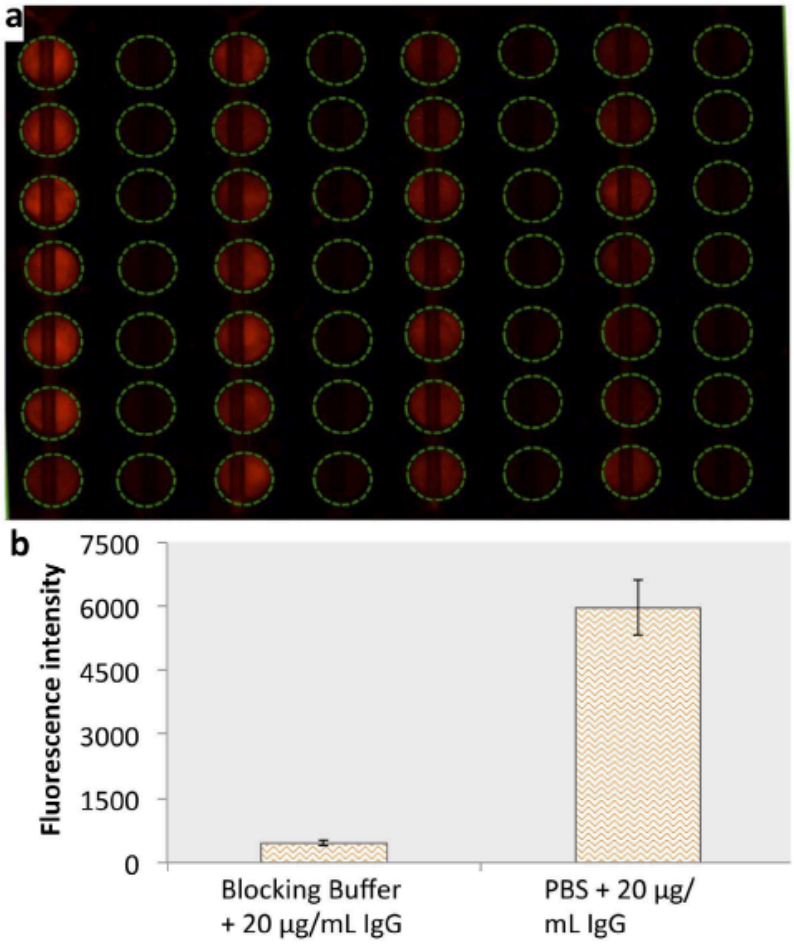

Figure 5.4: Rapid immobilization of antibodies (a) and effectiveness of blocking buffer (b) for ELISA on the hybrid device. (a) Fluorescence image of Cy3-labeled IgG immobilized on the hybrid device. Different concentrations of IgG include; 100 µ g/mL, PBS, 50 µ g/mL, PBS, 25 µ g/mL, PBS, 12.5 µ g/mL, and PBS, respectively, from left to right. (b) The mean fluorescence intensity of 20 µ g/mL of Cy-3 IgG immobilized on the hybrid device with and without the blocking buffer.

5.3.3 Optimization of incubation time for BCIP/NBT

It was observed that once BCIP/NBT was added to the chip, the substrate started to produce an insoluble diformazan end product, which was purple in color and could be observed visually (Figure 5.5). We observed that the lower concentration generated light purple color and

the higher concentration of the analyte produced dark purple color. The color intensity significantly increased to a certain time and then started fading away. To optimize the optimal incubation, on-chip ELISA of IgG (from 1 ng/mL-1 µg/mL) was performed. The chip was scanned every 5 minutes, starting from 10 minutes after the addition of BCIP/NBT. As seen from Figure 5.5, the purple color started fading away after 30 minutes, which led to decrease in corrected brightness value. In addition, lower signal/noise ratios (the noise was derived from the column with PBS only) were observed starting at 30 minutes. Colour intensity of 20-minute incubation was almost similar to that of 25-minute incubation, but 20-minute incubation had a higher background noise. It can also be noticed that the deviation started increasing slightly after 25 minutes. Therefore, considering the signal/noise ratio, deviation, and the time required, 25 minutes incubation time was considered optimum and was used in subsequent experiments.

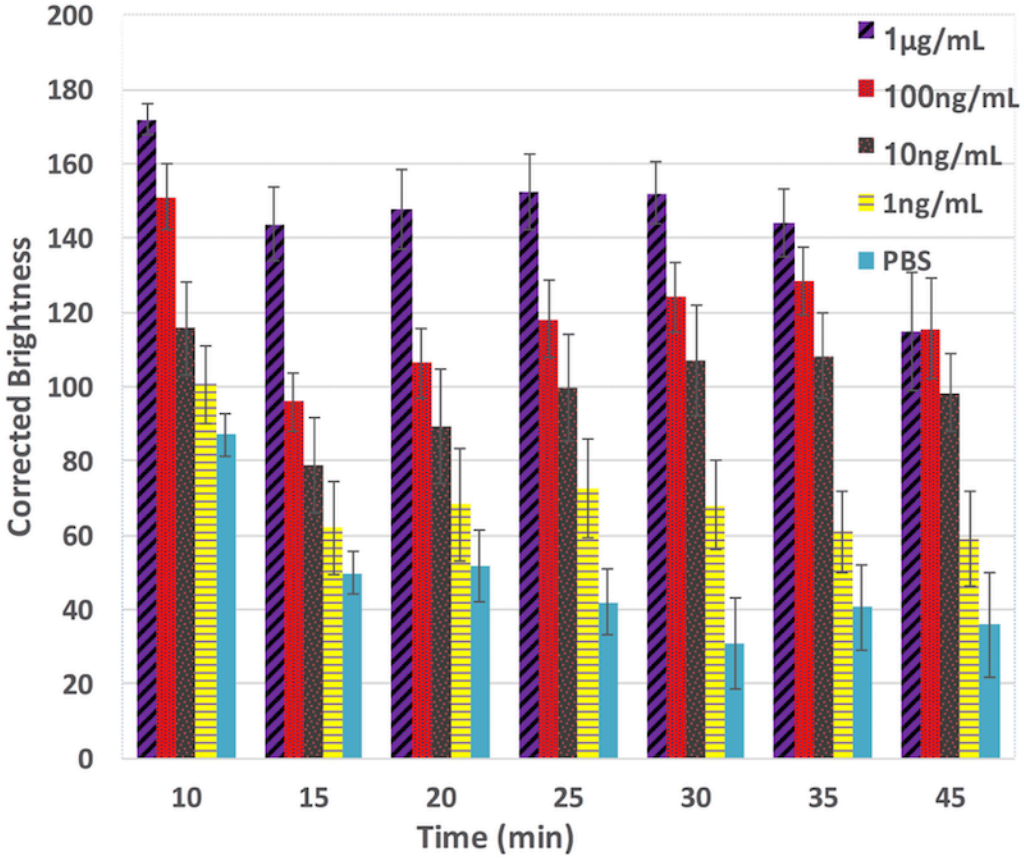

Figure 5.5: Optimization of the incubation time for BCIP/NBT. The graph shows the corrected brightness value of the enzymatically-developed color as measured by ImageJ for different IgG concentrations against the incubation time.

5.3.4 Rapid quantitative detection of IgG

IgG is the most common type of antibody found in the human circulation (75% of serum antibodies). The measurement of IgG can be a diagnostic tool for conditions like autoimmune hepatitis.[186] IgG levels are indicative of the immune status of diseases such as measles, mumps, and rubella (MMR), hepatitis B virus, and varicella.[187] In addition, IgG can serve as a specific marker for Neuromyelitis Optica, an inflammatory demyelinating disease.[188] Thus, we first demonstrated the application of our hybrid microfluidic plate for rapid detection of IgG (0.1 ng/mL-100 μg/mL). For the on-chip ELISA, all reagents were loaded sequentially from the inlets in the upper layer of the PMMA chip, the reagent delivery system. No external power or device was used for the addition of reagents, except a micropipette. After ELISA was completed, the result could be viewed by the naked eye, or a portable office scanner can be used to scan the device. Figure 5.6a shows a scanned image for IgG detection from an office scanner. It was found that the color intensity increased as the IgG concentration increased from 0.1 ng/mL to 100 μg/mL (from right to left) with the blank in the rightmost column. Signal intensities of the scanned images were calculated using ImageJ. Figure 5.6b shows the calibration curve of IgG over a concentration range of 1×10^2 pg/mL to 1×10^8 pg/mL. A sigmoidal curve (Figure 5.6b) was observed over the whole concentration range, while the linearity lies between 1×10^3 pg/mL to 1×10^7 pg/mL (inset Figure 5.6b) with a linear regression of $y = 18.35 \log (x) + 48.74$ ($R^2 = 0.99$), which illustrates a typical immunoassay characteristic.

The LOD for IgG was calculated to be 1.6 ng/mL based on 3 folds of standard deviation (SD) above the blank value, which was comparable to commercial 96-well microplate ELISA (LOD, 1.6-6.25 ng/mL).[154] The conventional 96-well microplate ELISA not only consumes more reagents (50-100 μL), and requires overnight incubation, but also rely on specialized instruments like a microplate reader. However, our method only needs 5 μL samples, and 1 h to complete the whole assay, without using any specialized instruments. As to PMMA devices, they require complicated surface modification with APTES and long incubation time (i.e. 12 hours), and the LOD was only 0.12 μg/mL even with a fluorescence microscope.[109]

Although 96-zone paper-based ELISA did not require surface modification,[128] it required time-consuming repeated micropipetting, making it less user-friendly and incapable of high-throughput detection. Additionally, the LOD of paper-based ELISA was 54 fmol/zone, much higher than that of our hybrid system (53.6 amol/zone), which might be attributed to efficient washing from our hybrid system.

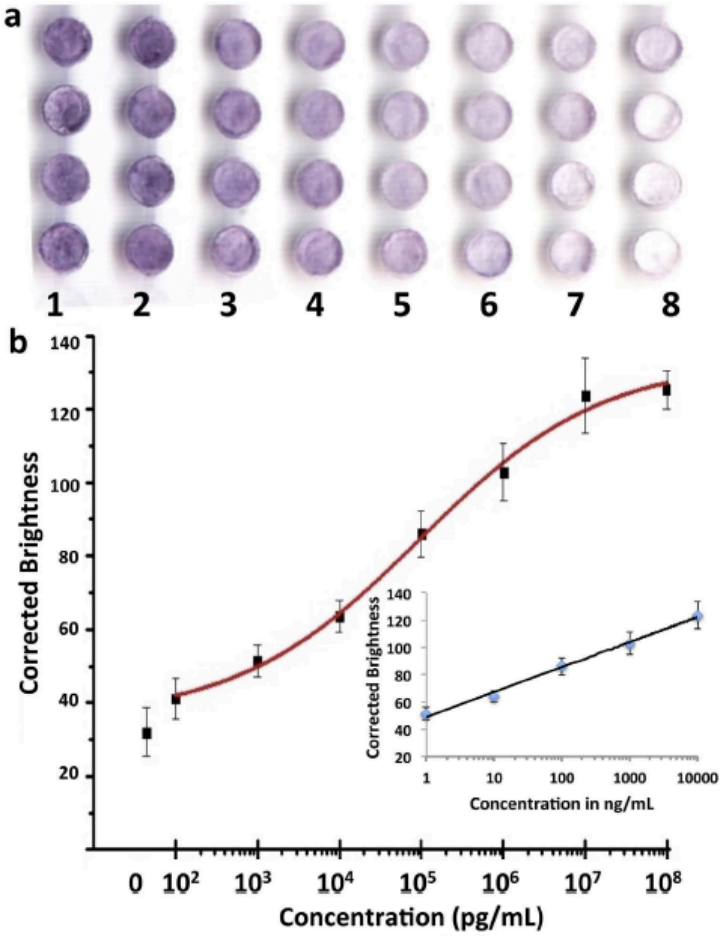

Figure 5.6: Rapid detection of IgG by on-chip ELISA on a hybrid microfluidic microplate. (a) Partial scanned image of the microfluidic microplate with different IgG concentrations by an office scanner: (1) 100 μ g/mL, (2) 10 μ g/mL, (3) 1 μ g/mL, (4) 100 ng/mL, (5) 10 ng/mL, (6) 1 ng/mL, (7) 0.1 ng/mL and (8) 0 ng/mL. (b) The sigmoidal plot of the corrected brightness of microwells versus different IgG concentrations. The inset shows the calibration curve of IgG where the range of linearity lies between 1 ng/mL to 1×10^4 ng/mL.

5.3.4 Rapid quantitative detection of HBV

HBV infection is a major cause of chronic hepatic damage and of hepatocellular carcinomas worldwide.[17] HBsAg, a serological biomarker for an HBV infection, can diagnose acute and chronic hepatitis B virus.[189-191]

Slightly different from the IgG detection, the ELISA for the detection of HBsAg and HBcAg was based on a sandwich-type immunoassay. As illustrated in the inset of Figure 5.7b, the antigen HBsAg was first immobilized on the paper surface in the hybrid microfluidic microplate, followed with reactions with the primary antibody (i.e. rabbit anti-HBsAg) and the secondary antibody goat anti-rabbit IgG conjugated with ALP. After the formation of the sandwich structure, the enzymatic reaction between ALP and the colorimetric substrate BCIP/NBT produces the purple color, similar to IgG detection. Different concentrations of HBsAg ranging from 0.34 ng/mL to 340 μg/mL were analyzed by the hybrid microfluidic microplate. Figure 5.7a shows a scanned image for HBsAg detection from an office scanner. The purple color intensity increased with increasing concentrations from 0.34 ng/mL to 340 μg/mL (from right to left) with the blank in the rightmost column. Figure 5.7b shows the calibration curve of HBsAg over a concentration range from 3.4×10^2 pg/mL to 3.4×10^8 pg/mL. A sigmoidal curve (Figure 5.7b) was observed over the whole detected concentration range as in IgG. In case of HBsAg, the range of linearity was observed between 3.4×10^2 pg/mL to 3.4×10^7 pg/mL (inset Figure 5.7b) with a linear regression of $y = 17.37 \log (x) + 56.71$ ($R^2 = 0.99$). The LOD for HBsAg was found to be 1.3 ng/mL, comparable to commercial ELISA kits.[192]

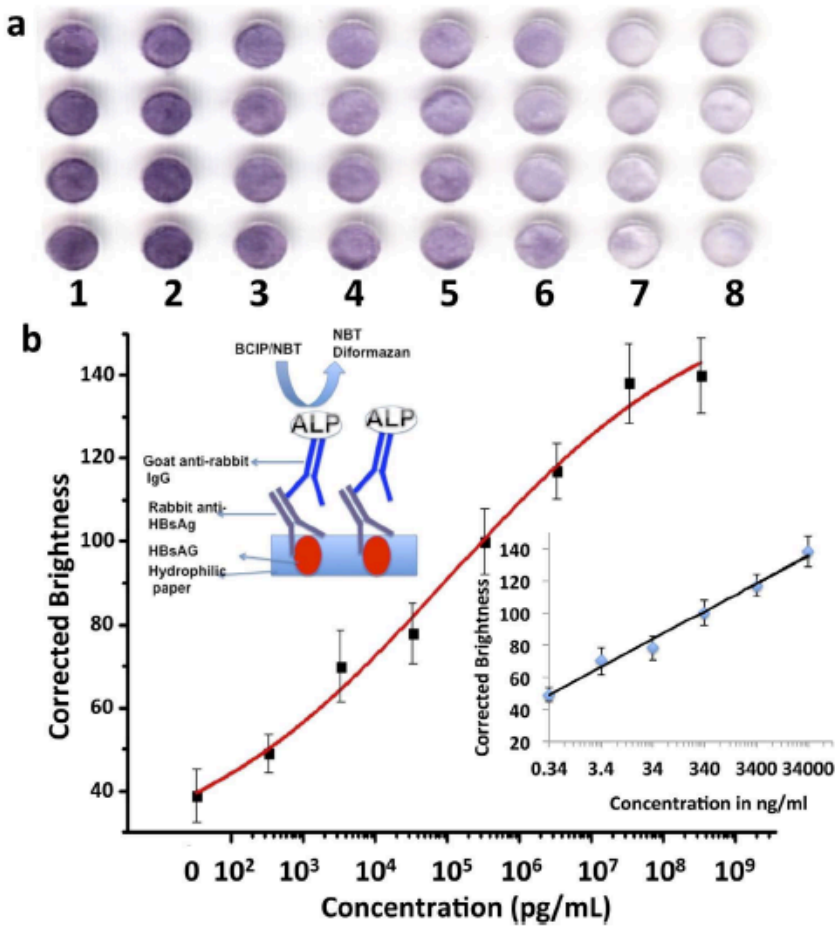

Figure 5.7: Detection of HBsAg by ELISA on a hybrid microfluidic microplate. (a) Partial scanned image of the microfluidic microplate with different HBsAg concentrations by an office scanner: (1) 340 µg/mL, (2) 34 µg/mL, (3) 3.4 µg/mL, (4) 340 ng/mL, (5) 34 ng/mL, (6) 3.4 ng/mL, (7) 0.34 ng/mL, and (8) 0 ng/mL. (b) The sigmoidal curve of the corrected brightness of HBsAg over a concentration range from 3.4×10^2 pg/mL to 3.4×10^8 pg/mL. The upper inset is the schematic of the colorimetric ELISA for detection of HBsAg, where a primary antibody (rabbit anti-HBsAg) and an ALP-conjugated secondary antibody (goat anti-rabbit IgG) are used together to form a sandwich-type immunoassay. The lower inset shows the calibration curve of HBsAg where the range of linearity lies between 0.34 ng/mL to 3.4×10^4 ng/mL.

As seen from Figure 5.8A, ELISA of HBcAg was performed in the hybrid microfluidic microplate with concentrations ranging from 1 ng/mL to 100 µg/mL. As seen from the corrected brightness value from Figure 5.8B, it can be observed that the color intensity increased till 10 µg/mL, after which it started to saturate. The calibration curve of HBcAg was linear over the range of 1 ng/mL to 1×10^4 ng/mL, after which there is a plateau with no more increase in purple

color intensity. The linear regression of y = 10.36 log (x) + 29.32 (R^2 = 0.98) was observed with the LOD of 1.1 ng/mL, comparable to commercial ELISA kits.[192]

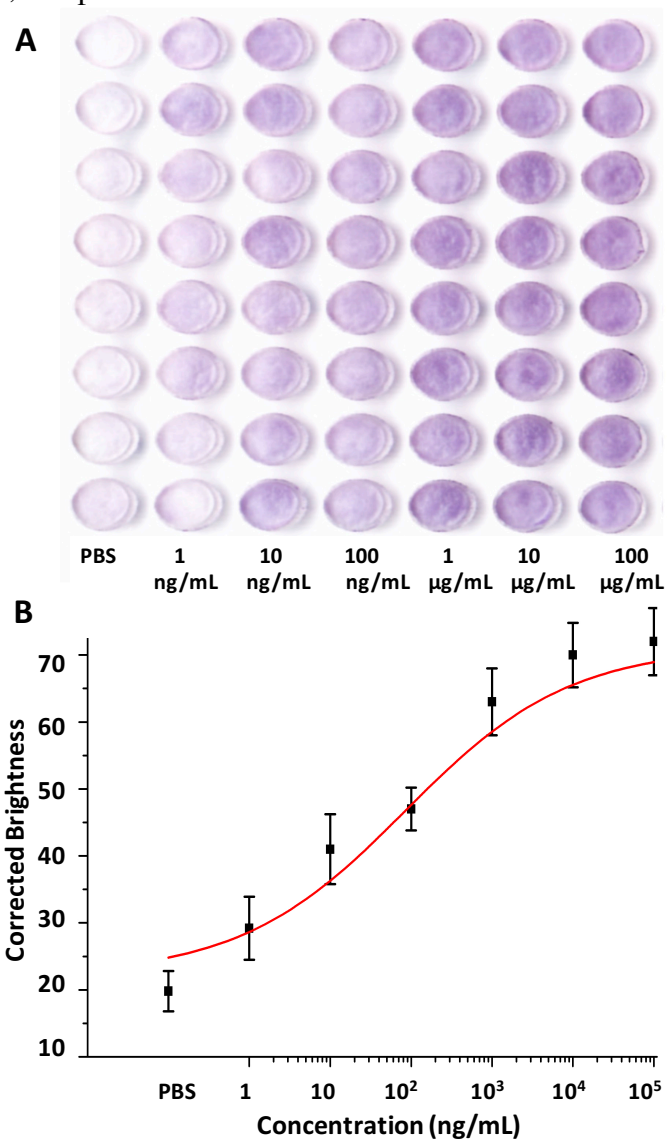

Figure 5.8: Detection of HBcAg in a hybrid microfluidic microplate. (A) Scanned image of the microfluidic microplate with different HBcAg concentrations by an office scanner ranging from 1 ng/mL to 100 µg/mL and a negative control (PBS). (B) The sigmoidal curve of the corrected brightness of HBcAg over a concentration range from 1 ng/mL to 10^5 ng/mL.

5.3.5 Rapid quantitative detection of HCVcAg

Different concentrations of HCVcAg ranging from 0.1 ng/mL to 10 µg/mL were analyzed by the hybrid microfluidic microplate for the detection of HCV. Figure 5.9A shows a scanned image for HCVcAg detection from an office scanner. The figure clearly shows that the purple color

intensity increased with increased concentrations of HCVcAg from 0.1 ng/mL to 10 μg/mL (from left to right) with the blank in the leftmost column. Figure 5.9B shows the calibration curve of HBcAg over a concentration range from 0.1 ng/mL to 1×10^4 ng/mL. A sigmoidal curve (Figure 5.9B) was observed over the whole detected concentration range. No plateau was observed in the color production as the maximum concentration of HCVcAg was only 10 μg/mL and the range of linearity was observed between 0.1 ng/mL to 10 μg/mL with a linear regression of $y = 11.24 \log (x) + 41.76$ ($R^2 = 0.98$). The LOD of HCVcAg was found to be 0.8 ng/mL. The sensitivity of the hybrid device was comparable to commercial ELISA kits[192] and slightly better than nano-composite modified electrochemical immunosensor (LOD of 1 ng/mL).[193]

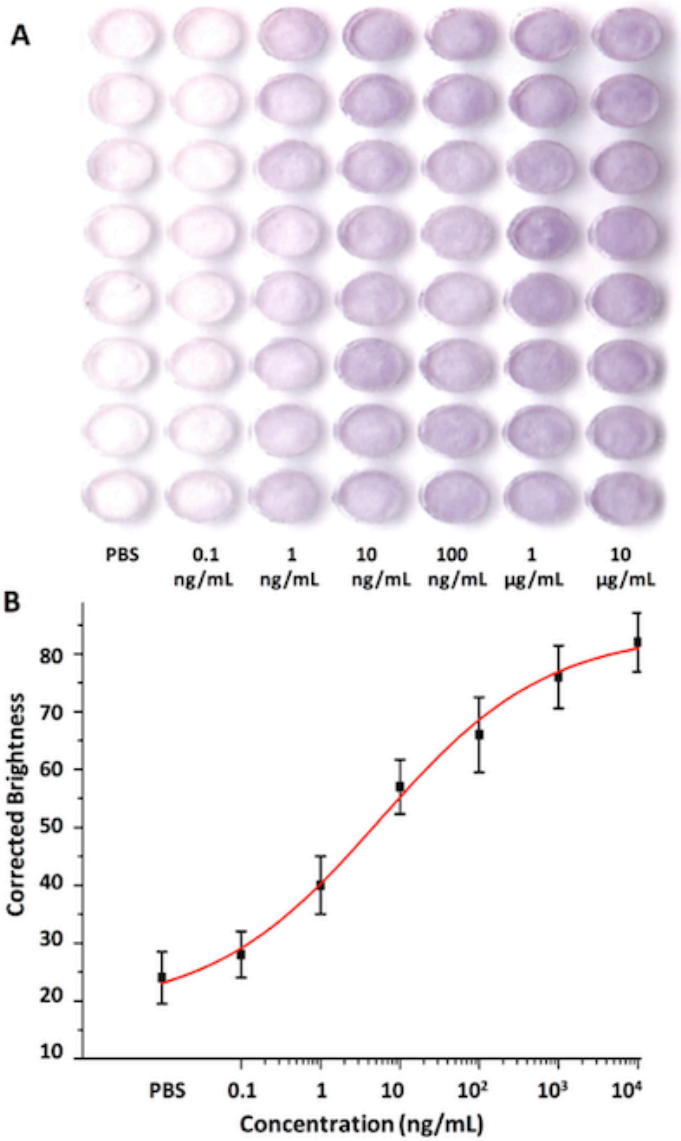

Figure 5.9: Colorimetric detection of HCVcAg in a paper/PMMA hybrid microfluidic microplate. (A) Scanned image of enzymatic converted substrate in different columns of the chip with concentrations from left to right: blank (PBS), 0.1 ng/mL, 1 ng/mL, 10 ng/mL, 100 ng/mL, 1 µg/mL, and 10 µg/mL respectively. (B) The sigmoidal curve of the corrected brightness of HBcAg over a concentration range of 0.1 ng/mL to 10^4 ng/mL.

5.3.6 Colorimetric Multiplex detection of HBsAg and HBcAg in the hybrid device

For the demonstration of the efficiency of multiplex detection of various biomarkers in the hybrid microfluidic platform, simultaneous colorimetric detection of biomarkers of hepatitis B virus i.e., HBsAg and HBcAg were performed. As we observed from Figure 5.10A, there was no color development in the first column as it was negative control (PBS) without any antigen. Second and fifth columns developed color as they had respective antibody for the capture

antigen, but third and fourth columns didn't develop color as they didn't have the respective antibody against the capture antigen. This assay also showed high specificity for anti-HBsAg and anti-HBcAg as they could only bind to their respective antigen. All the last three columns (sixth, seventh, and eighth) developed color as they had both the capture antigen i.e., HBsAg and HBcAg. Figure 5.10B shows the bar graph for the corrected brightness for different columns of the hybrid microfluidic microplate.

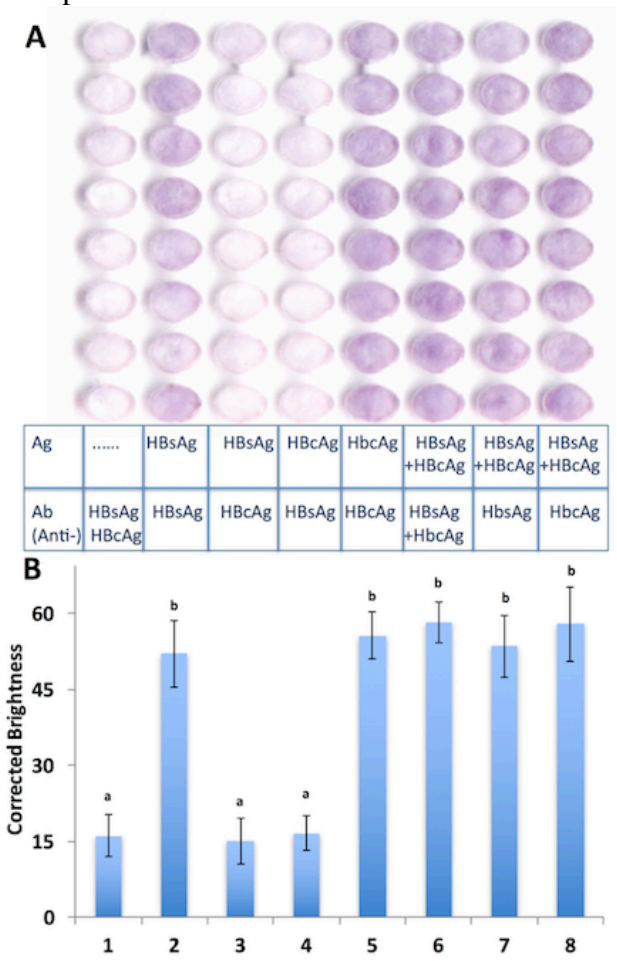

Figure 5.10: Colorimetric multiplex assay of HBsAg and HBcAg on a paper/PMMA hybrid microfluidic microplate. Scanned image of the enzyme-catalyzed substrate, (A) and bar plot of the corrected brightness of the scanned image (B). From left to right: immobilized probe, none (1), HBsAg (2) and (3), HBcAg (4) and (5), and HBsAg + HBcAg (6), (7), and (8), respectively. Test: From left to right, solution containing, anti-HBsAg and anti-HBcAg (1) and (6), HBsAg (2), (4), and (7), and HBcAg (3), (5), and (8). "a" and "b" shows that the data are significantly different from each other at $p = 0.05$.

5.3.7 Colorimetric anti-interference test of HBsAg in the hybrid device

The anti-interference assay showed that there was no interference or cross-reaction of the target protein with other proteins and biomolecules present in the matrix. Figure 5.11 shows the detection of 200 ng/mL of HBsAg with and without various concentrations of interfering proteins (HBcAg, CEA, BSA, and PSA). There was no production of purple color in the first four columns from the left as anti-HBsAg did not bind with any of the interfering proteins (1 μg/mL HBcAg in the first column, 100 ng/mL CEA in the second column, 250 μg/mL BSA in the third column, and 10 ng/mL PSA in the fourth column). As seen from Figure 5.11B, the color intensity for the detection of 200 ng/mL of HBsAg in the presence of different interfering proteins (column 5, 6, and 7) was similar to the detection of 200 ng/mL of HBsAg without the interfering proteins (column 8). It demonstrated that even 1,250 times concentrated interfering proteins did not influence the specific detection of HBsAg in the hybrid microfluidic microplate.

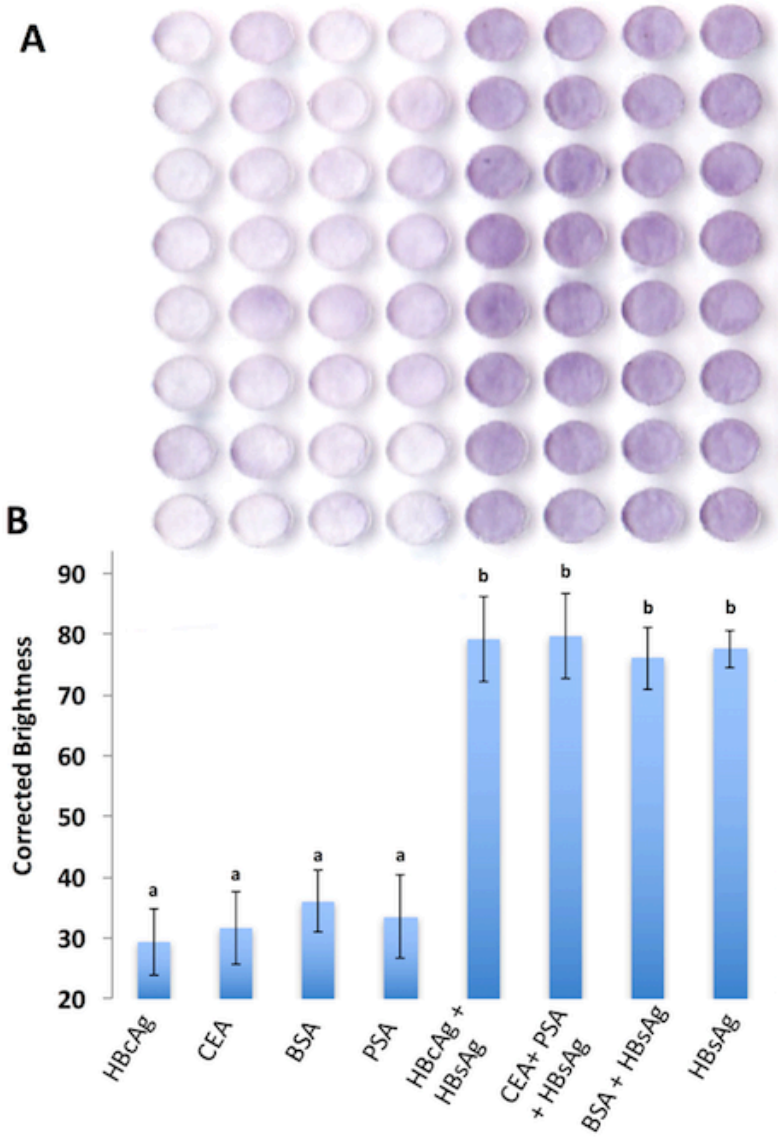

Figure 5.11: Colorimetric anti-interference test for the detection of HBsAg in a paper/PMMA hybrid microfluidic microplate. The scanned image of the chip (A) and the corrected brightness of the scanned image of ELISA in the hybrid device (B) for the detection of HBsAg. The left four columns are for detection of 0 ng/mL of HBsAg in the solution containing 1μg/mL HBcAg (1), 100 ng/mL CEA (2), 250 μg/mL BSA (3), and 10 ng/mL PSA (4), respectively. The right four columns are for the detection of 200 ng/mL of HBsAg in 1μg/mL HBcAg (5), 100 ng/mL CEA + 10 ng/mL PSA (6), 250 μg/mL BSA (7), and PBS (8), respectively. "a" and "b" shows that the data are significantly different from each other at $p = 0.05$.

5.3.8 Rapid quantitative detection of HBsAg in human serum samples

To validate the analytical accuracy and to determine its feasibility for detection of real human samples of HBV, normal human serum was spiked with different concentrations of standard HBsAg. Four different concentrations of HBsAg (3.4 ng/mL, 34 ng/mL, 0.34 μg/mL,

and 3.4 µg/mL) within the range of linearity and above the LOD were chosen for spiking and recovery tests. As can be seen from Table 5.1, the intensity of purple color increased from lower concentrations to higher concentrations of the spiked human serum samples, consistent with ELISA results using standard HBsAg (Figure 5.7). The analytical recoveries of the serum samples ranging from 91.1-109.1 % were obtained and were within the acceptable criteria for bio-analytical validation.[194, 195]

Table 5.1: Detection of HBsAg spiked in human serum sample by colorimetric ELISA on a hybrid microfluidic microplate.

Serum Sample Number	Serum HBsAg concentration	Color changes	Measured Values	Recovery (%)
Control	0	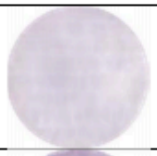		
No.1	3.4 ng/mL		3.71 ng/mL	109.1
No.2	34 ng/mL		36.45 ng/mL	107.2
No.3	0.34 µg/mL	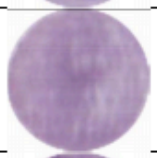	0.31 µg/mL	91.1
No.4	3.4 µg/mL		3.17 µg/mL	93.2

5.3.9 Chemiluminescence ELISA on the hybrid microfluidic microplate

For the device to be used in high-end laboratories and hospitals, the hybrid device was redesigned to make it compatible with traditional microplate readers (Figure 5.12). The microwells in the hybrid device were designed according to the dimensions of the standard 384

well plates as discussed in Section 3.2.2. Chemiluminescence ELISA of IgG, HBV, and HCV was performed in the hybrid device. Once the chemiluminescence substrate for ELISA was added to the chip, the chip was incubated for two minutes. The chip was then scanned using microplate reader M3 (Molecular Devices, San Jose, CA). Since the dimensions of the chip were similar to the 384-wells microplate, the desired area of scanning was chosen from the standard 384-wells microplate. The chemiluminescence intensity of SuperSignal® ELISA Pico Chemiluminescent substrate was measured at 425 nm to draw the calibration curve.

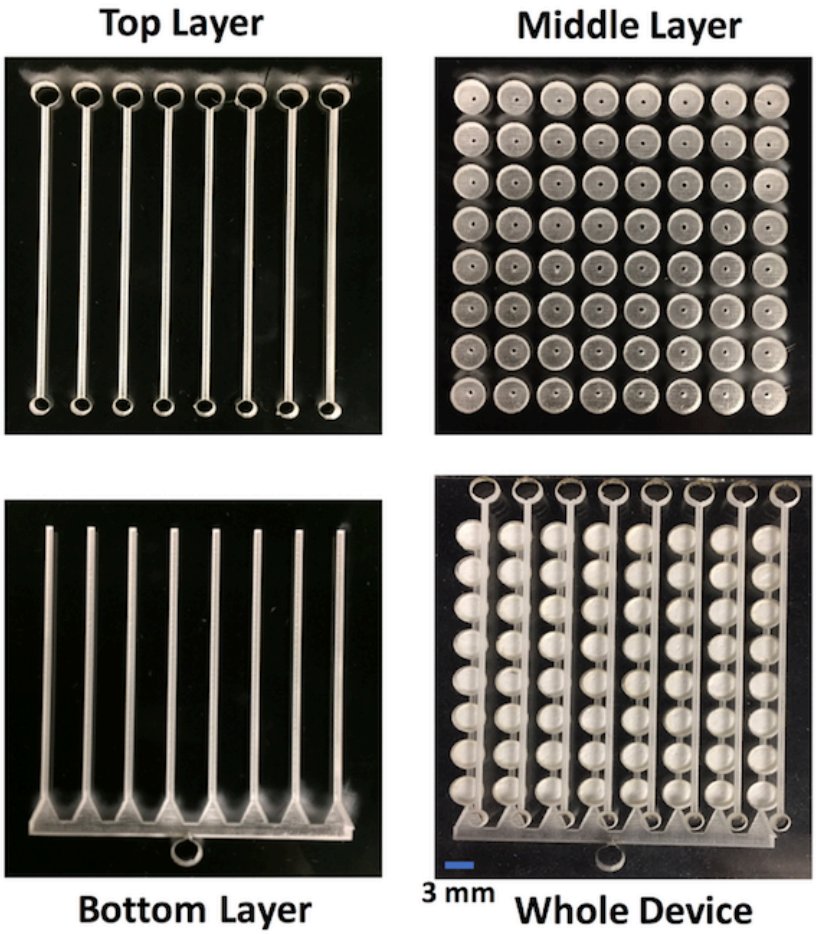

Figure 5.12: Photographs of the PMMA/paper hybrid microfluidic microplate consisting of three different layers. The top layer for fluid delivery consists of inlet reservoirs and fluid distribution channels. The middle layer consists of 64 funnel-shaped microwells where paper disks can be inserted. The lowermost layer for fluid removal consists of outlet channels which lead to a common outlet reservoir.

5.3.10 Optimization of incubation time for chemiluminescence substrate

Once the chemiluminescence substrate was added to the hybrid device, after washing the device three times with PBST following the addition of enzyme-linked secondary antibody, chemiluminescence was measured. To optimize the incubation time of the substrate to get the maximum signal, kinetic ELISAs were performed for 30 min after the addition of the substrate and reading was taken every 30 seconds. Chemiluminescence signal was measured using a microplate reader after the completion of the assay. On-chip ELISA was performed at three different concentrations, 1 ng/mL, 1 μg/mL, and 100 μg/mL of IgG along with the negative control. As we can see from Figure 5.13 the chemiluminescence intensity increased until 2 min for higher concentration (1 μg/mL and 100 μg/mL) and until 2.5 min for lower concentration (1 ng/mL) and then started to decrease rapidly. The increase in chemiluminescence intensity from 2 min to 2.5 min in lower concentration was not significant. The maximum signal to noise (PBS) ratio was also observed at 2 min. Therefore, 2 min was considered as the optimum time for the incubation of chemiluminescence substrate and reading was taken at 2 min after the addition of the substrate.

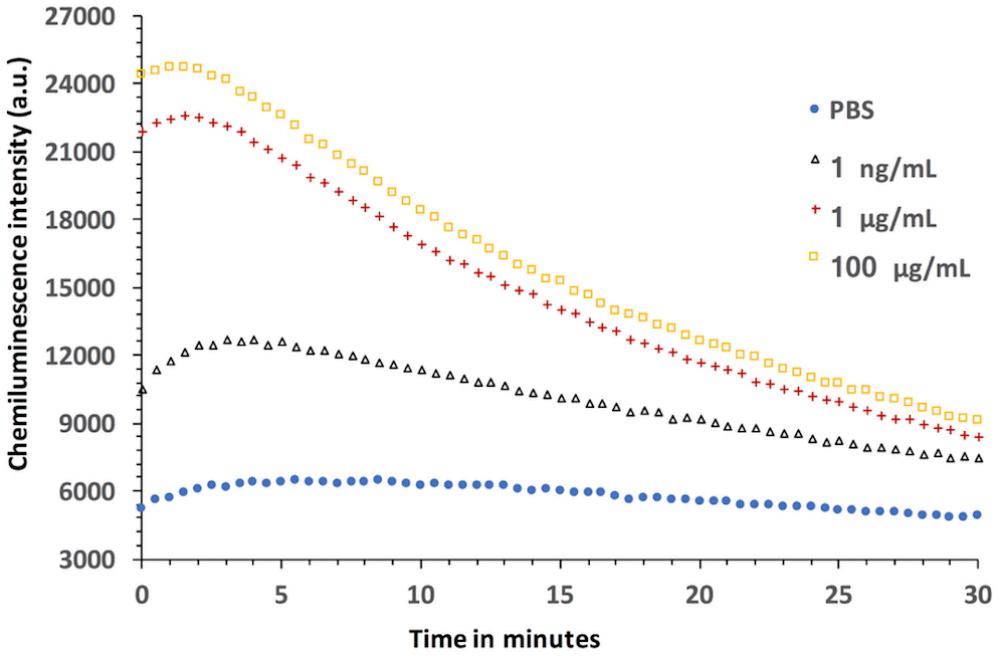

Figure 5.13: Optimization of the incubation time for the chemiluminescent substrate (luminol and peroxide). Kinetic chemiluminescence ELISAs of different concentrations of IgG were performed in the hybrid device for 30 min.

5.3.11 Rapid chemiluminescence detection of IgG

For the on-chip chemiluminescence ELISA of IgG in the hybrid microfluidic microplate, all the reagents were loaded sequentially from the inlets in the upper layer of the hybrid device. The reagents flowed through all the wells in the middle layer avoiding the manual pipetting to all the wells. After ELISA was completed, the device was scanned using a microplate reader at 425 nm. Figure 5.14A shows the fitted sigmoidal curve for on-chip chemiluminescence detection of IgG as chemiluminescence intensity versus the concentration of IgG. It can be seen from Figure 5.14A that the chemiluminescence intensity increased rapidly until the concentration reached 10^3 ng/mL, after which the intensity got saturated. Figure 5.14B shows the assay had a very wide linear range of detection ranging from 0.01 ng/mL to 1×10^3 ng/mL with a linear regression of $y = 2389.4 \log (x) + 11722$ ($R^2 = 0.99$). The LOD of IgG was found to be 20 pg/mL. The assay was found to be 80-fold more sensitive as compared to our hybrid colorimetric device (LOD, 1.6 ng/mL) and 100-fold more sensitive than traditional microplate ELISA.[5] Our device also has a better sensitivity as compared to APTES modified PMMA (0.12 µg/mL),[109] the paper-based

device (54 f/mol/zone),[128] and poly(ethyleneimine) modified PMMA using fluorescence microscope.[111]

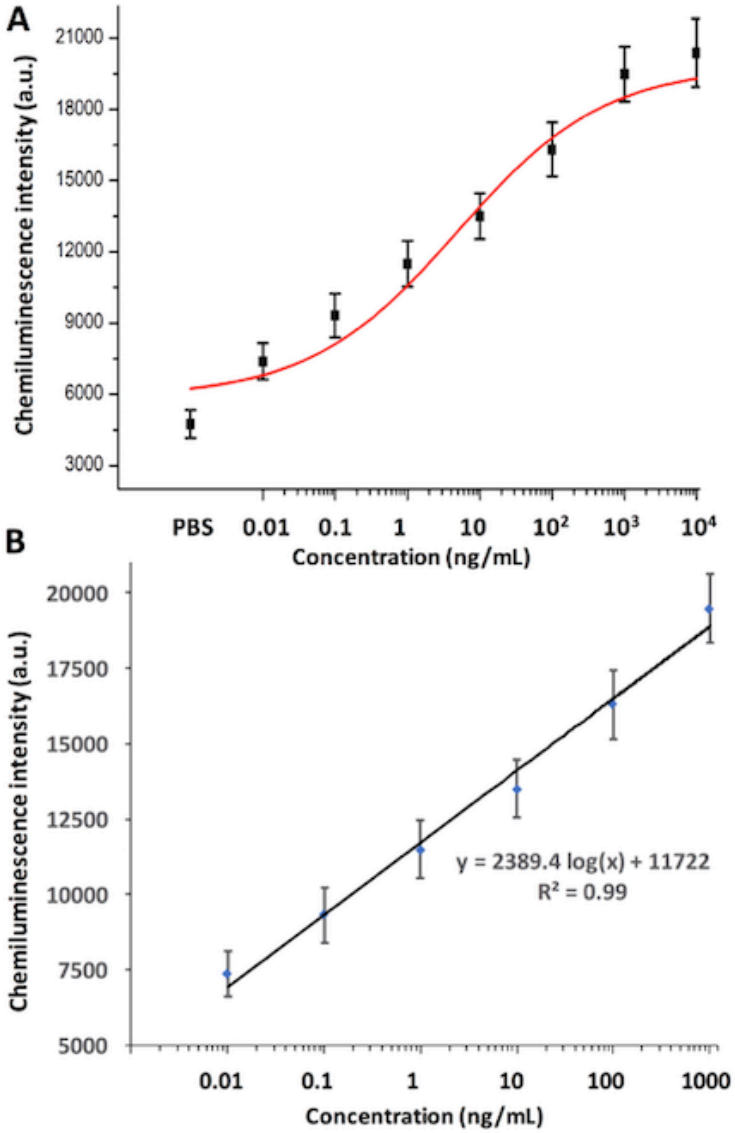

Figure 5.14: Rapid chemiluminescence detection of IgG in the hybrid microfluidic microplate. (A) The fitted sigmoidal curve of the chemiluminescence intensity over a concentration range from 0.01 ng/mL to 10^4 ng/mL and a negative control (PBS). (B) Calibration plot of IgG where the range of linearity lies between 0.01 ng/mL to 1000 ng/mL.

5.3.12 Rapid chemiluminescence detection of HBsAg

Similar to on-chip chemiluminescence ELISA of IgG, chemiluminescence ELISA of HBsAg was also performed in the hybrid microfluidic microplate. As we could observe from Figure 5.15, chemiluminescence intensity of HBsAg increased with the increase in the

concentration of HBsAg from 0.034 ng/mL to 3.4×10^4 ng/mL. Figure 5.15A shows the sigmoidal fitted curve for the detection of HBsAg with chemiluminescence intensity against the concentration of HBsAg. Figure 5.15B showed that the assay had very wide linear range of detection ranging from 3.4×10^1 pg/mL to 3.4×10^7 pg/mL with a linear regression of $y = 2415.8 \log (x) + 10492$ ($R^2 = 0.98$). The LOD of HBsAg was found to be 50 pg/mL. The chemiluminescence hybrid device was more sensitive than commercial ELISA kits, HBsAg assay by Yazdani *et al*. (LOD of 0.7 ng/mL), and our previous colorimetric hybrid device with LOD of 1.3 ng/mL.[5, 160] Our device had better sensitivity than the device by Xu *et al*. (LOD of 0.1 ng/mL), which required experiment in class-100 clean room,[139] capillary chemiluminescence with a sensitivity of 0.3 ng/mL, and copper oxide nanoparticles and nanocomposite-based chemiluminescence assay (LOD of 1.8 and 0.85 ng/mL).[196, 197] The sensitivity was comparable to gold nanoparticle-based chemiluminescence detection of HBsAg with LOD of 14 pg/mL.[198]

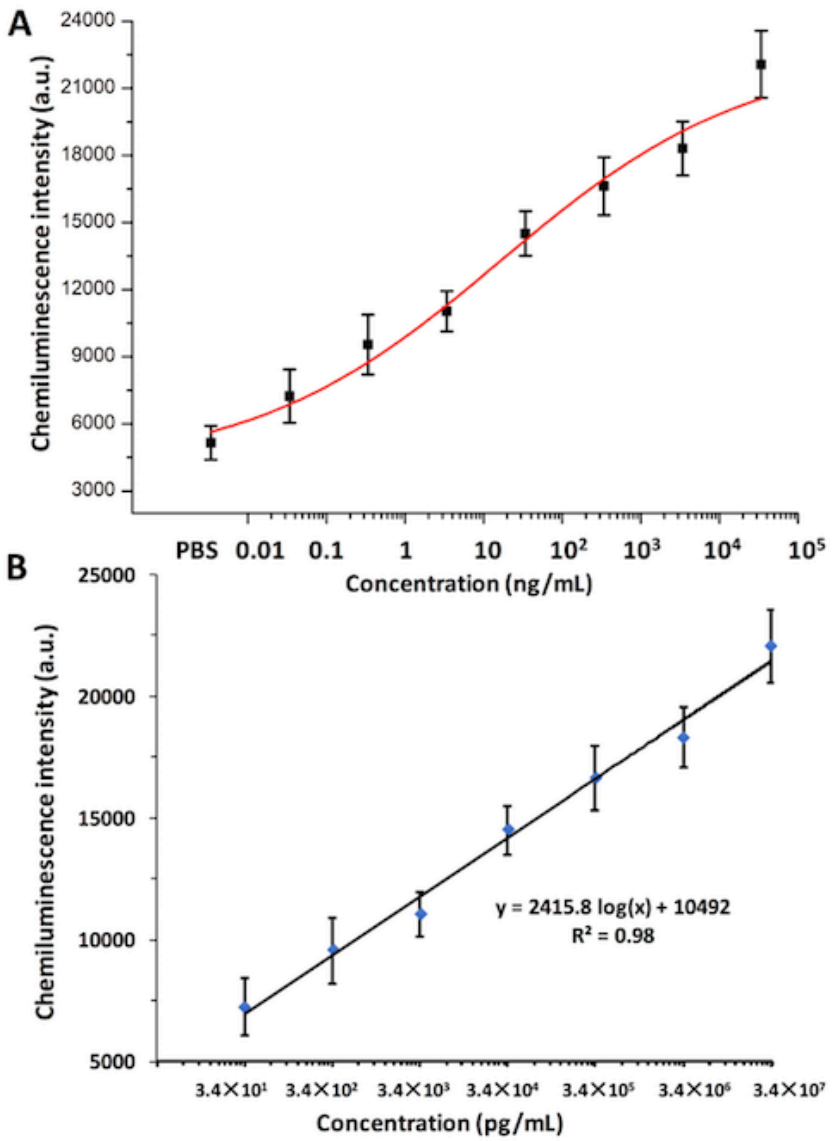

Figure 5.15: Rapid chemiluminescence detection of HBsAg in the hybrid microfluidic microplate. (A) The fitted sigmoidal curve of the chemiluminescence intensity over a concentration range from 0.034 ng/mL to 34 × 10^4 ng/mL and a negative control (PBS). (B) Calibration plot of HBsAg where the range of linearity lies between 3.4 × 10^1 pg/mL to 3.4 × 10^7 pg/mL.

5.3.13 Rapid chemiluminescence detection of HBcAg

On-chip chemiluminescence ELISA of HBcAg was performed similar to the ELISA of IgG and HBsAg in the hybrid microfluidic microplate. Figure 5.16A shows that chemiluminescence intensity of HBcAg increased with the increase in the concentration of HBcAg from 0.01 ng/mL to 10^3 ng/mL. There was no significant increase in the intensity from

10^3 ng/mL to 10^4 ng/mL, which may indicate that the chemiluminescence intensity was getting saturated. As seen in Figure 5.16A chemiluminescence intensity against the concentration of HBcAg gave a sigmoidal fitted curve over the whole range of concentrations. Figure 5.16B shows the assay had very wide linear range of detection ranging from 0.01 ng/mL to 1×10^4 ng/mL with a linear regression of $y = 2349 \log (x) + 10065$ ($R^2 = 0.98$). The LOD of HBcAg was found to be 35 pg/mL which was similar to chemiluminescence detection of HBsAg.

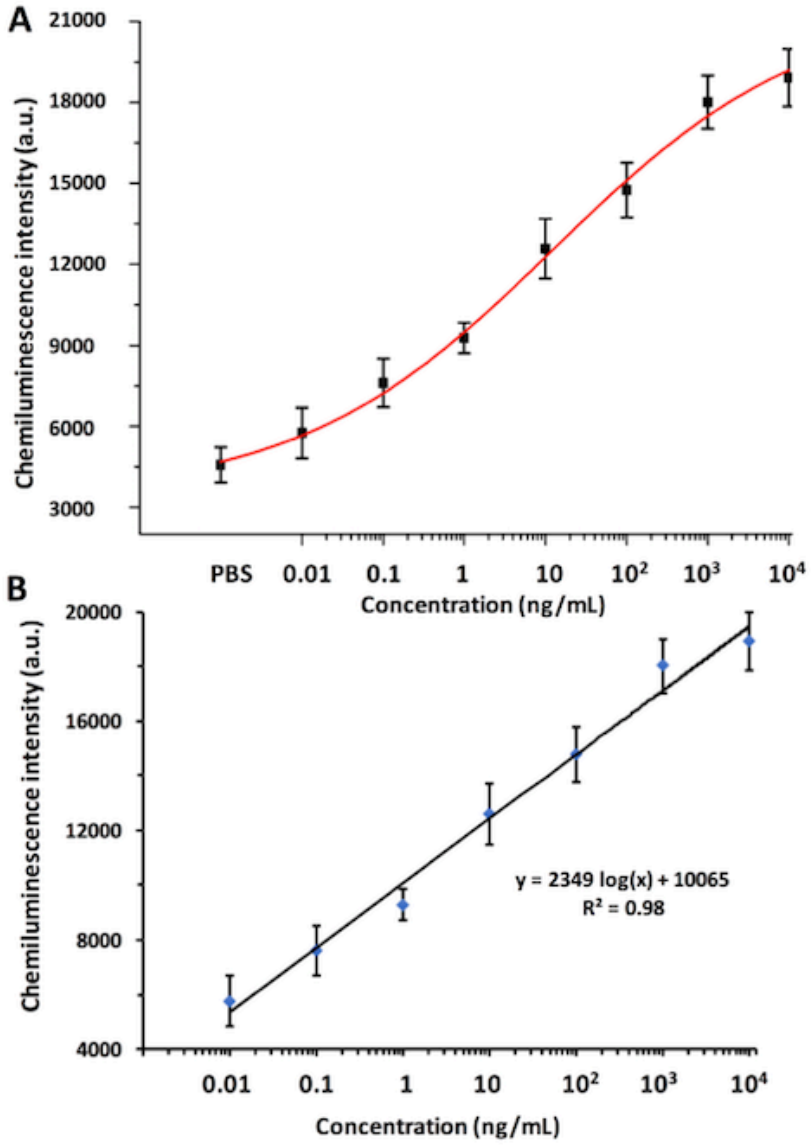

Figure 5.16: Rapid chemiluminescence detection of HBcAg in the hybrid microfluidic microplate. (A) The fitted sigmoidal curve of the chemiluminescence intensity over a

concentration range from 0.01 ng/mL to 10^4 ng/mL and a negative control (PBS). (B) Calibration plot of HBcAg where the range of linearity lies between 0.01 ng/mL to 10^4 ng/mL.

5.3.14 Rapid chemiluminescence detection of HCVcAg

Infection by hepatitis B and C virus cause acute and chronic liver disease and they can coexist and result in fulminant hepatitis and HCC.[199] Both the viruses are the causal agents for a chronic liver infection. Therefore, after the completion of on-chip chemiluminescence ELISA for the detection of HBV (HBsAg and HBcAg), detection of HCV was carried out using HCVcAg. For the detection of HCVcAg, samples ranging from 10^4 ng/mL to 0.01 ng/mL were taken. Figure 5.17 shows that there was minimum chemiluminescence intensity for the negative control (PBS) and the chemiluminescence intensity of HCVcAg escalated with the increase in the concentration of HCVcAg from 0.01 ng/mL to 10^3 ng/mL, after which a plateau can be observed, indicating saturation of the chemiluminescence intensity. Chemiluminescence intensity against the concentration of HCVcAg gave a sigmoidal fitted curve as seen in Figure 5.17A. Figure 5.17B shows that the assay had a wide linear range of detection ranging from 0.01 ng/mL to 1×10^4 ng/mL with a linear regression of $y = 2075.5 \log (x) + 11569$ ($R^2 = 0.99$). The LOD of HCVcAg was found to be 10 pg/mL. The device was found to be more sensitive than the label-free immunosensor for HCVcAg detection (LOD of 0.17 ng/mL), nano-composite modified electrochemical immunosensor (LOD of 1 ng/mL).[193, 200] The LOD was comparable to gold nanoparticle-enhanced microwell plate-based ELISA of HCV antibody with LOD of 122 pg/mL.[201]

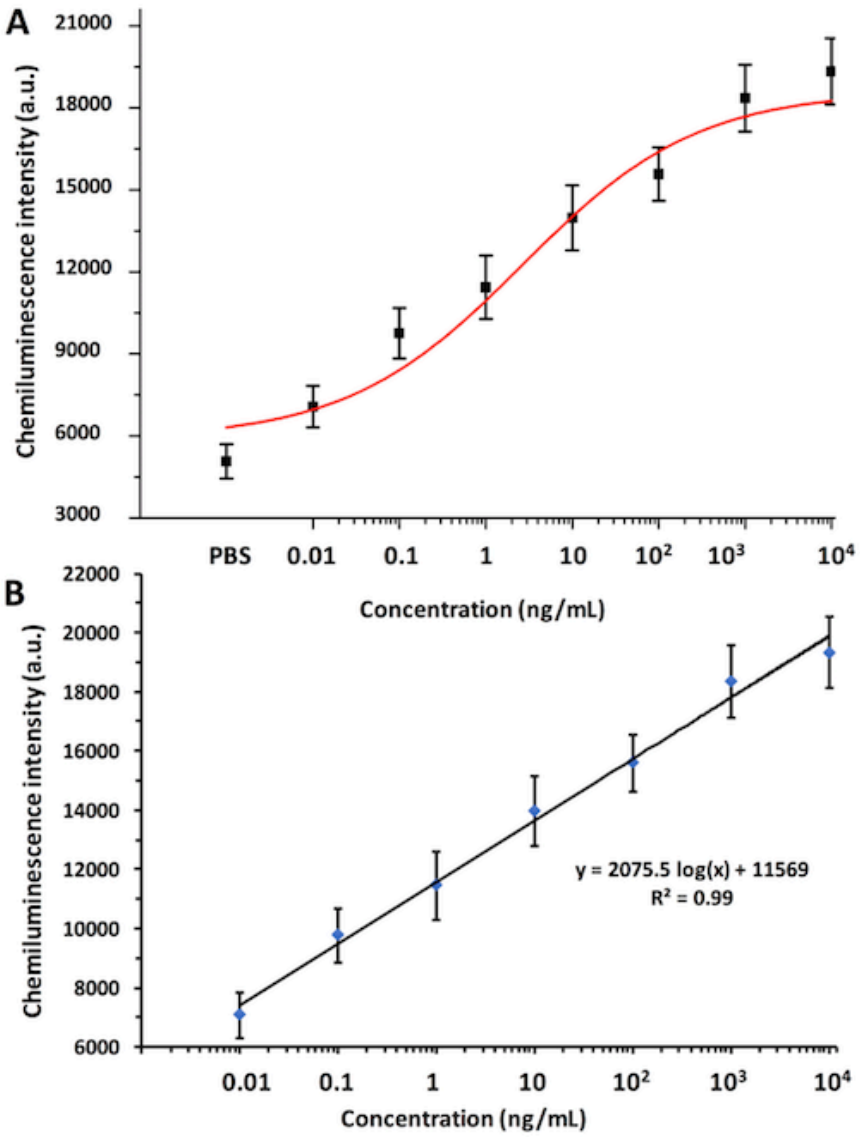

Figure 5.17: Rapid chemiluminescence detection of HCVcAg in the hybrid microfluidic microplate. (A) The fitted sigmoidal curve of the chemiluminescence intensity over a concentration range from 0.01 ng/mL to 10^4 ng/mL and a negative control (PBS). (B) Calibration plot of HCVcAg where the range of linearity lies between 0.01 ng/mL to 10^4 ng/mL.

5.3.15 Multiplex chemiluminescence detection of HBcAg and HBsAg

Similar to the colorimetric multiplex assay, simultaneous chemiluminescence detection of HBsAg and HBcAg was performed in the hybrid microfluidic platform. As we could observe from Figure 5.18, there was minimum chemiluminescence intensity in the first column as it was negative control (PBS) without any antigen. The second and fifth columns showed high chemiluminescence intensity as they had respective antibody for the capture antigen but third

and fourth columns showed minimum chemiluminescence intensity as they didn't have the respective antibody against the capture antigen. Last three columns (sixth, seventh, and eighth) had high chemiluminescence intensity as they had both the capture antigen i.e., HBsAg and HBcAg. The assay shows that multiple biomarkers can be detected at a same time in the hybrid device. The device has a potential to detect eight different biomarkers in eight columns of the hybrid chip.

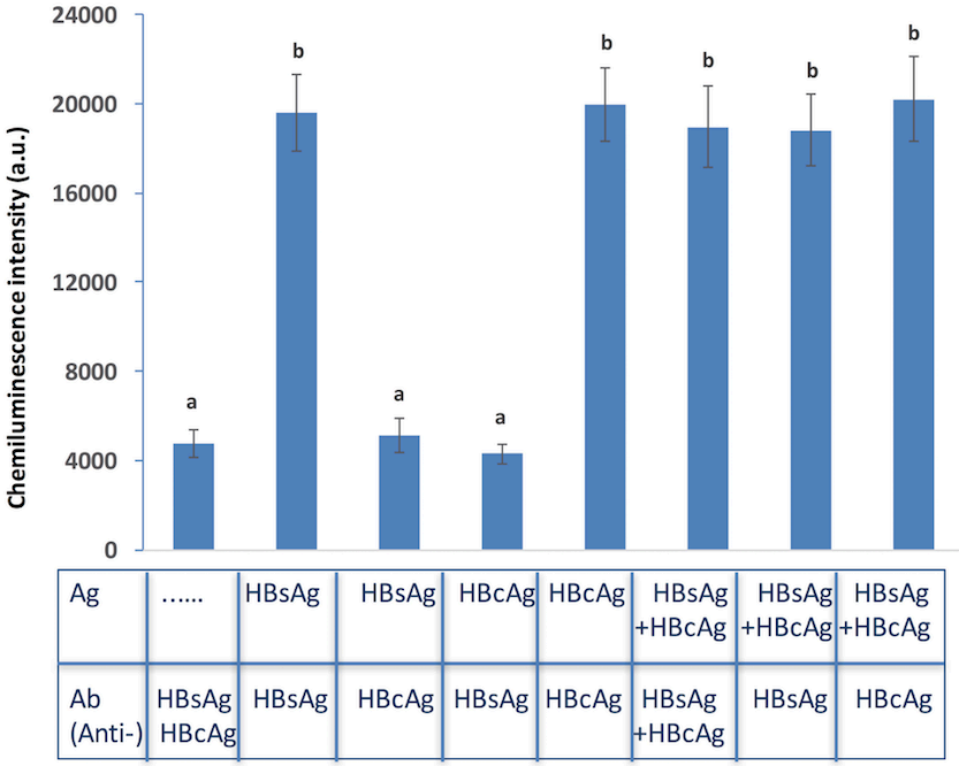

Figure 5.18: Multiplex chemiluminescence assay of HBsAg and HBcAg in a paper/PMMA hybrid microfluidic microplate. From left to right: immobilized probe, none (1st), HBsAg (2nd) and (3rd), HBcAg (4th) and (5th), and HBsAg + HBcAg (6th), (7th), and (8th), respectively. Test: From left to right, solution containing, anti-HBsAg and anti-HBcAg (1st) and (6th), HBsAg (2nd), (4th), and (7th), and HBcAg (3rd), (5th), and (8th). "a" and "b" shows that the data are significantly different from each other at $p = 0.05$.

5.3.16 Chemiluminescence anti-interference test for HBsAg

Similar to the colorimetric anti-interference assay, the on-chip chemiluminescence anti-interference assay for HBsAg was performed. The assay procedure was similar to the colorimetric assay except for the secondary antibody (HRP-linked antibody instead of ALP-

linked antibody) and its chemiluminescence substrate along with the scanning method. Figure 5.18 shows that the first four columns are negative controls without any target protein (i.e. HBsAg) and produce minimum chemiluminescence intensity, while the last four columns contain 200 ng/mL of the target protein, HBsAg in the presence of other interfering proteins and produced high chemiluminescence intensity. The chemiluminescence intensity of 200 ng/mL of HBsAg was similar to the intensity of 200 ng/mL of HBsAg with different interfering proteins. Similar to the colorimetric assay, it demonstrated that even 1,250 times concentrated interfering proteins did not influence the specific detection of HBsAg in the hybrid microfluidic microplate.

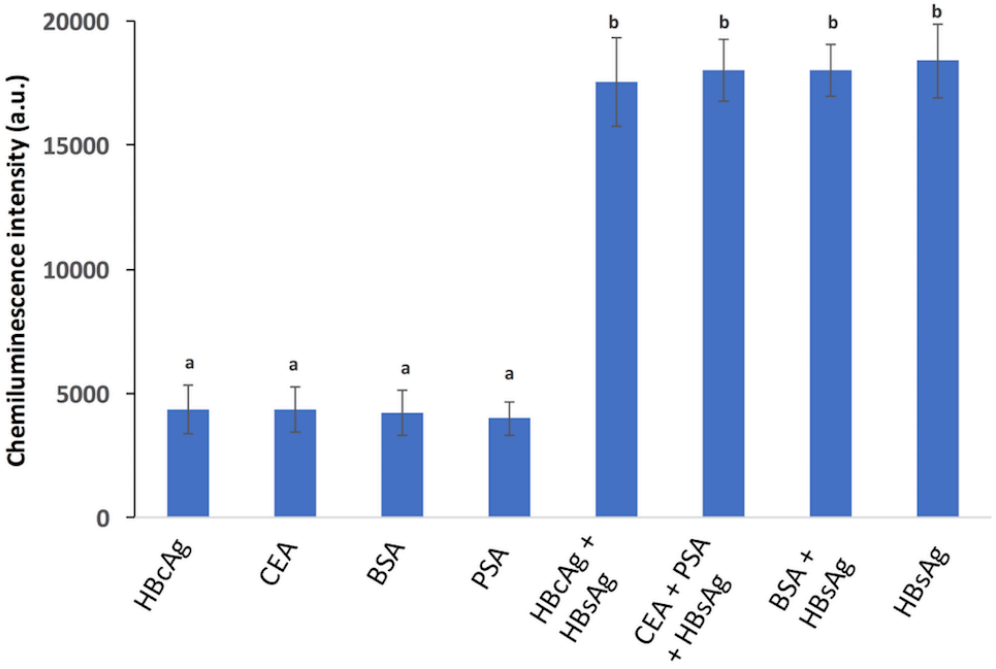

Figure 5.19: Chemiluminescence anti-interference test for the detection of HBsAg on a paper/PMMA hybrid microfluidic microplate. The left four columns: detection of 0 ng/mL of HBsAg in the solution containing 1µg/mL HBcAg (1st), 100 ng/mL CEA (2nd), 250 µg/mL BSA (3rd), and 10 ng/mL PSA (4th), respectively. The right four columns: detection of 200 ng/mL of HBsAg in 1µg/mL HBcAg (5th), 100 ng/mL CEA + 10 ng/mL PSA (6th), 250 µg/mL BSA (7th), and PBS (8th), respectively. "a" and "b" shows that the data are significantly different from each other at $p = 0.05$.

5.3.17 Chemiluminescence detection of HBsAg and HCVcAg in a human serum sample

To determine the feasibility for the detection of the real human sample and to validate the analytical accuracy of the proposed chemiluminescence assay in the hybrid device,

chemiluminescence ELISA of HBsAg and HCVcAg was performed with the human serum sample. For the chemiluminescence assay, normal human serum was first spiked with various concentrations of standard HBsAg and HCVcAg. Five different concentrations of both HBsAg (3.4 ng/mL, 34 ng/mL, 340 ng/mL, 3.4 µg/mL, and 34 µg/mL) and HCVcAg (0.1 ng/mL, 1 ng/mL, 10 ng/mL, 100 ng/mL, and 1 µg/mL) were taken. All the concentrations of HBsAg and HCVcAg chosen for spiking and recovery tests were within the range of linearity and above the LOD. We can see from Table 5.2 that the analytical recoveries of the serum samples obtained ranged from 90.00–109.64 % and were within the acceptable criteria for bio-analytical validation.[194, 195]

Table 5.2: Detection of HBsAg and HCVcAg spiked in human serum sample by chemiluminescence ELISA on a hybrid microfluidic microplate.

Sample Number	Serum type	Spiked serum concentration	Measured values	Recovery (%)
1	HBsAg	3.40 ng/mL	3.72 ng/mL	109.41
2	HBsAg	34 ng/mL	37.14 ng/mL	109.24
3	HBsAg	340 ng/mL	363.08 ng/mL	106.79
4	HBsAg	3.40 µg/mL	3.24 µg/mL	95.29
5	HBsAg	34 µg/mL	31.62 µg/mL	93.00
6	HCVcAg	0.10 ng/mL	0.09 ng/mL	90.00
7	HCVcAg	1 ng/mL	0.97 ng/mL	97.00
8	HCVcAg	10 ng/mL	9.33 ng/mL	93.30
9	HCVcAg	100 ng/mL	109.64 ng/mL	109.64
10	HCVcAg	1 µg/mL	1.07 µg/mL	107.00

5.4 Summary

We have developed a simple, portable, and POC paper/PMMA hybrid microfluidic microplate for rapid and sensitive detection of infectious diseases and other bio-analytes. To the best of our knowledge, this is the first report of paper/PMMA hybrid microfluidic device, which draws more benefits from both substrates. The innovative use of 3D micro-porous paper in funnel-shaped microwells of this hybrid microplate facilitated rapid immobilization of

antibody/antigen and avoided complicated surface modifications. ELISA assays can be completed within one hour, and results can be observed by the naked eye or scanned by an office scanner for quantitative analysis. In addition, smartphone cameras can also be used to capture the image and the signals can be processed using different applications or cloud-based systems[57]. Although the basic system shown here can only perform 8 seven-repeated experiments (7x8 microwells), the design can be simply modified to perform as many experiments and repeats as desired. For instance, the hybrid microfluidic microplate can be expanded to 96 wells or 384 wells according to different needs simply by increasing the number of wells and channels, where the basic architecture remains the same. Without using any specialized laboratory equipment, the LOD of 1.6 ng/mL for IgG was achieved, which is comparable to that of commercial ELISA kits using spectrometers or microplate readers. The hybrid microfluidic microplate significantly reduces the sample and reagent volume compared to commercial ELISA and shows great promise as a POC device for rapid, sensitive, and quantitative detection of biomarkers, especially in low-resource settings, such as small clinics, rural areas, border regions and developing nations.

For the device to be used in the settings of laboratories and hospitals, the hybrid device was redesigned to make it compatible with traditional microplate readers. The microwells in the hybrid device were designed according to the dimensions of the standard 384-well plates so that any commercial microplate reader can be used to read the device. Chemiluminescence assay of different biomarkers was performed in the hybrid device and the LODs of 20 pg/mL for IgG, 50 pg/mL for HBsAg, 35 pg/mL for HBcAg, and 10 pg/mL for HCVcAg were achieved. The hybrid device can be used in high-end laboratories and hospitals having microplate reader for detection of infectious diseases and cancer biomarkers. As the device is around 100-fold more sensitive than commercial 96- or 384-well plates, it can be used to detect a low-concentration analyte. Because ELISA and microplates are widely used, this hybrid paper/PMMA microfluidic microplate will have broad applications from biology and clinical diagnosis to various biochemical analyses.

Chapter 6: A Reusable PMMA/Paper Hybrid Plug-and-Play Microfluidic Device for High-sensitivity Immunoassay

---

- This chapter introduces a reusable, cost-effective, and eco-friendly PMMA/paper hybrid plug-and-play (PnP) device for analyte enrichment and detection.
- The sample flows back and forth through the low-cost 3D paper substrate within the PMMA channels thereby enriching the amount of analyte adsorbed and dramatically decreasing the incubation time.
- The paper substrate can be replaced so that the device can be reused.
- The sandwich-type immunoassay of IgG and HBsAg was performed in the hybrid device with LOD of 200 pg/mL and 270 pg/mL, respectively which is at least 10 times more sensitive than commercial ELISA kits.
- The hybrid PnP device can be used for low-cost, reusable, and reproducible enrichment and detection of infectious diseases, cancers, and other biomolecules.

6.1 Introduction

Infectious diseases caused by bacteria, viruses or fungi lead to around 13.2 million deaths, which is 25% of the deaths worldwide and accounts for more than half of all the infant deaths.[202, 203] In addition, 95% of these deaths are due to the lack of cost-effective medical interventions.[204] Although advanced and sophisticated technologies including polymerase chain reaction (PCR) and enzyme-linked immunosorbent assay (ELISA) are extensively used in developed countries, they are not widely available in developing countries because of limited funds and skilled manpower. These techniques along with other methods such as cell culture, western blotting, and flow cytometry are often laborious and time-consuming. So, point-of-care (POC) detection in resource-limited settings is still a challenge.[170, 205144] Although ELISAs performed in 96-well plates are the most commonly used laboratory methods, they require overnight incubation, consume a large volume of valuable samples and expensive reagents, and require laboratory settings with bulky and expensive robotic pipettors, plate washers, and optical detectors.[52, 145] Likewise, the other major problem is the detection of low-concentration analytes. The ability to enrich biological samples such as proteins is important in bio-analysis and medical diagnosis to increase the sensitivity of detection. In order to make LOC devices as competitive as traditional techniques, the development of novel methods to improve detection limits and enrich analytes for chip-based detection is required.[206] One of the most important boons of pre-concentration of samples before analysis is to improve the detection of low-concentration analytes, typically faced in the real-world samples.[206] Sample enrichment or pre-concentration have been done on microfluidic devices either by electrophoretic methods or non-electrophoretic extraction methods (liquid/liquid extraction, solid-phase extraction). Such techniques require careful consideration of electrical behavior, background electrolyte composition, and ion concentrations.[207, 208] Likewise, complicated on-chip column-based chromatography method followed by detection using mass spectroscopy has also been used for enrichment of biomarkers.[209] Carbon-based nanomaterials such as fullerenes, graphene, nanodiamonds, and nanofibers have also been frequently utilized as adsorbents for sample pre-treatment and

enrichment.[210] Most of the developed techniques of analyte enrichment require complicated synthesis and cross-linking steps along with expensive detection units and are not suitable in POC settings.

Microfluidic devices fabricated by microelectromechanical systems (MEMS) technology incorporate different fields including electronics, mechanics, optics, biological detection, and sensors.[147, 211] The small volume of micro-channels and high surface-to-volume ratios in these low-cost and portable microfluidic devices, significantly decreases the analysis time and can integrate various bio-sensing elements.[6237] Microfluidic lab-on-a-chip (LOC) devices greatly reduce the volume of samples and reagents, without compromising specificity and sensitivity.[212] Disposable devices such as paper-based devices further reduce the cost of diagnosis. Paper-based devices have been widely used as platforms for POC analysis.[55, 128] Paper having a high surface-to-volume ratio can rapidly immobilize different sensors and biomolecules, yet doesn't require clean room for fabrication, and can be easily disposed. Furthermore, it is abundant, inexpensive and easy to use.[55] Colorimetric paper-based devices are the most widely employed detection platforms since the paper substrate offers a bright, high-contrast, and colorless background for color change readings as described in Section 1.5.3. PMMA has also been widely used in LOC devices due to its low cost of manufacturing and ease of use and fabrication as discussed in Section 1.5.2. Likewise, it is bio-disposable, transparent, rigid, and can rapidly transfer reagents. However, PMMA requires complicated surface modification for the immobilization of proteins and immune-sensors. Darain *et al*. activated the PMMA surface with O_2 plasma and functionalized it with APTES for stable antibody immobilization.[109] The on-chip ELISA was detected using fluorescence microscopy with LOD of 0.12 μg/mL. Zhou *et al*. treated PMMA under ultrasonic water bath and oxygen plasma before coupling the capture antibody with 1-ethyl-3-(3-dimethylaminopropyl) carbodiimide reagent and required a pumping system and a microplate reader.[135] Yu *et al*. developed a QD-linked immune-diagnostic assay where myeloperoxidase antibodies were covalently linked to PMMA after treating it with polyethylene glycol followed by glutaraldehyde and required expensive fluorescence setup for detection.[136]

Liu *et al*. modified the PMMA using PEI for electrochemical detection of a biomarker of neurological disease and required an electrochemical workstation.[137] Sun *et al*. performed sandwich ELISA of staphylococcal enterotoxin B by functionalizing antibody with carbon nanotube before immobilizing it to the PMMA.[125] All of these assays require complicated and time-consuming functionalization along with bulky and expensive detection systems and cannot be used in POC settings.

Each microfluidic substrate has its own nobilities and drawbacks. The combination of different substrates can enable integration of different functionalities, taking advantages of different materials and excluding some limitations of certain materials. Recently hybrid microfluidic devices have been broadly applied for diverse applications including detection of infectious diseases and cell culture studies as discussed in Section 1.5.4.[55, 148, 149, 213]

In response to the aforementioned challenges, we have developed a simple reusable PMMA/paper hybrid plug-and-play (PnP) microfluidic device for analyte enrichment and highly sensitive immune-detection. The PMMA substrate has multiple laser-ablated slots where a pre-patterned 3D microporous paper substrate can be plugged in. The sample flows back and forth through the paper within the PMMA channel, hence increasing the amount of analyte immobilized and decreasing the incubation time. After the enrichment assay through the 3D matrix of the paper, paper substrate can be simply plugged out of the device to view the result and a new paper substrate can be plugged in for the next assay. ELISA of IgG and HBsAg were performed in the PnP hybrid microfluidic device and LODs of 200 pg/mL and 270 pg/mL were obtained, respectively, without the use of any specialized detection system like the microplate reader. Compared to regular paper-based and PMMA microfluidic devices, our hybrid method showed significantly improved sensitivity and a wide linear range of five orders of magnitude for IgG and six orders of magnitude for HBsAg. The sensitivity of the PnP device was at least 10 folds better than that the commercial ELISA kits.

6.2 Experimental

6.2.1 Chemicals and materials

All chemicals and materials are listed in Section 2.1.

6.2.2 Design and fabrication of microfluidic platform

PnP hybrid microfluidic platform was designed with the aid of Adobe Illustrator CS5. The PMMA chip was then fabricated with a laser cutter (Epilog Zing 16, Golden, CO) by mask-less laser ablation where the beams of the laser move in x- and y-directions as devised in the chip design. The final design of the PnP hybrid device was as shown in Figure 6.1. The hybrid PnP microfluidic device has varying depths in each of the PMMA layers. Thus, we have used laser ablation as a rapid alternative to the photolithography, where the high-powered laser removes the material from the desired substrate as defined in the pattern.

The PnP hybrid device consists of three layers as shown in the 3D schematic of the exploded device in Figure 6.1A, with top, middle, and bottom layers. The top and middle layers consist of two inlet microwells, four slots, and two micro-reservoirs. Inlet microwells in the middle layer are connected to the reservoir microwells via slots by microchannels in the middle layer. Two sets of the two-replica assays can be performed in the shown device. The bottom layer consists of four slots. Figure 6.1B shows a 3D view of the assembled PnP hybrid microfluidic device, while Figure 6.1C shows the photograph of the actual assembled PnP hybrid microfluidic device.

A reversible sealing of the PnP device was obtained by clamping different PMMA layers together within glass slabs in an oven at 115-120 °C for 35 minutes. The PnP device can be used for enrichment and assay after plugging the paper substrate in the slots after the chip cools down to room temperature.

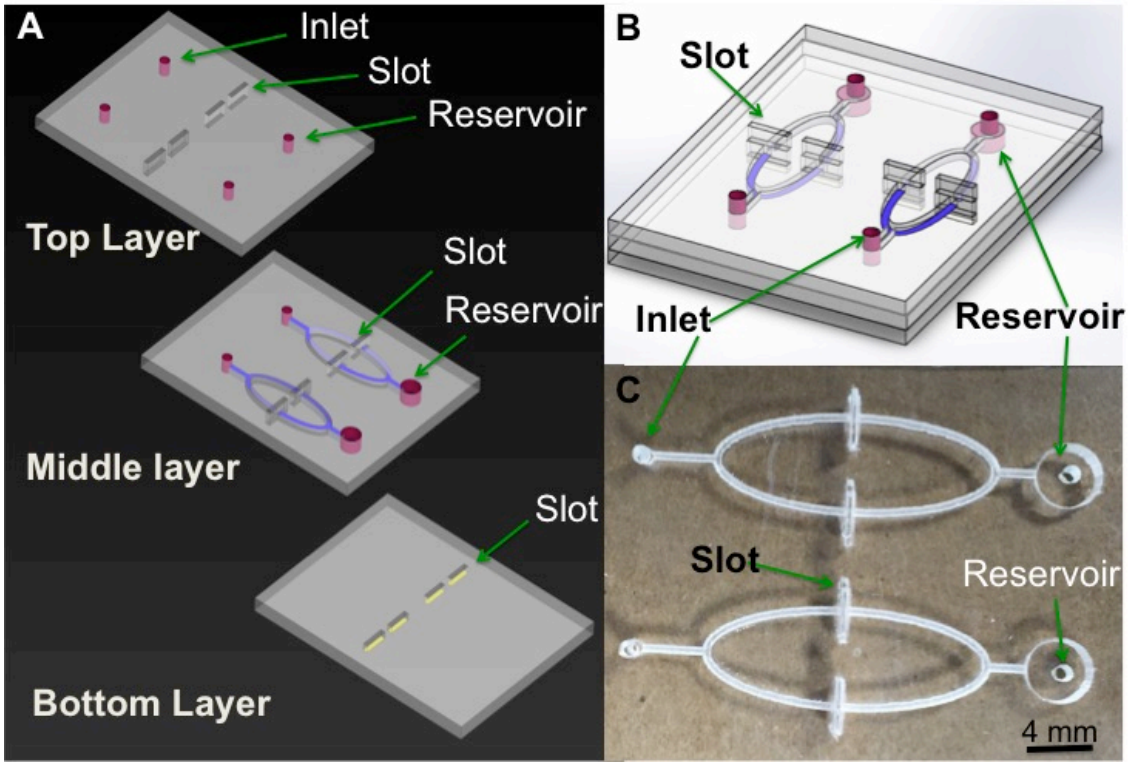

Figure 6.1: Chip design of hybrid PnP device. (A) 3D schematic of the exploded PnP hybrid microfluidic device with top, middle, and the bottom layer. (B) 3D view of the assembled PnP hybrid microfluidic device. (C) The photograph of the assembled PnP hybrid microfluidic device.

6.2.3 Optimization of parameters effecting colorimetric signals

ELISAs of different biomarkers were performed in the hybrid PnP microfluidic device. Varieties of factors including flow rate, incubation time, and repeat time influences the sensitivity of ELISA. A thorough study was performed to optimize the conditions of ELISA to get a better result and sensitivity. Finally, the ELISA of IgG and HBsAg were performed with the optimized conditions.

6.2.4 Optimization of the flow rates in the hybrid device

To determine the relationship between the flow rate and signal intensity, ELISA of IgG was performed with different flow rates. Samples/reagents were injected into the microwells by polyethylene tubing (BD Diagnostics, Sparks, MD) connected to a syringe pump (kdScientific, Holliston, MA) and the inlet microwells to control the flow rate. 1 ng/mL of IgG and the

negative control (PBS) were added to each inlet microwell present in the first layer. To optimize the flow rate of the analyte, ELISA was performed with different flow rates (15 μL/min, 20 μL/min, 25 μL/min, 30 μL/min, and 35 μL/min). 50 μL of the analyte/PBS was added to the chip with these different flow rates (so that each micro-zone receives 25 μL of the analyte). Once 50 μL of the analyte was added and incubated for 5 minutes, analyte was withdrawn back to the syringe so that it flows through the paper surface within the channel. This process was repeated for 5 times in order to maximize enrichment of the analyte onto the paper surface. After the completion of the colorimetric assay, the flow rate with the highest net brightness (signal) difference between the analyte and the negative control was taken as the optimum flow rate and further experiments were done with the same flow rate.

6.2.5 Optimization of the incubation time and repeat times in the hybrid device

Incubation time was defined as the time of incubation after the analyte was completely injected or withdrawn from the PnP hybrid microfluidic device in each repeat cycles. Incubation time was optimized similar to the optimization of the flow rate. Once the analyte was completely injected to the device or withdrawn from the device using the optimum flow rate, the paper substrate was incubated for different times (0 min, 1 min, 3 min, 5 min, and 10 min) and the process was repeated for 5 times. Finally, the colorimetric assay was completed to measure the net brightness difference between the analyte and the negative control. For the optimization of the repeat times, the complete injection and withdrawal of the analytes were repeated for several times (1, 2, 3, and 4) with the optimized flow rate and incubation time. The signal intensities were compared against repeat times after the assay and the repeat times with the highest net brightness difference between the analyte and the negative control was considered as the optimum repeat times.

6.2.6 Detection of IgG and HBsAg using the hybrid PnP microfluidic device

The hybrid PnP device was used for the detection of IgG and HBsAg. Standard samples of IgG were prepared by diluting a stock solution of IgG (2 mg/mL in 10 mM, pH 8.0 PBS) to

different concentrations ranging from 0.1 ng/mL to 10 μg/mL. 50 μL of IgG/PBS was injected into the hybrid PnP device from different inlet microwells in the top layer of the chip. The analyte was injected from the syringe pump via polyethylene tubing to the inlet microwells at the speed of 20 μL/min. The device was incubated for 3 min, then the analyte was withdrawn back to the syringe pump at the same speed of 20 μL/min followed by incubation time of 3 min. The injection and withdrawal of the analytes were repeated for 3 times with the same speed and incubation time. After the enrichment step, the paper surface was blocked with a 4.5 % BSA to block the non-specific binding sites. After incubating for 10 min, the device was washed with washing buffer. 6 μg/mL of anti-rabbit IgG linked with alkaline phosphatase was added for 7 min, which was followed by a three-time wash with PBST. A light yellow colored BCIP/NBT, which is a substrate for alkaline phosphatase was then added. The substrate produces a visually observable purple color, the intensity of which depends on the concentration of the analyte. Finally, the paper substrate was plugged out of the device after 10 minutes and scanned with a scanner or an image cab be taken by a cell-phone camera.

For the on-chip enrichment and detection of HBsAg, a sandwich immunoassay was performed with a procedure similar to IgG. HBsAg was first bound to the surface of the paper followed by blocking the unreacted surfaces. Next, anti-HBsAg was added followed by the addition of anti-rabbit IgG, which was linked with alkaline phosphatase. Unbound secondary antibody in the sandwich structure was then washed with PBST and finally the colorimetric substrate, BCIP/NBT was added.

6.2.7 Comparison of the PnP device with paper-based devices for the detection of HBsAg

For the detection of HBsAg in a paper-based device, 40-microzone-paper substrate with an array (8 × 5) of circular zones was prepared and colorimetric ELISA ranging from 0.34 ng/mL-340 μg/mL was performed. 10 μL of different concentrations of HBsAg was first added to each microzone and incubated for 10 min followed by blotting-dry by keeping the paper-based device over a kimwipe (Kimtech, Roswell, GA). The paper substrate was then blocked with a blocking buffer (5 μL per zone) for 10 min and washed with PBST. The paper-based device was

blotted dry after each step. Anti-HBsAg was then added for 10 min followed by washing and the addition of ALP-linked anti-rabbit IgG. Finally, BCIP/NBT was added after washing it three times with PBST. The paper-based device was scanned with a desktop scanner for quantitative measurement.

6.3 Results and discussion

6.3.1 Hybrid PnP microfluidic device

The PnP hybrid microfluidic device was designed to meet three specific requirements: (i) generation of multiple slots with interconnected channels, where the paper substrate can be placed so that the analyte can pass back and forth through the channel, rapidly immobilizing more and more analyte in the porous paper substrate. (ii) the paper substrate which can be plugged into the device to perform the assay (PnP) and be replaced with a new one for another assay. (iii) a temporary reservoir to store the analyte so that all the analyte from the syringe can pass through the slot.

Figure 6.2 explains the working principle of the PnP hybrid microfluidic device. As shown in Figure 6.2A, the top layer (I) has inlet microwells (a) from which reagents/analytes can be added. The top inlet microwell continues with microwell in the middle layer (II), which is placed just below the inlet microwell so that the reagents can fall directly into the middle layer. The microwell in the middle layer continues to the channels (c) in the middle layer through which reagents flow towards the opposite end of the reservoir (d). The reagent flows through the slots (e) where the paper substrate (f) is plugged in vertically as shown in Figure 6.2B. The reservoir in the middle layer is open as a reservoir in the top layer with a smaller diameter (b). The slot is open in the top and middle layer but it is closed towards the lower side of the bottom layer so that the reagent does not fall down from the chip. The analyte passes through the paper substrate and gets stored in the reservoir. The analyte is then withdrawn back to the syringe pump through the paper substrate. The process is continued for a couple of times so that the higher amount of sample could be immobilized to the surface of the paper.

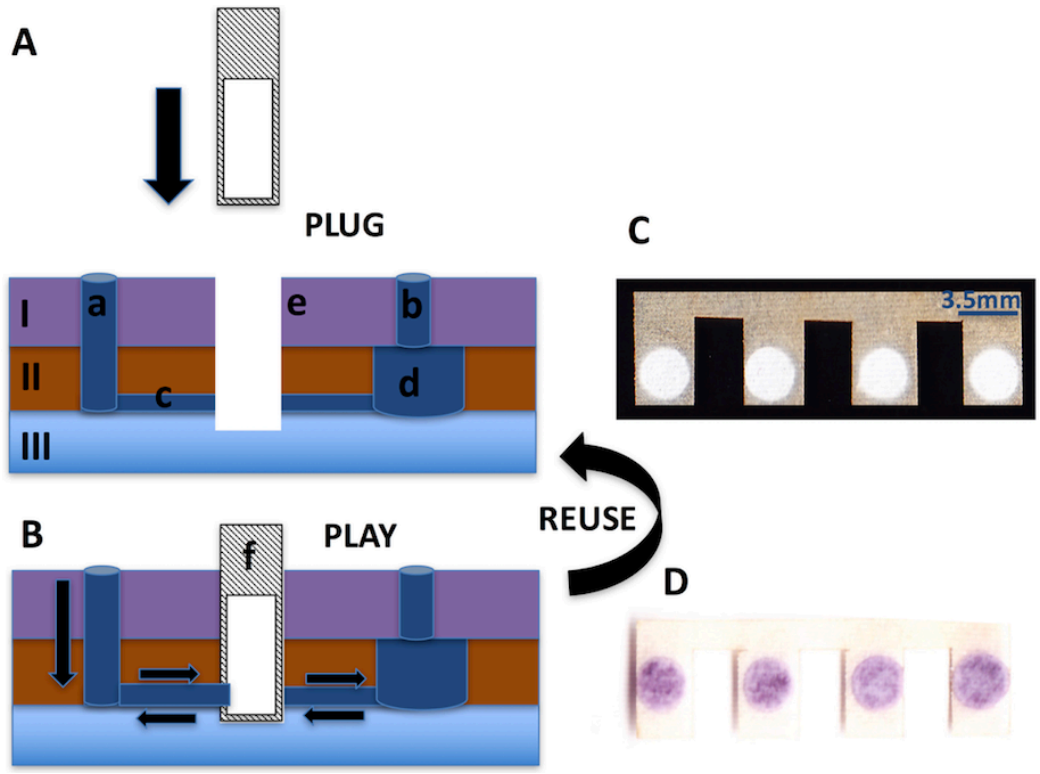

Figure 6.2: Working principle and cross-section view of PnP hybrid microfluidic device. The figure shows the cross-section view of the PnP hybrid microfluidic device without the paper substrate (A) and with the paper substrate (B). The top layer consists of inlet microwell (a) and reservoir microwell (b). The middle layer consists of channels (c) and reservoir (d). Slots (e) pass through the top, middle and half of the bottom layer where the paper substrate (f) can be plugged in vertically. Scanned image of the SU-8 treated paper substrate before the immunoassay (C) and after the immunoassay (D).

6.3.1 Optimization of the flow rates

The flow rate of the sample through the paper-strip affects the immobilization or the enrichment efficiency of the analyte on the surface of the paper. Therefore, the optimum flow rate of the sample which can immobilize maximum amount of analyte was determined. IgG was chosen as the model analyte for optimization studies. IgG, the most prevalent antibody in the human circulation can be used for diagnosis of Neuromyelitis Optica[188] and autoimmune hepatitis[186] and is the major constituent of the secondary immune response to different kinds of infectious agents.[214] IgG levels in the human body also indicates the immune status of different diseases including measles, mumps, and rubella (MMR), hepatitis B virus, and varicella.[187] For the optimization of the flow rate of the injection and the withdrawal of the sample, different flow

rates of IgG (15 μL/min, 20 μL/min, 25 μL/min, 30 μL/min, and 35 μL/min) were tested. After the completion of ELISA, the paper substrate was scanned and ImageJ was used to measure the brightness value. As we could observe from Figure 6.3, there was a significant increase in the net brightness difference between the analyte (1 ng/mL of IgG) and the negative control (phosphate-buffered saline, PBS) from 15 μL/min to 20 μL/min. The decrease in the net brightness difference between the analyte and the negative control was observed from 20 μL/min to 35 μL/min. At 15 μL/min, the pressure may not be strong enough for the analyte to go through the paper substrate properly. However, we hypothesized that with the flow rate higher than 20 μL/min, the analytes passed the paper substrate too fast, so they could not bind to the paper surface properly. The flow rate of 20 μL/min, which gave the highest net difference between the analyte and the negative control, was considered as the optimized flow rate and was used in the following experiments.

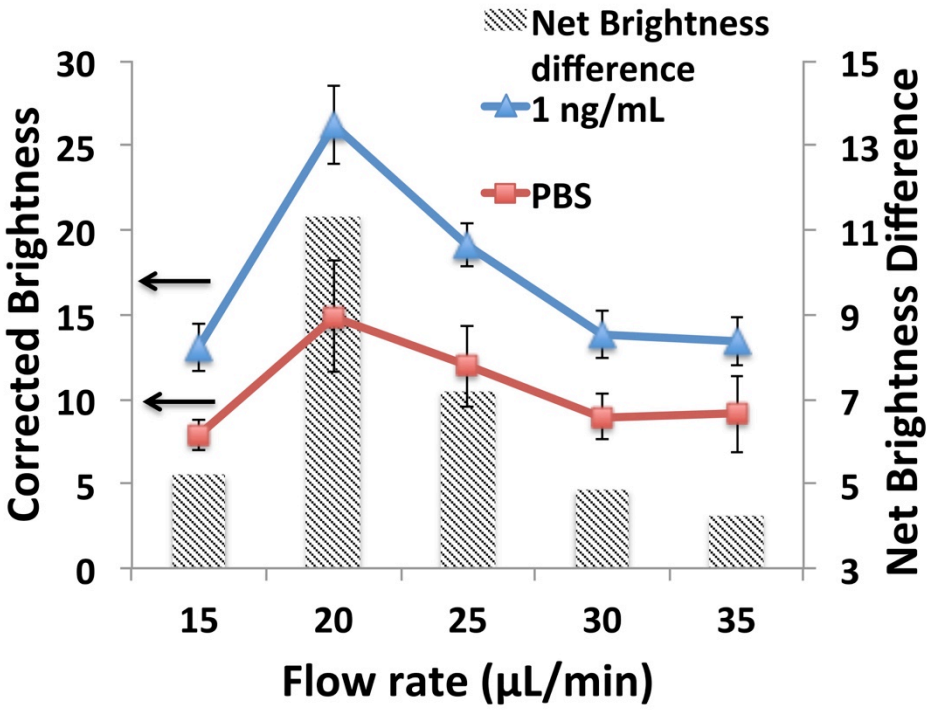

Figure 6.3: Optimization of the flow rate of the analyte. The graph shows the relationship between flow rate and the net brightness difference between the analyte and the negative control.

6.3.2 Optimization of the incubation time and repeat times

Diagnostic devices which have higher sensitivity, but lower assay time are preferred. Therefore, the minimum incubation time which can obtain the highest enrichment of the analyte, ultimately leading to increase in sensitivity was determined in the optimization of incubation time. Once the flow rate of the analyte was optimized, different incubation times (0 min, 1 min, 3 min, 5 min, 10 min) were evaluated to optimize the incubation time for the analyte. As seen from Figure 6.4A, there was a slight increase in the net brightness difference between the analyte and the negative control, from 0 min to 3 min. After 3 min of incubation time, there was no significant increase in the net brightness difference. In addition, the standard deviation at 0 and 1 min was much higher as compared to 3 min. The incubation time of 3 min was considered as the optimum incubation time as we could observe from Figure 6.4A, where the graph of net brightness difference against incubation time showed plateau starting from 3 min. Therefore, the incubation time of 3 min was used in all the subsequent experiments.

We also optimized the repeat time for the injection and withdrawal of the analyte to determine the minimum repeat time with the maximum difference between the positive and negative control so as to increase the sensitivity while achieving the minimum time possible. A few repeat times may not be sufficient to enrich the analyte while too many repeats may ultimately lead to washing off the immobilized analyte or more time consumption. The injection and withdrawal of the analyte were repeated for several times (1 time, 2 times, 3 times, and 4 times). As we could observe from Figure 6.4B, the net brightness difference between the analyte and the negative control increased with the increase in repeat times for up to 3 repeats. After 3 repeats, there was no significant increase in the net brightness difference as the graph of net brightness difference against repeat time showed plateau starting from 3 repeats. It showed that signal to noise difference reached a maximum at 3 repeats and any further increase in repeat time did not increase the enrichment of analyte, so 3 repeats were enough to immobilize maximum amount of analyte. Hence, the repeat times of 3 repeats were considered as optimum repeat times and the same parameter was used in all the subsequent experiments.

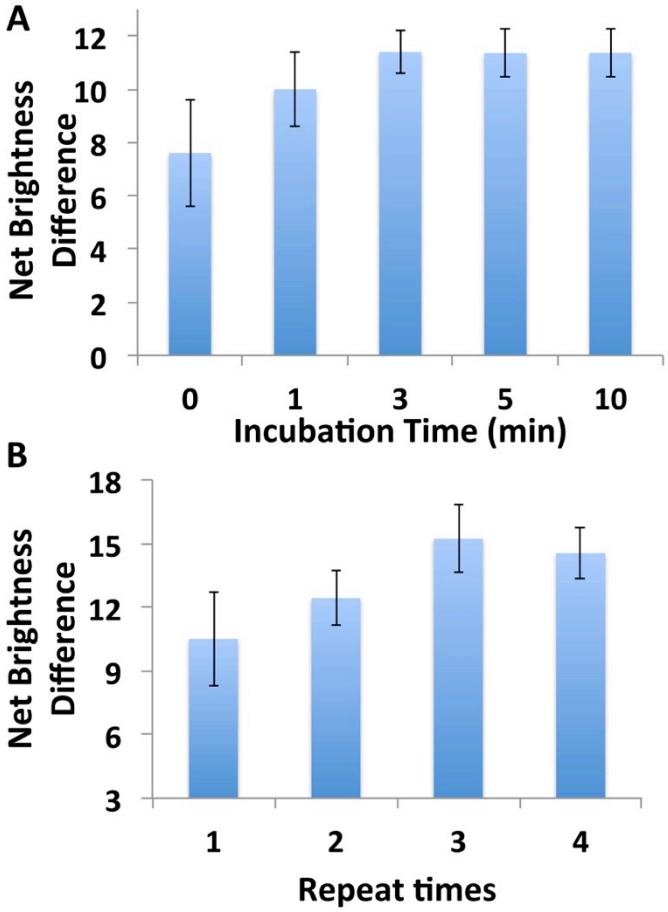

Figure 6.4: Optimization of incubation time and repeat times for immunoassay in PnP hybrid microfluidic device. (A) The relationship between incubation time and net brightness difference between the analyte and the negative control. (B) The relationship between repeat times and net brightness difference between the analyte and the negative control.

6.3.3 Rapid quantitative detection of IgG in the hybrid PnP device

The hybrid PnP microfluidic device can be used for the enrichment and detection of several disease biomarkers. We first performed the on-chip ELISA of IgG in our hybrid PnP microfluidic device. Different concentrations of IgG ranging from 0.1 ng/mL to 10 μg/mL were injected into the device using the syringe pump to perform the colorimetric ELISA. The result was observed with the naked eye and a portable desktop scanner was used to scan the paper substrate for quantitative analysis. Figure 6.5 shows the gray image scanned by the desktop scanner for IgG immunodetection on the PnP hybrid microfluidic device along with its

corresponding corrected brightness against the concentration of IgG. We could observe that the brightness of the hydrophilic zones was directly related to the concentration of IgG. As seen from Figure 6.5, the detection zone containing PBS had the brightest color and the detection zone containing 10^7 pg/mL of IgG had the darkest color. The brightness of other concentrations decreased from 10^2 pg/mL to 10^7 pg/mL, from left to right. ImageJ was used to measure the average brightness/intensity of the signal from the scanned images. Similarly, a wide linearity range was found over the whole concentration range from 10^2 pg/mL to 10^7 pg/mL with a linear regression of $y = 5.30 \log (x) + 15.72$ ($R^2 = 0.99$). LOD of IgG using the hybrid PnP microfluidic device was calculated to be 200 pg/mL based on 3 folds of SD above the blank value. Our device is around 10-folds more sensitive compared to the commercial ELISA of IgG, which has LOD of 1.6–6.25 ng/mL.[154] Our hybrid PnP device (200 pg/mL) was also more sensitive than the paper-based device,[128] the modified PMMA (0.12 μg/mL),[109] the complementary metal oxide semiconductor (10 ng/mL),[166] and the paper/polymer hybrid microfluidic microplate (1.6 ng/mL).[215]

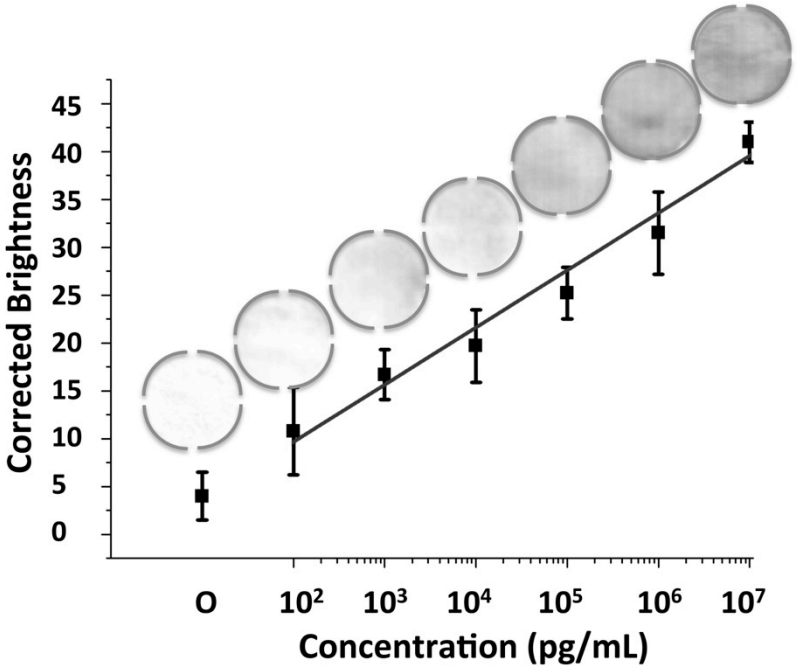

Figure 6.5: Rapid detection of IgG by hybrid PnP microfluidic device. The figure shows a linear plot of the corrected brightness of IgG over a concentration range from 10^2 pg/mL to 10^7 pg/mL. The inset shows the gray image obtained by converting the RGB image of the paper substrate

with different IgG concentrations. The RGB image was obtained by scanning the paper substrate from an office scanner.

6.3.4 Rapid quantitative detection of HBsAg in the hybrid PnP device

HBV is a major cause of chronic hepatic damage and of hepatocellular carcinomas worldwide[17] and roughly 30% of world's population show serological evidence of current or past infection.[16 216] 25% of people acquiring HBV infection in childhood develop primary liver cancer or cirrhosis when they grow up.[217] HBsAg, a serological biomarker for an HBV infection, appears 2-10 weeks after the exposure to HBV and persistence beyond 6 months is due to the progression to chronic infection.[16] Globally, 248 million individuals were estimated to be HBsAg positive.[218] HBsAg can diagnose acute and chronic hepatitis B virus[189-191] and the titer indicates the level of infection and severity of the disease.[15, 191] Thus, HBsAg was used as the biomarker for the detection of HBV. Figure 6.6A shows the image scanned by the desktop scanner for the detection of HBsAg in the PnP microfluidic device. The detection zone with PBS showed the brightest color and the one with 340 μg/mL HBsAg showed the darkest purple color, while the purple color intensity of other concentrations increased from 0.34 ng/mL to 340 μg/mL. Signal intensity of the scanned image was calculated by ImageJ and a calibration curve of HBsAg over a concentration range from 34×10^{1} pg/mL to 34×10^{7} pg/mL was obtained (Figure 6.6B). In addition, a wide linearity range was found over the whole concentration range from 34×10^{1} pg/mL to 34×10^{7} pg/mL with a linear regression of $y = 10.89 \log (x) + 33.16$ ($R^2 = 0.99$). LOD of HBsAg using the hybrid PnP microfluidic device was found to be 270 pg/mL based on 3 folds of SD above the blank value. Our device was more sensitive than the device developed by Yazdani *et al*. for detection of HBsAg (LOD of 0.5 ng/mL, which was comparable to commercial ELISA kits).[160] This shows that the proposed method is more sensitive than the commercial ELISA kits and the paper/polymer hybrid microfluidic microplate with a LOD of 1.3 ng/mL.[215]

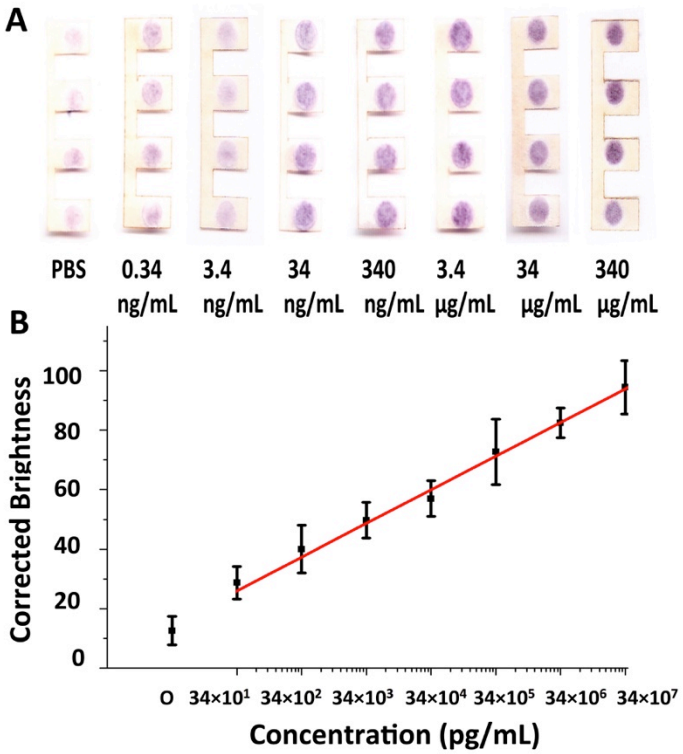

Figure 6.6: Rapid detection of HBsAg by hybrid PnP microfluidic device. (A) Scanned image of the paper substrate with different HBsAg concentrations by an office scanner. (B) Linear plot of the corrected brightness of HBsAg over a concentration range from 34×10^1 pg/mL to 34×10^7 pg/mL.

6.3.5 Comparison of the PnP device with paper-based devices for the detection of HBsAg

To compare the sensitivity of ELISA and the dynamic linearity range, ELISA of HBsAg was performed in the paper-based device. Figure 6.7A shows the image scanned by the desktop scanner for HBsAg immunodetection on the paper-based device. Similar to detection of HBsAg on hybrid PnP microfluidic device, the intensity of the purple color increased from 0.34 ng/mL to 340 µg/mL from left to right. However, the purple color intensity only increased slightly from 0.34 ng/mL to 3.4 ng/mL and then got saturated at 34 µg/mL. The intensity of the signal of the scanned images was calculated using ImageJ as described before. Figure 6.7B is the calibration curve of HBsAg over a concentration range from 34×10^1 pg/mL to 34×10^7 pg/mL. Unlike the hybrid PnP device, the linearity range was only found in the concentration between 34×10^2 pg/mL and 34×10^5 pg/mL with a linear regression of $y = 7.80 \log (x) + 28.73$ ($R^2 = 0.96$). LOD of HBsAg using the paper-based device was found to be 2.9 ng/mL, which was 10 folds higher than

the hybrid PnP device. In addition, repeated washing steps required in ELISA led to decrease in hydrophobicity of the paper surrounding the hydrophilic zone. Similarly, we observed that repeated washing in the hydrophilic zone of the paper substrate led to spreading of the reagents over the hydrophobic area, which may lead to cross-contamination. Finally, as seen from Figure 6.7A, analytes and color production in the paper-based device tend to agglomerate at the center of the hydrophilic zone. In contrast, the adsorption of the analyte and hence the color production in PnP hybrid microfluidic devices are distributed more evenly (Figure 6.6 A) compared to those in the paper-based devices. In the absence of external force, water tends to form droplets because of the surface tension and get agglomerated at the center of the hydrophilic zone, thus analytes get adsorbed mostly at the center and hence the color production. The tendency to form the droplet increases with the increase in storage time of SU-8 fabricated paper substrate as the hydrophilic zones turns more hydrophobic. In contrast, even distribution of the analyte and color production may be due to the repeated back and forth flow of the sample through the paper substrate with the help of syringe pump, which increases the uniformity of protein absorption as the analyte flows more uniformly and does not form droplets. This led to significant increase in dynamic linearity range from 3 orders of magnitude (34×10^{2} pg/mL to 34×10^{5} pg/mL) in the paper-based device, to 6 orders of magnitude (34×10^{1} pg/mL to 34×10^{7} pg/mL) in the PnP hybrid microfluidic device.

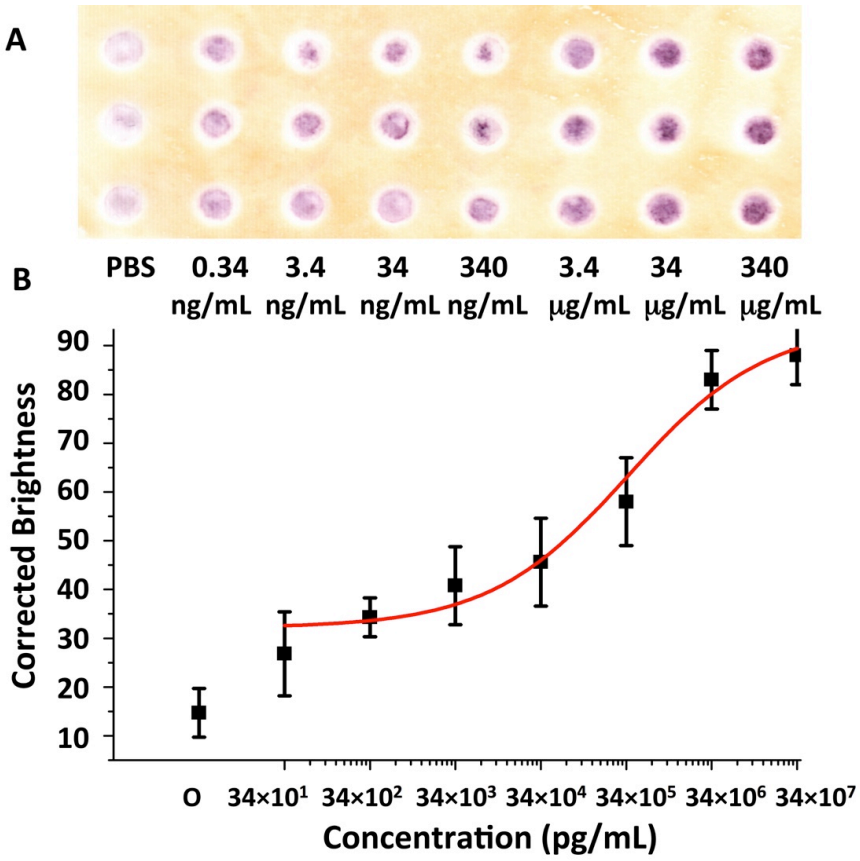

Figure 6.7: ELISA of HBsAg on the paper-based device. (A) Scanned image of the paper substrate with different HBsAg concentrations by an office scanner. (B) Linear plot of the corrected brightness of HBsAg over a concentration range from 34×10^{1} pg/mL to 34×10^{7} pg/mL.

6.4 Summary

The goal of this study was to develop a highly sensitive and eco-friendly device for the enrichment and detection of disease biomarkers. We developed a simple and portable hybrid PnP microfluidic device that takes advantages of both paper and PMMA substrates. The hybrid device provides a unique and low-cost platform to carry out the colorimetric assay of different biomolecules at very low reagent and sample volume. The hybrid PnP microfluidic device has four important features as compared to regular paper-based or PMMA microfluidic devices. (i) The entire sample passes back and forth through the paper substrate with a certain flow rate enriching the amount of analyte immobilized, ultimately increasing the sensitivity of the device so that low-concentration analyte typically faced in real-world samples can be measured. (ii) The paper substrate can be replaced with a new substrate after the completion of the assay so that the

main PMMA framework can be used for multiple times in this PnP microfluidic device. (iii) Reagents/analytes can be easily and rapidly transferred through the microchannels to the paper substrate, avoiding the slower flow in the paper-based device. The flow of the reagent can be controlled through the use of syringe pump as the rate of flow of the analyte plays an important role in the overall sensitivity of the device. (iv) Due to the unique installation of the 3D micro-porous paper substrate with high surface-to-volume ratio within the PMMA slot, proteins can be rapidly immobilized within few minutes as compared to overnight incubation in traditional microplates, which also avoids the complicated surface modification of PMMA.

The results of the assay could be viewed within 70 min with the naked eye or scanned by a simple desktop scanner for quantitative analysis. Without the use of any specialized equipment, LODs of 200 pg/mL for IgG and 270 pg/mL for HBsAg were achieved, which were at least 10 folds better than those using commercial ELISA kits. In addition, the hybrid device showed a wide linear range of five orders of magnitude for IgG and six orders of magnitude for HBsAg. The hybrid PnP microfluidic device can be used for the rapid enrichment and immobilization of the analyte for highly sensitive and quantitative detection of infectious diseases, cancers, and other bio-molecules. It also remarkably reduces the reagent volume and can be reused simply by replacing the paper substrate. This hybrid PnP microfluidic device could be immensely valuable in resource-poor settings including rural areas, small clinics, border regions, and developing countries, where the expensive diagnostic equipment such as microplate readers is not easily available.

Chapter 7: A Paper in Polymer Pond (PiPP) Hybrid Microfluidic Device for the Detection of Cancer Biomarkers

---

- This chapter introduces a cost-effective paper in polymer pond (PiPP) hybrid device for detection of cancer biomarkers.
- Sandwich type immunoassays of cancer biomarkers including CEA and PSA were performed with LODs of 0.32 ng/mL and 0.20 ng/mL, respectively.
- The hybrid PiPP device can be used for low-cost and reproducible detection of infectious diseases, cancer biomarkers, and other biomolecules.

7.1 Introduction

Cancer, characterized by uncontrolled growth and spread of abnormal cells in the body has been the leading cause of death as discussed in Section 1.2. Cancer also causes a tremendous burden to the society in terms of economic cost. In addition, cancer survival rate is very low due to late-stage diagnosis and limited access to adequate and standard treatment. Early detection of cancer biomarker proteins holds immense potential for the effective toxicity monitoring and successful treatment or personalized therapy.[219] The major goal in the field is to develop reliable, low-cost, and highly sensitive biomarker detection methods to indicate cancer risk or early detection and classification of the tumor, so the patient can get appropriate treatment and be monitored.[220] Detection of infectious diseases, cancer biomarkers, and other biomolecules can be done with high precision, sensitivity, and specificity in the laboratory which needs expensive instrumentation, and well-trained personnel and requires tiresome sample preparation methods. Conventional methods including ELISA, PCR, LC/MS are limited either by analysis time, sample volume required, or complexity for routine diagnosis.

Miniaturization of the device using microfluidic LOC technology to develop POC devices with a minimum volume of sample/reagent but with precision and sensitivity as that of traditional instruments including PCR, flow-cytometer, and microplate ELISA is in great need.[221] Different kinds of POC devices including agglutination and lateral flow assays are being developed for immunoassay test but most of the time they are limited by the lack of quantitative assay and multiplex analysis.[222]

As discussed in Section, 1.5.3, the paper is an inexpensive and widely used substrate with the basic principle of creating hydrophilic microchannels and reaction surface surrounded by hydrophobic patterning materials such as wax, polymers, and inks. Similarly, PMMA remains another widely used substrate as mentioned in Section 1.5.2. It requires surface modification for immobilization of the biomolecules. In contrast, paper-based devices can rapidly immobilize biomolecules but do not offer high performance in flow control. Hybrid microfluidic devices which can extract benefits from both the substrates are being used for different applications.

Herein, we have developed a paper in PMMA pond (PiPP) hybrid microfluidic device for low-cost detection of cancer biomarkers. Porous 3D paper with high surface-to-volume ratio kept over the PMMA pond can easily immobilize capture antibodies within 10 min, thereby decreasing the assay time to 1 hr compared to 16 hr in traditional microplates. Presence of the pond-shaped structure avoids the addition of paper substrates to individual microwells separately, as a single paper substrate cut by laser cutter as the shape of the pond can be added ti the PiPP device. The flow-through pond also acts as outlet channels to direct the waste reagents to the outlet microwell. The vertical flow-through reservoirs which pass through the paper substrate to the outlet layer ensures maximum immobilization of the protein and efficient washing, thereby increasing the sensitivity and decreasing the background noise. Simultaneous sandwich type multiplex immunoassay of cancer biomarkers including PSA and CEA was performed in the hybrid device and sensitivity better than traditional microplates was obtained without the use of any sophisticated instruments like a microplate reader.

7.2 Experimental

7.2.1 Chemicals and materials

All chemicals and materials are listed in Section 2.1.

7.2.2 Microfluidic platform design and fabrication

The microfluidic device used in this study was designed in Adobe Illustrator CS5 and fabricated using the laser cutter. As seen in Figure 7.1, the device consists of three different PMMA layers. The top layer has eight different fluid delivery channels connected to each inlet microwells. The reagents added from the top reagent delivery layer flow through the fluid delivery channel into the six reservoirs (2 mm diameter) kept just below each channel in the middle layer. The bottom layer of the device consists of interconnected pond-shaped structures. Each pond-shaped structure (0.6 mm in height) in the same column is connected to each other. Finally, all the outlets for the ponds are connected to a common horizontal outlet which has a higher depth (1.5 mm) as compared to the vertical outlet channels so that the waste reagent does not flow back to the same or different outlet channels. SU-8 treated paper is cut by laser cutter as

the shape of the ponds and kept over the bottom layer, so that all the reservoir in the middle layer fall just above the hydrophilic layer of the paper (3.5 mm diameter). In this way, the reagents added from the inlet microwell flow through the channel to the six reservoirs below each channel and pass through the paper into the outlet pond and to the outlet. All the reagents flow through the hydrophilic paper layer so that maximum amount of protein gets immobilized onto the surface of the paper substrate.

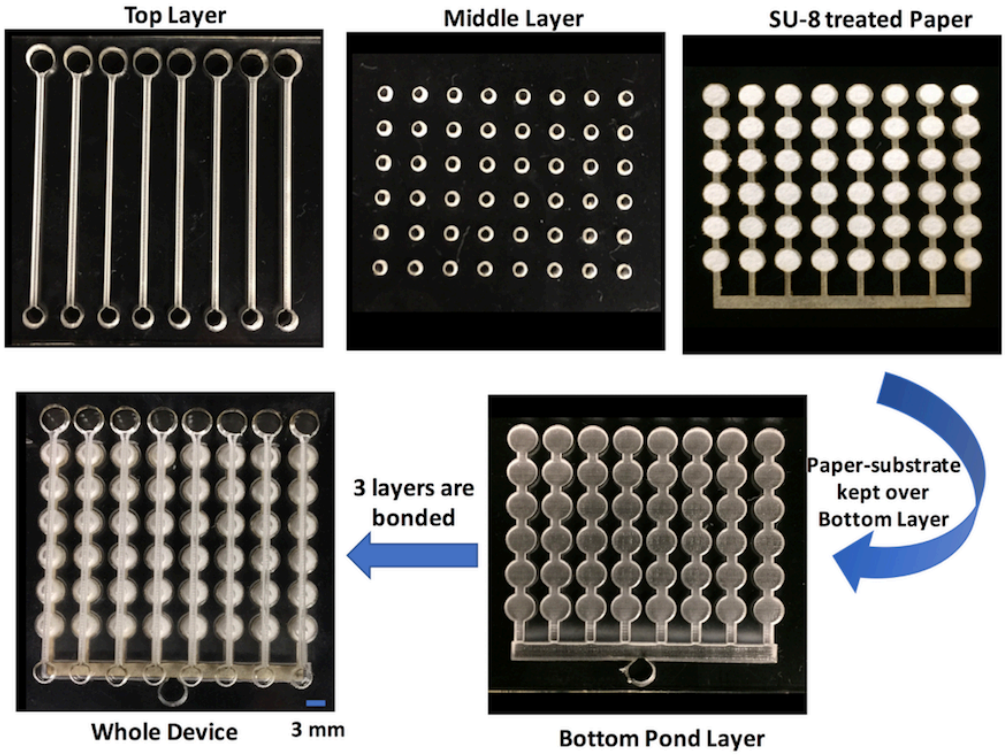

Figure 7.1: Paper on PMMA Pond hybrid device consisting of a top layer, middle layer, and bottom pond layer with the paper substrate kept over the bottom pond layer. The top layer has inlet microwells and reagent delivery channels. The middle layer has 6 × 8 reservoirs. The bottom layer has pond-shaped structure connected to a common outlet channel leading to an outlet microwell.

7.2.3 Optimization of the concentration of capture antibody

The immunoassay of CEA was performed with different concentrations of anti-CEA capture antibody for the optimization of the concentration of capture antibody as shown in Figure 7.2. First, different concentrations of anti-CEA capture antibody (1 μg/mL, 5 μg/mL, 10 μg/mL, 15 μg/mL, 20 μg/mL, 25 μg/mL, and 30 μg/mL in 10 mM, pH 8.0 PBS) were added to the hybrid device and incubated for 10 min. The device was then blocked with blocking buffer for

another 10 min followed by washing with PBST. For one set of device positive sample antigen (500 ng/mL of CEA) was added, while for the other, negative control (PBS) was added. After incubating the positive and negative control for 10 min, the device was washed with PBST and 10 μg/mL of anti-CEA secondary antibody was added. The device was washed with PBST after 10-min incubation followed by adding of 10 μg/mL ALP-linked IgG for 7 min. Finally, the device was washed for three times with PBST and colorimetric substrate BCIP/NBT was added. The device was disassembled 10 min after the addition of the substrate and the bottom pond layer with paper substrate was scanned using an office scanner. ImageJ was used to obtain the brightness value which was used for further study.

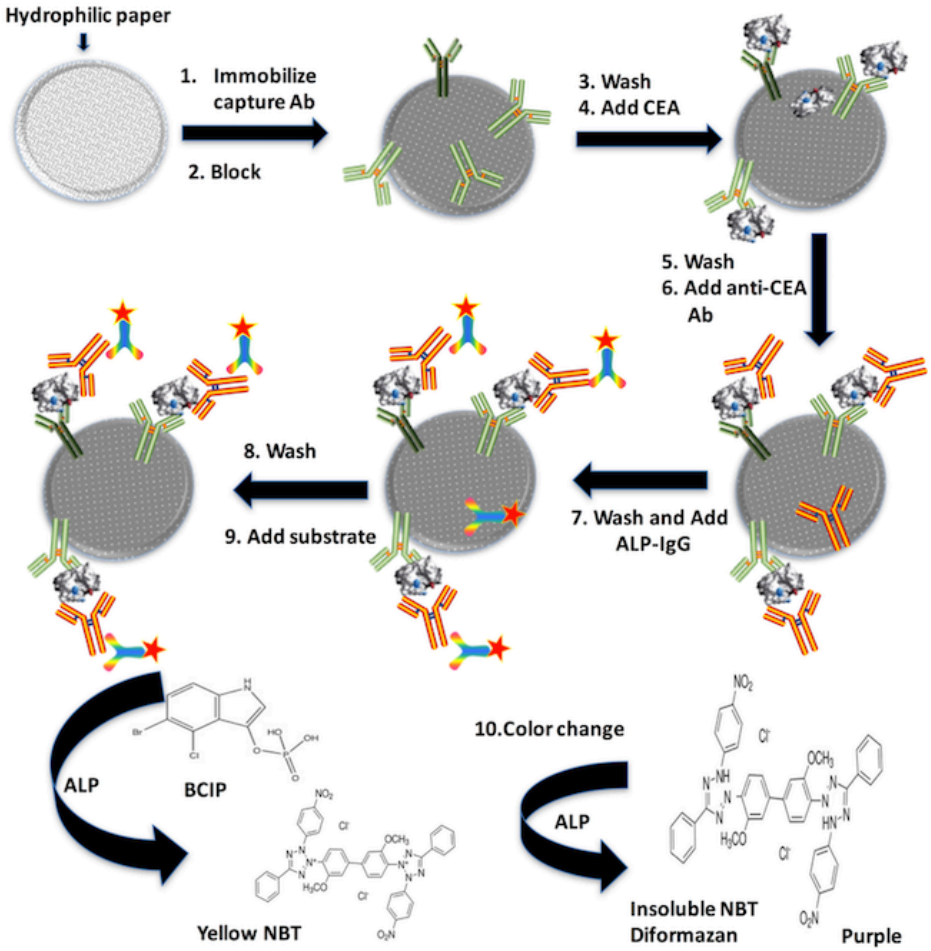

Figure 7.2: Schematic of the approach of immunoassay of CEA on the paper in polymer pond microfluidic device, comprising of ten steps: (1) Immobilizing of the capture antibody in the paper substrate, (2) Blocking, (3) Washing, (4) Addition of CEA, (5) Washing, (6) Addition of anti-CEA antibody, (7) Washing and addition of ALP-linked IgG, (8) Washing, (9) Addition of the substrate, and (10) Enzymatic production of insoluble NBT diformazan.

7.2.4 Optimization of the concentration of anti-CEA secondary antibody

Optimization of the concentration of anti-CEA secondary antibody was performed with the optimized concentration of capture antibody. First, 20 μg/mL capture antibody was added to the hybrid device and incubated for 10 min followed by blocking with blocking buffer for another 10 min and washing with PBST. 500 ng/mL of CEA was added as a positive control and PBS was added as a negative control. The device was washed with PBST after a 10-min incubation. Different concentrations of anti-CEA secondary antibody (1 μg/mL, 5 μg/mL, 10 μg/mL, 15 μg/mL, and 20 μg/mL) were added to both the positive and negative control for 10 min and washed with PBST. ALP-linked IgG (10 μg/mL) was then added for 7 min and washed for three times with PBST. Finally, BCIP/NBT was added for 10 min and the device was disassembled to scan the bottom pond layer with the paper substrate using a simple office scanner.

7.2.4 Optimization of the concentration of enzyme-linked secondary antibody

After the optimization of the concentration of capture antibody and the anti-CEA secondary antibody, concentration of enzyme-linked secondary antibody (ALP-IgG) was optimized. First, 20 μg/mL capture antibody was added to the hybrid device and incubated for 10 min followed by blocking with blocking buffer for another 10 min. The device was washed with PBST followed by the addition 500 ng/mL of CEA as a positive control and PBS as a negative control. The device was incubated for 10 min and washed with PBST followed by the addition of 10 μg/mL of anti-CEA secondary antibody. The device was then incubated for 10 min and washed with PBST. Different concentrations of ALP-linked IgG (1 μg/mL, 3 μg/mL, 6 μg/mL, 9 μg/mL, 12 μg/mL, and 15 μg/mL) were then added for 7 min and washed for three times with PBST. Finally, BCIP/NBT was added for another 10 min and the device was disassembled for scanning.

7.2.5 Colorimetric detection of cancer biomarkers

The paper in PMMA pond hybrid device can be used for the detection of a wide range of biomolecules. Herein, CEA and PSA were detected in the PiPP device with all the optimized

concentrations of different antibodies. For the detection of CEA, 20 μg/mL of capture antibody was added to the device and incubated for 10 min followed by blocking with blocking buffer for another 10 min (Figure 7.2). Different concentrations of CEA (0.1 ng/mL, 1 ng/mL, 5 ng/mL, 10 ng/mL, 25 ng/mL, 50 ng/mL, and 100 ng/mL) were then added to the device and incubated for 10 min. The device was then washed with PBST followed by the addition of 10 μg/mL of anti-CEA secondary antibody. 6 μg/mL of ALP-linked IgG was then added for 7 min and washed for three times with PBST. Finally, BCIP/NBT was added for another 10 min and the device was disassembled for scanning.

Similar to the detection of CEA, detection of PSA was performed by addition of 20 μg/mL of anti-PSA capture antibody and incubation for 10 min. After the substrate was blocked with blocking buffer, different concentrations of PSA (0.1 ng/mL, 1 ng/mL, 5 ng/mL, 10 ng/mL, 25 ng/mL, 50 ng/mL, and 100 ng/mL) were added and incubated for another 10 min. Finally, the anti-PSA secondary antibody (10 μg/mL) was added followed by the addition of ALP-linked IgG (6 μg/mL). The device was scanned 10 min after the addition of the substrate, BCIP/NBT.

7.3 Results and discussion

7.3.1 Optimization of the concentration of capture antibody

Optimization of the concentration of capture antibody was carried out by performing the immunoassay of CEA with varying concentrations of anti-CEA capture antibody. As seen from Figure 7.3, the corrected brightness value of positive control (500 ng/mL of CEA) increased with the increase in the concentration of capture antibody from 1 μg/mL to 20 μg/mL. It reached a plateau at 20 μg/mL and remained constant with further increase in the concentration of the capture antibody. For the negative control (PBS) the corrected brightness value remained constant with the increase in the concentration of capture antibody from 1 μg/mL to 20 μg/mL. As the concentration of capture antibody increased further from 20 μg/mL there was a slight increase in the corrected brightness value (background noise). It could also be observed from Figure 7.3 that the signal difference between the positive control and the negative control was maximum at the capture antibody concentration of 20 μg/mL. Therefore, 20 μg/mL of capture

antibody was considered as the optimum concentration and all the further assays were performed with the same concentration.

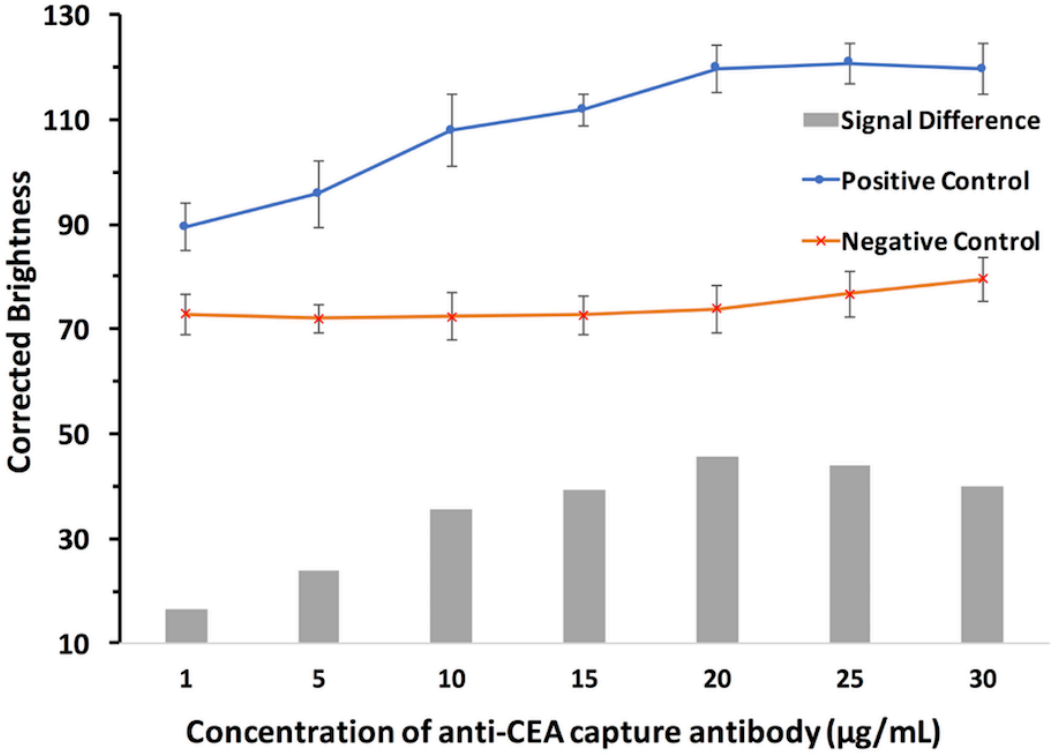

Figure 7.3: Optimization of the concentration of anti-CEA capture antibody. The line graph shows the corrected brightness value for the positive (500 ng/mL of CEA) and negative (PBS) control with 10 μg/mL of anti-PSA secondary antibody and 10 μg/mL of ALP-linked IgG. The bar graph shows the signal difference between the positive and negative control.

7.3.2 Optimization of the concentration of anti-CEA secondary antibody

The concentration of anti-CEA secondary antibody was optimized after the optimization of the concentration of capture antibody. As seen from Figure 7.4, the corrected brightness value of positive control (500 ng/mL of CEA) increased with the increase in the concentration of anti-CEA secondary antibody from 1 μg/mL to 10 μg/mL after which it reached a plateau. The average brightness value of positive control remained almost constant with concentration more than 10 μg/mL. For the negative control (PBS) the corrected brightness value remained constant with the increase in the concentration of capture antibody from 1 μg/mL to 10 μg/mL. As the concentration of anti-CEA secondary antibody increased further from 10 μg/mL, there was a rapid increase in the corrected brightness value (background noise). It could also be observed

from Figure 7.4 that the signal difference between the positive control and the negative control was maximum at the anti-CEA secondary antibody concentration of 10 μg/mL. Therefore, 10 μg/mL of anti-CEA secondary antibody was considered as an optimum concentration and all the further assays were performed with 20 μg/mL of capture antibody and 10 μg/mL of anti-CEA secondary antibody.

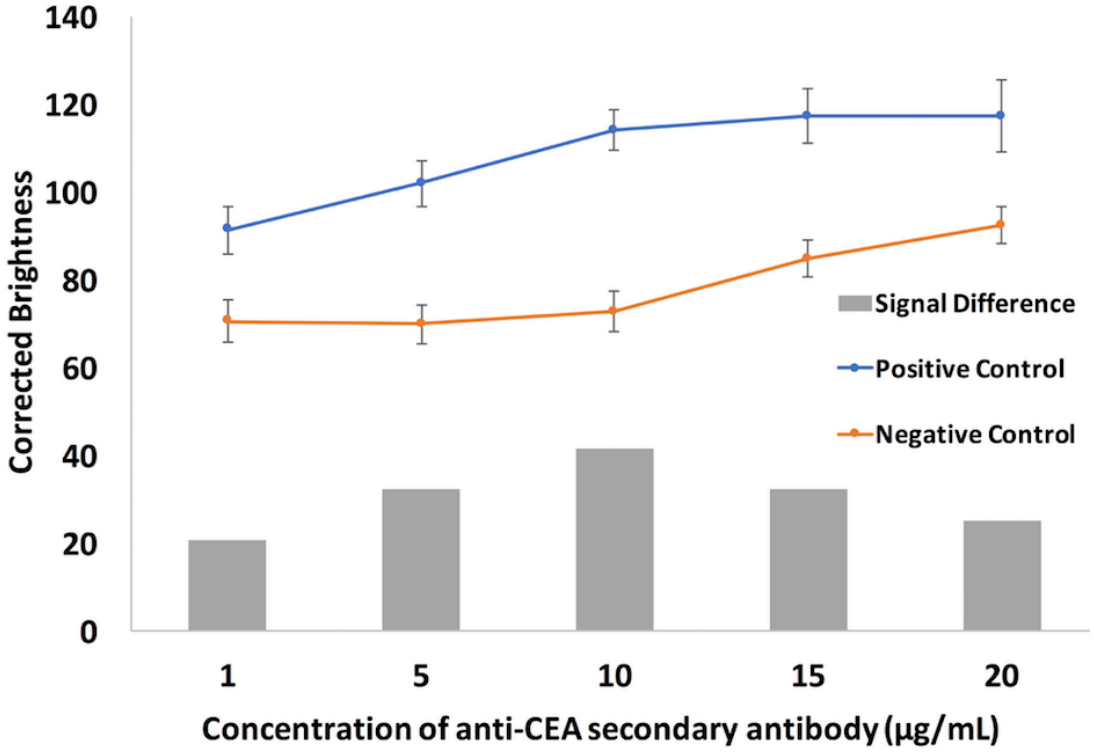

Figure 7.4: Optimization of the concentration of anti-CEA secondary antibody. The line graph shows the corrected brightness value for the positive (500 ng/mL of CEA) and negative (PBS) control with 20 μg/mL of capture antibody and 10 μg/mL of ALP-linked IgG. The bar graph shows the signal difference between the positive and negative control.

7.3.3 Optimization of the concentration of enzyme-linked secondary antibody

The optimal concentration of ALP-linked IgG was optimized after the optimization of the concentration of capture antibody and anti-CEA secondary antibody. As seen from Figure 7.5, the corrected brightness value of positive control (500 ng/mL of CEA) increased with the increase in concentration of ALP-linked IgG from 1 μg/mL to 6 μg/mL after which it reached a plateau and remained almost constant with any further increase in concentration of ALP-linked IgG from 6 μg/mL to 15 μg/mL. For the negative control (PBS) the corrected brightness value

remained constant with the increase in the concentration of ALP-linked IgG from 1 μg/mL to 6 μg/mL. As the concentration of ALP-linked IgG increased further from 6 μg/mL to 15 μg/mL, there was a rapid increase in the corrected brightness value (background noise). It could also be observed from Figure 7.5 that the signal difference between the positive control and the negative control was maximum at the ALP-linked IgG concentration of 6 μg/mL. Therefore, 6 μg/mL of ALP-linked IgG was considered as the optimum concentration and all the further assays were performed with 20 μg/mL of capture antibody, 10 μg/mL of anti-CEA secondary antibody, and 6 μg/mL of ALP-linked IgG.

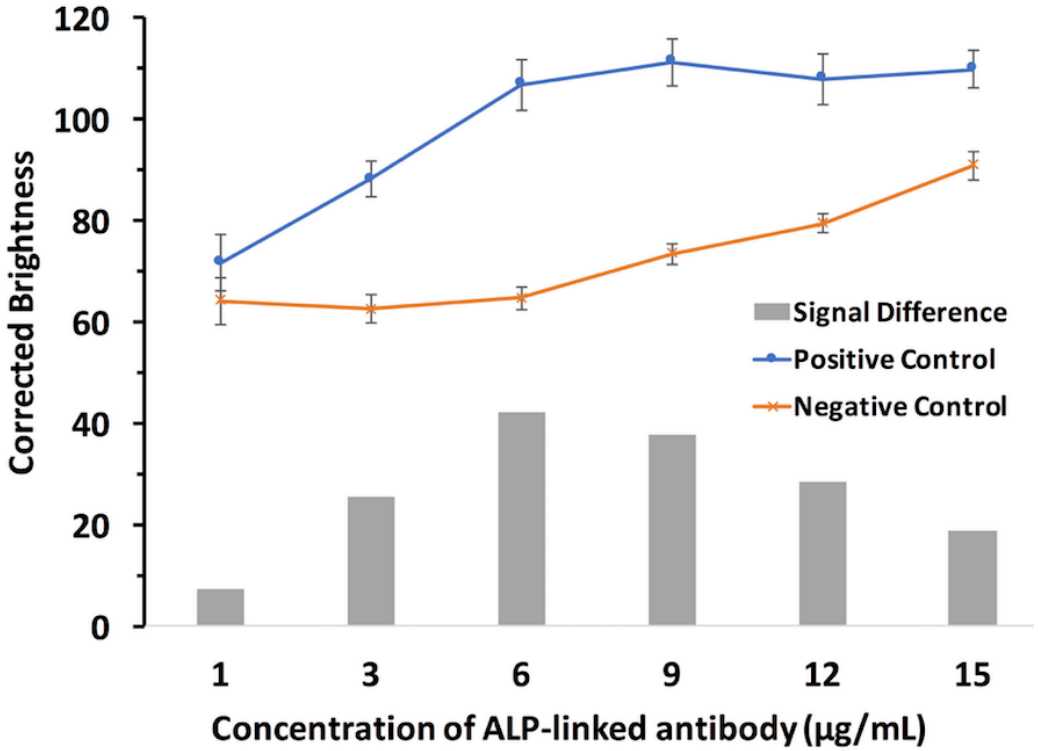

Figure 7.5: Optimization of the concentration of ALP-linked antibody. The line graph shows the corrected brightness value for the positive (500 ng/mL of CEA) and negative (PBS) control with 20 μg/mL of capture antibody and 10 μg/mL of anti-CEA secondary antibody. The bar graph shows the signal difference between the positive and negative control.

7.3.4 Colorimetric detection of cancer biomarkers in PiPP device

Rapid ELISA of the cancer biomarkers including CEA and PSA was achieved in the paper in PMMA pond hybrid device. Figure 7.6A shows the image scanned by a desktop scanner for the detection of CEA in a PiPP hybrid microfluidic device. It could be observed from the

figure that PBS showed the brightest color and 100 ng/mL CEA showed the darkest purple color, while the purple color intensity of other concentrations increased from 0.1 ng/mL to 100 ng/mL. After calculating the signal intensity of the scanned images by ImageJ, a calibration curve of concentration of CEA against the corrected brightness was plotted as seen in Figure 7.6B. Inset in Figure 7.6B shows that a linearity range was found over the clinically relevant range from 1 ng/mL to 100 ng/mL with a linear regression of $y = 27.05 \log (x) + 95.86$ ($R^2 = 0.98$). LOD of CEA using the hybrid PiPP microfluidic device was found to be 0.32 ng/mL based on 3-fold of SD above the blank value which was sensitive enough to detect the clinical cut off value of 5 ng/mL. Our device was more sensitive as compared to colorimetric immunoassay based upon gold nanoparticles (LOD of 2.32 ng/mL) and distance-based assay on microfluidic paper (LOD of 2 ng/mL).[223, 224] The sensitivity was comparable to microfluidic electrochemical detection (LOD of 0.20 ng/mL) and paper-based microfluidic device (LOD of 0.3 ng/mL).[225, 226]

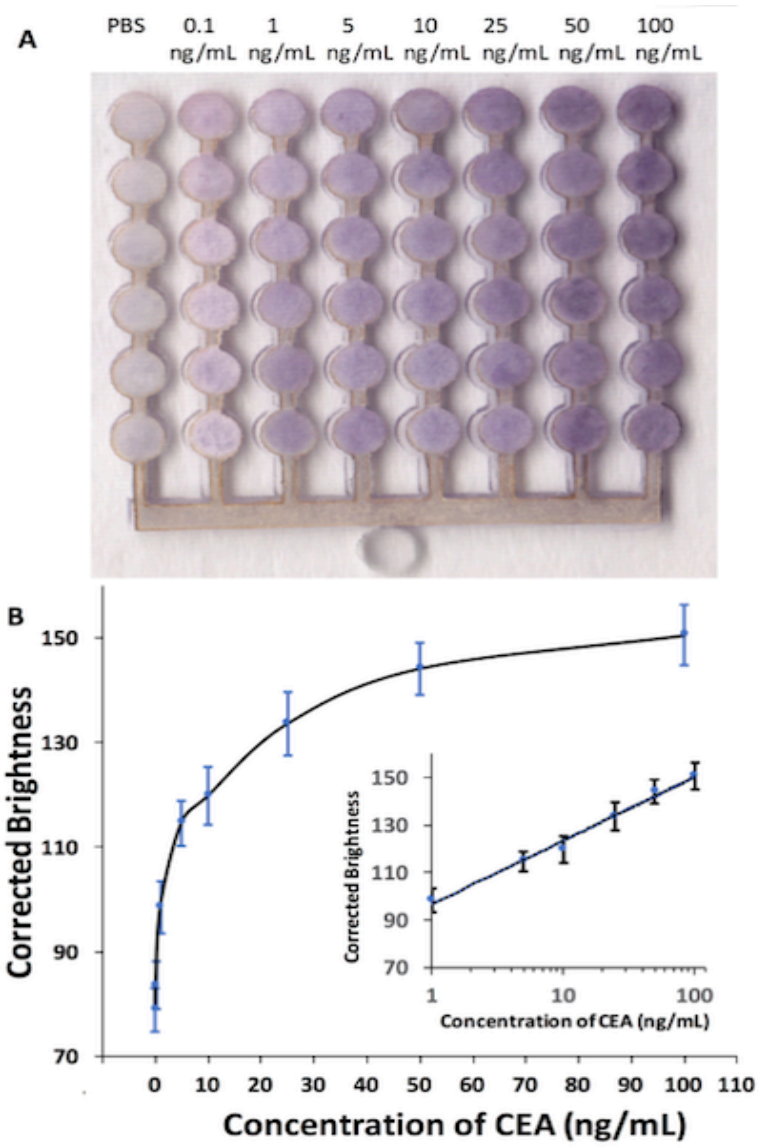

Figure 7.6: Rapid detection of CEA in a hybrid PiPP microfluidic device. (A) Scanned image of the paper substrate after the assay with negative control (PBS) and different CEA concentrations ranging from 0.1 ng/mL to 100 ng/mL by an office scanner. (B) Calibration curve for the detection of CEA as corrected brightness against the concentration of CEA. Inset shows the linear plot of the corrected brightness of CEA over a logarithmic concentration range from 1 ng/mL to 100 ng/mL.

Rapid colorimetric detection of PSA was carried out in the PiPP hybrid microfluidic device similar to the detection of CEA using the same optimized concentrations of different antibodies. Detection of PSA was performed in the range of 0.1 ng/mL to 100 ng/mL. Figure 7.7A shows the image scanned by a desktop scanner for the detection of PSA in a PiPP hybrid

microfluidic device. It could be observed that PBS showed the brightest color and 100 ng/mL PSA showed the darkest purple color. Figure 7.7B shows the calibration curve for the corrected brightness of different concentrations of PSA. Inset in Figure 7.7B shows that a linearity range was found over the clinically relevant range from 0.1 ng/mL to 100 ng/mL with a linear regression of $y = 16.26 \log (x) + 116.74$ ($R^2 = 0.988$). LOD of PSA using the hybrid PiPP microfluidic device was found to be 0.20 ng/mL based on 3-fold of SD above the blank value, which is sensitive enough to detect the clinical cut off value of 4 ng/mL. The sensitivity of the device was better than our previous nanoparticle-mediated bioassay using a thermometer (LOD of 1 ng/mL) and colorimetric assay (LOD of 1 ng/mL).[144, 145] Our device was also found to be equally sensitive as the microfluidic electrochemical detector which required a syringe pump (LOD of 0.20 ng/mL).[225]

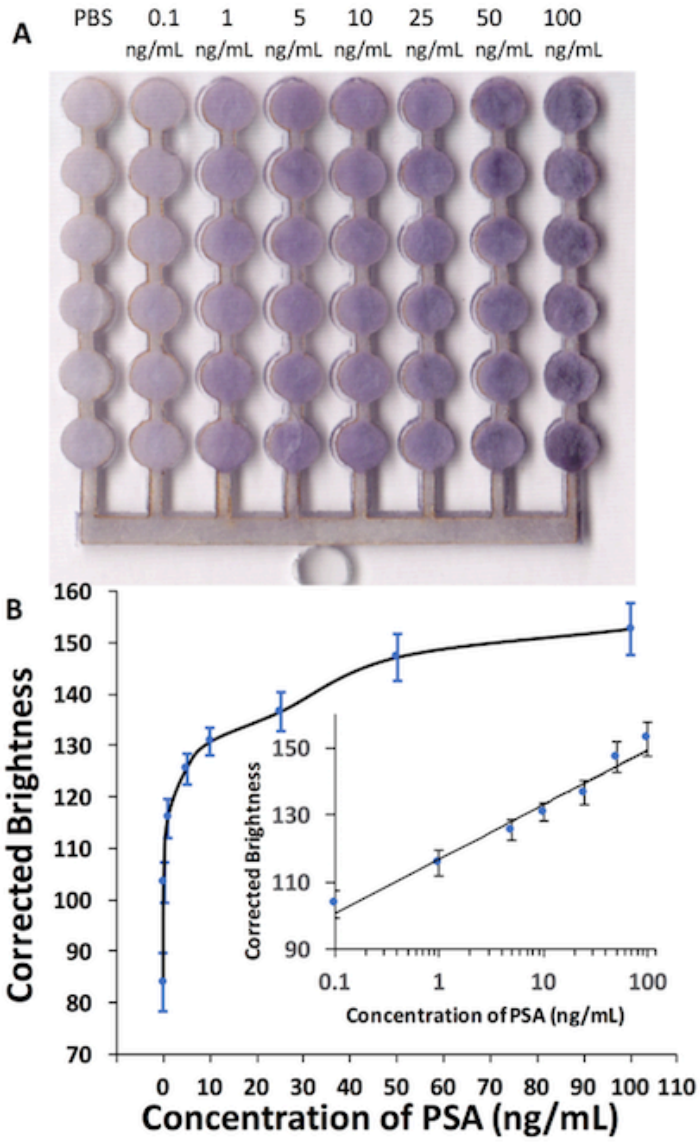

Figure 7.7: Rapid detection of PSA in a hybrid PiPP microfluidic device. (A) Scanned image of the paper substrate after the assay with negative control (PBS) and different PSA concentrations ranging from 0.1 ng/mL to 100 ng/mL by an office scanner. (B) Calibration curve for the detection of PSA as corrected brightness against the concentration of CEA. The inset shows the linear plot of the corrected brightness of CEA over a logarithmic concentration range from 1 ng/mL to 100 ng/mL.

7.4 Summary

The goal of this study was to develop a simple, POC paper in PMMA pond (PiPP) hybrid microfluidic device for the detection of cancer biomarkers. We have developed a highly sensitive colorimetric hybrid PiPP microfluidic device taking advantages of both the paper and PMMA substrates. The presence of the 3D micro-porous paper substrate within the pond-shaped

structure of the hybrid device ensures that proteins are immobilized within a short period of time without any complicated surface modifications, so that the assay can be completed within an hour and observed by the naked eye or can be scanned by a simple desktop scanner for quantitative analysis. A single paper substrate pre-fabricated using SU-8 can be added to the pond due to the presence of interconnected pond-shaped structure, which avoids the addition of paper substrate to individual microwells. Because of the presence of reagent delivery top layer and flow-through reservoirs kept just over the paper substrate, manual addition of reagent into each assay zone is eliminated. In addition, the flow-through reservoir aids in efficient washing thus decreasing the background noise and increasing the sensitivity of the ELISA. After the optimization of different antibodies, sandwich ELISA for cancer biomarkers including CEA and PSA was performed without the use of any specialized equipment. LODs of 0.32 ng/mL for CEA and 0.20 ng/mL for PSA were achieved, which were at least 10 folds better than commercial ELISA kits. This hybrid PiPP microfluidic device could be immensely valuable in POC settings for the screening of cancer biomarkers and may have wide application as a rapid, highly sensitive, and quantitative detection of infectious diseases, cancers, and other biomolecules.

Chapter 8: Conclusions and Perspectives

- This chapter describes the concluding remarks and future directions of the research work in this dissertation.

8.1 Concluding remarks

Five PMMA and paper/polymer hybrid microfluidic microplates have been developed for the detection of disease biomarkers. These devices provide low-cost, POC, and rapid detection of diseases. In this dissertation, sensitive and specific detection of infectious diseases including Hepatitis B and Hepatitis C and cancer biomarkers for Prostate and Colorectal cancer has been successfully demonstrated using these microfluidic microplates. In conclusion:

1. Surface modified PMMA microplate could remarkably increase the efficiency of surface immobilization of biomolecules including proteins in a short period of time (20 min) due to covalent immobilization. Multiplex detection of various biomarkers including IgG, HBsAg, and HBcAg were performed with LODs of 200 pg/mL, 180 pg/mL, and 300 pg/mL, respectively, which are 10-fold more sensitive than traditional microplates.
2. Different substrates have their own advantages and limitations. Polymer/paper hybrid microfluidic devices can draw more benefits from both the polymer and paper substrates and avoid some of their limitations.
3. Introduction of the low-cost 3D paper substrate with a high surface to volume ratio within the funnel-shaped, flow-through microwells in the paper/polymer hybrid device ensures rapid immobilization of proteins within 10 min and efficient washing, decreasing the background noise.
4. The top reagent delivery channels in the hybrid device can transfer reagents to multiple flow-through microwells, avoiding repeated manual pipetting to all the microwells or the use of costly robots. LODs of 1.3 ng/mL and 1.6 ng/mL for IgG and HBsAg were achieved without any specialized equipment, which were comparable to commercially used microplate ELISA.
5. In addition, for the device to have wider applications in high-end laboratories and hospitals, the hybrid device was redesigned to make it compatible with traditional microplate readers. Chemiluminescence ELISAs of HBsAg, HBcAg, and HCVcAg

were performed in the hybrid device with LODs of 50 pg/mL, 35 pg/mL, and 10 pg/mL, respectively, using commercial microplate reader to read the device. The sensitivity was about 100-fold better than the traditional microplates.

6. To further increase the sensitivity of the colorimetric device to measure low-concentration analytes, a reusable plug-and-play hybrid device was developed. The sample flows back and forth through the 3D paper substrate within the PMMA channels thereby enriching the amount of analyte adsorbed and dramatically decreasing the incubation time. The paper substrate could be replaced so that the device can be reused. LODs of 200 pg/mL and 270 pg/mL were obtained for IgG and HBsAg, respectively, which were 10-fold better than commercial microplate readers. A wide linear range of five and six orders of magnitude were obtained for IgG and HBsAg, respectively.
7. The broader application of our microfluidic approach was further demonstrated by simultaneous multiplex detection of cancer biomarkers including PSA and CEA with high specificity and sensitivity. LODs of CEA and PSA were found to be 0.32 ng/mL and 0.20 ng/mL, respectively, which were 10-fold more sensitive than the clinical cut off value of 5 ng/mL and 4 ng/mL for CEA and PSA, respectively.
8. PMMA and paper/polymer hybrid microfluidic microplates demonstrated great potential applications in both underdeveloped and developed countries for low-cost, sensitive, and high-throughput bioassays of infectious diseases, cancer biomarkers, and other bio-molecules.

8.2 Future directions

8.2.1 On-chip separation of blood plasma

Pure protein samples dissolved in PBS was used for the detection of Immunoglobulin G, Hepatitis B surface antigen, Hepatitis B core antigen, Hepatitis C virus core antigen, Prostate-specific antigen, and Carcinoembryonic antigen in this dissertation. But, for the validation of the

reliability of the proposed colorimetric and chemiluminescence assay, the detection of the biomarkers was carried out in the real human serum sample. Blood serum is usually obtained by using a centrifuge. After the clotting of blood at room temperature, serum is separated by centrifuging at around 1,600 g for 15 min, which is not suitable for POC detection. There are different kind of POC devices to separate serum from the blood which are commercially available. But the on-chip separation of blood plasma followed by detection of disease biomarkers within the single biochip would be ideal. Plasma could be separated within the device by using different techniques such as placing a blood filtering membrane inside the inlet microwell which can separate plasma from pure blood. Other techniques such as lateral displacement and hydrodynamic flow separation could also be used but are relatively more complicated than filtration. That kind of devices will find broader application in POC settings.

8.2.2 Test of clinical samples

As mentioned earlier the validation of the reliability of the proposed colorimetric and chemiluminescence assay was performed by spiking the pure protein in human serum samples. The hybrid and surface modified devices need to be further validated by testing clinical samples of Hepatitis B, Hepatitis C, Prostate cancer, and Colorectal cancer. The data can be further validated by performing the ELISA of these biomarkers using commercially available 96-well ELISA kits. The data obtained from the microfluidic devices need to be compared statistically with the standard method including PCR and microplate ELISA to see if the result matches the performance of the established techniques. In addition, sensitivity, specificity, false positive, and false negative values need to be calculated with preferably 50 or more clinical samples.

8.2.3 Field validation

The major aim of this kind of microfluidic devices is to have a broad application in POC settings. Therefore, instead of conducting these assays in a clean and well-equipped laboratory setting, field validation and testing of hepatitis B & C at a physician's offices, a school/college health center or other resource-limited settings is needed in the future. For instance, detection of

hepatitis B could be directly performed in the field using patient's blood sample in underdeveloped places like African region. In this way, the utility of PMMA and paper/polymer hybrid microfluidic microplates for detection of infectious diseases and cancer biomarkers can be validated.

8.2.4 Mobile application for data analysis

All the colorimetric data analysis for different projects in this dissertation was accomplished using a desktop-based ImageJ after scanning devices with a common office scanner. For POC analysis, cell phone camera can be used to take the image of the device. Although different kinds of application including an application based upon ImageJ is available for data analysis, these applications are not user-friendly for our devices. It is difficult to measure so many microwells using the cell phone based application. In future, it is better to develop the application which can easily take a picture or upload the existing picture of our device with assay result and give the final result in a user-friendly way. It would be ideal if the application could recognize the pattern of the device and measure the value of all the microwells at a time.

8.2.5 Broad application of the hybrid devices

This dissertation demonstrates the application of several PMMA and paper/polymer hybrid microfluidic microplates for the detection of disease biomarkers. By changing the capture antibody, other pathogens that cause epidemics, such as Zika, foodborne pathogens, chikungunya, cholera, and Ebola could be tested on the microfluidic devices for rapid POC detection. Likewise, different kinds of cancer such as lung cancer and breast cancer could also be detected at early stages using our microfluidic microplates. In addition, the hybrid microfluidic devices should have a variety of applications, such as 3D cell culture, drug discovery and drug test, chemical synthesis, and so on.

8.2.6 Panel-based detection of diseases

The hybrid device could be further modified to perform a panel-based detection of different diseases. For instance, it could be simultaneously used for detection of viral sexually

transmitted diseases (STDs). Different kind of STDs can co-exist together and it could save a lot of money and resources if different STDs including HIV, Herpes, hepatitis B virus could be detected in a single chip. In future, different conditions could be optimized so that rapid 5 min test can be performed with this kind of device.

References:

(1) Aydin, S. A short history, principles, and types of ELISA, and our laboratory experience with peptide/protein analyses using ELISA, *Peptides* **2015**, *72*, 4-15.

(2) Martinez, A. W.; Phillips, S. T.; Wiley, B. J.; Gupta, M.; Whitesides, G. M. FLASH: a rapid method for prototyping paper-based microfluidic devices, *Lab on a Chip* **2008**, *8*, 2146-2150.

(3) Dou, M.; Dominguez, D. C.; Li, X.; Sanchez, J.; Scott, G. A versatile PDMS/paper hybrid microfluidic platform for sensitive infectious disease diagnosis, *Analytical chemistry* **2014**, *86*, 7978-7986.

(4) Brown, L.; Koerner, T.; Horton, J. H.; Oleschuk, R. D. Fabrication and characterization of poly (methylmethacrylate) microfluidic devices bonded using surface modifications and solvents, *Lab on a Chip* **2006**, *6*, 66-73.

(5) Sanjay, S. T.; Dou, M.; Sun, J.; Li, X. A paper/polymer hybrid microfluidic microplate for rapid quantitative detection of multiple disease biomarkers, *Scientific reports* **2016**, *6*, 30474.

(6) Tsai, H.; Chan, J.; Li, Y.; Cheng, F.; Fuh, C. B. Determination of hepatitis B surface antigen using magnetic immunoassays in a thin channel, *Biosensors and Bioelectronics* **2010**, *25*, 2701-2705.

(7) Lozano, R.; Naghavi, M.; Foreman, K.; Lim, S.; Shibuya, K.*, et al*. Global and regional mortality from 235 causes of death for 20 age groups in 1990 and 2010: a systematic analysis for the Global Burden of Disease Study 2010, *The lancet* **2012**, *380*, 2095-2128.

(8) Nelson, K. E.; Williams, C. M. *Infectious disease epidemiology*; Jones & Bartlett Publishers, 2013.

(9) Yang, S.; Rothman, R. E. PCR-based diagnostics for infectious diseases: uses, limitations, and future applications in acute-care settings, *The Lancet infectious diseases* **2004**, *4*, 337-348.

(10) Jones, K. E.; Patel, N. G.; Levy, M. A.; Storeygard, A.; Balk, D.*, et al*. Global trends in emerging infectious diseases, *Nature* **2008**, *451*, 990-993.

(11) Morens, D. M.; Folkers, G. K.; Fauci, A. S. The challenge of emerging and re-emerging infectious diseases, *Nature* **2004**, *430*, 242-249.

(12) Fauci, A. S.; Morens, D. M. The perpetual challenge of infectious diseases, *New England Journal of Medicine* **2012**, *366*, 454-461.

(13) Delaney, W. E. Molecular virology of chronic hepatitis B and C: parallels, contrasts and impact on drug development and treatment outcome, *Antiviral research* **2013**, *99*, 34-48.

(14) Hollinger, F. B.; Lau, D. T.-Y. Hepatitis B: the pathway to recovery through treatment, *Gastroenterology Clinics of North America* **2006**, *35*, 425-461.

(15) Ganem, D.; Prince, A. M. Hepatitis B virus infection—natural history and clinical consequences, *New England Journal of Medicine* **2004**, *350*, 1118-1129.

(16) Trépo, C.; Chan, H. L.; Lok, A. Hepatitis B virus infection, *The Lancet* **2014**, *384*, 2053-2063.

(17) Lai, C. L.; Ratziu, V.; Yuen, M.-F.; Poynard, T. Viral hepatitis B, *The Lancet* **2003**, *362*, 2089-2094.

(18) Organization, W. H. O, 2014.

(19) El-Serag, H. B. Epidemiology of viral hepatitis and hepatocellular carcinoma, *Gastroenterology* **2012**, *142*, 1264-1273. e1261.

(20) Weinbaum, C. M.; Williams, I.; Mast, E. E.; Wang, S. A.; Finelli, L., *et al*. Recommendations for identification and public health management of persons with chronic hepatitis B virus infection, *MMWR Recomm Rep* **2008**, *57*, 1-20.
(21) Marcellin, P.; Gane, E.; Buti, M.; Afdhal, N.; Sievert, W., *et al*. Regression of cirrhosis during treatment with tenofovir disoproxil fumarate for chronic hepatitis B: a 5-year open-label follow-up study, *The Lancet* **2013**, *381*, 468-475.
(22) Rosenberg, S. Recent advances in the molecular biology of hepatitis C virus1, *Journal of molecular biology* **2001**, *313*, 451-464.
(23) Mohd Hanafiah, K.; Groeger, J.; Flaxman, A. D.; Wiersma, S. T. Global epidemiology of hepatitis C virus infection: New estimates of age‐specific antibody to HCV seroprevalence, *Hepatology* **2013**, *57*, 1333-1342.
(24) Perz, J. F.; Armstrong, G. L.; Farrington, L. A.; Hutin, Y. J.; Bell, B. P. The contributions of hepatitis B virus and hepatitis C virus infections to cirrhosis and primary liver cancer worldwide, *Journal of hepatology* **2006**, *45*, 529-538.
(25) Lavanchy, D. Evolving epidemiology of hepatitis C virus, *Clin Microbiol Infec* **2011**, *17*, 107-115.
(26) Howlader, N.; Noone, A.; Krapcho, M.; Garshell, J.; Miller, D., *et al*., 2014.
(27) Siegel, R. L.; Miller, K. D.; Jemal, A. Cancer statistics, 2015, *CA: a cancer journal for clinicians* **2015**, *65*, 5-29.
(28) Ferlay, J.; Soerjomataram, I.; Dikshit, R.; Eser, S.; Mathers, C., *et al*. Cancer incidence and mortality worldwide: sources, methods and major patterns in GLOBOCAN 2012, *International Journal of Cancer* **2015**, *136*, E359-E386.
(29) Unger-Saldaña, K. Challenges to the early diagnosis and treatment of breast cancer in developing countries, *World journal of clinical oncology* **2014**, *5*, 465.
(30) Kanavos, P. The rising burden of cancer in the developing world, *Annals of oncology* **2006**, *17*, viii15-viii23.
(31) Grönberg, H. Prostate cancer epidemiology, *The Lancet* **2003**, *361*, 859-864.
(32) Ferlay, J.; Soerjomataram, I.; Dikshit, R.; Eser, S.; Mathers, C., *et al*. Cancer incidence and mortality worldwide: sources, methods and major patterns in GLOBOCAN 2012, *International journal of cancer* **2015**, *136*.
(33) Tenke, P.; Horti, J.; Balint, P.; Kovacs, B. In *Prostate Cancer*; Springer, 2007, pp 65-81.
(34) Sarrats, A.; Comet, J.; Tabarés, G.; Ramírez, M.; Aleixandre, R. N., *et al*. Differential percentage of serum prostate‐specific antigen subforms suggests a new way to improve prostate cancer diagnosis, *The Prostate* **2010**, *70*, 1-9.
(35) Aran, V.; Victorino, A. P.; Thuler, L. C.; Ferreira, C. G. Colorectal cancer: epidemiology, disease mechanisms and interventions to reduce onset and mortality, *Clinical colorectal cancer* **2016**, *15*, 195-203.
(36) Arnold, M.; Sierra, M. S.; Laversanne, M.; Soerjomataram, I.; Jemal, A., *et al*. Global patterns and trends in colorectal cancer incidence and mortality, *Gut* **2016**, gutjnl-2015-310912.
(37) Sanjay, S. T.; Fu, G.; Dou, M.; Xu, F.; Liu, R., *et al*. Biomarker detection for disease diagnosis using cost-effective microfluidic platforms, *Analyst* **2015**, *140*, 7062-7081.
(38) Brouwer, M. C.; Tunkel, A. R.; van de Beek, D. Epidemiology, diagnosis, and antimicrobial treatment of acute bacterial meningitis, *Clinical Microbiology Reviews* **2010**, *23*, 467-492.

(39) Dubos, F.; Moulin, F.; Gajdos, V.; De Suremain, N.; Biscardi, S., *et al*. Serum procalcitonin and other biologic markers to distinguish between bacterial and aseptic meningitis, *The Journal of Pediatrics* **2006**, *149*, 72-76.
(40) Fry, N. K.; Tzivra, O.; Li, Y. T.; McNiff, A.; Doshi, N., *et al*. Laboratory diagnosis of pertussis infections: the role of PCR and serology, *Journal of Medical Microbiology* **2004**, *53*, 519-525.
(41) Pai, M.; Flores, L. L.; Pai, N.; Hubbard, A.; Riley, L. W., *et al*. Diagnostic accuracy of nucleic acid amplification tests for tuberculous meningitis: a systematic review and meta-analysis, *The Lancet Infectious Diseases* **2003**, *3*, 633-643.
(42) Neuman, M. I.; Tolford, S.; Harper, M. B. Test Characteristics and Interpretation of Cerebrospinal Fluid Gram Stain in Children, *The Pediatric Infectious Disease Journal* **2008**, *27*, 309-313 310.1097/INF.1090b1013e31815f31853ba.
(43) Sidransky, D. Nucleic acid-based methods for the detection of cancer, *Science* **1997**, *278*, 1054-1058.
(44) Urdea, M.; Penny, L. A.; Olmsted, S. S.; Giovanni, M. Y.; Kaspar, P., *et al*. Requirements for high impact diagnostics in the developing world, *Nature* **2006**, *444*, 73-79.
(45) Cherry, J. D.; Grimprel, E.; Guiso, N.; Heininger, U.; Mertsola, J. Defining pertussis epidemiology: clinical, microbiologic and serologic perspectives, *The Pediatric infectious disease journal* **2005**, *24*, S25-S34.
(46) Wang, X.; Theodore, M. J.; Mair, R.; Trujillo-Lopez, E.; du Plessis, M., *et al*. Clinical validation of multiplex real-time PCR assays for detection of bacterial meningitis pathogens, *Journal of Clinical Microbiology* **2012**, *50*, 702-708.
(47) Lee, D.; Kim, E. J.; Kilgore, P. E.; Kim, S. A.; Takahashi, H., *et al*. Clinical evaluation of a loop-mediated isothermal amplification (LAMP) assay for rapid detection of Neisseria meningitidis in cerebrospinal fluid, *PloS One* **2015**.
(48) Resti, M.; Micheli, A.; Moriondo, M.; Becciolini, L.; Cortimiglia, M., *et al*. Comparison of the effect of antibiotic treatment on the possibility of diagnosing invasive pneumococcal disease by culture or molecular methods: a prospective, observational study of children and adolescents with proven pneumococcal infection, *Clinical Therapeutics* **2009**, *31*, 1266-1273.
(49) Kamili, S.; Drobeniuc, J.; Araujo, A. C.; Hayden, T. M. Laboratory diagnostics for hepatitis C virus infection, *Clin Infect Dis* **2012**, *55*, S43-S48.
(50) Gan, S. D.; Patel, K. R. Enzyme immunoassay and enzyme-linked immunosorbent assay, *Journal of Investigative Dermatology* **2013**, *133*, 1-3.
(51) Limbut, W.; Kanatharana, P.; Mattiasson, B.; Asawatreratanakul, P.; Thavarungkul, P. A reusable capacitive immunosensor for carcinoembryonic antigen (CEA) detection using thiourea modified gold electrode, *Analytica chimica acta* **2006**, *561*, 55-61.
(52) Kai, J.; Puntambekar, A.; Santiago, N.; Lee, S. H.; Sehy, D. W., *et al*. A novel microfluidic microplate as the next generation assay platform for enzyme linked immunoassays (ELISA), *Lab on a Chip* **2012**, *12*, 4257-4262.
(53) Salieb-Beugelaar, G. B.; Simone, G.; Arora, A.; Philippi, A.; Manz, A. Latest Developments in Microfluidic Cell Biology and Analysis Systems, *Analytical Chemistry* **2010**, *82*, 4848-4864.
(54) Volpatti, L. R.; Yetisen, A. K. Commercialization of microfluidic devices, *Trends in Biotechnology* **2014**, *32*, 347-350.

(55) Dou, M.; Sanjay, S. T.; Benhabib, M.; Xu, F.; Li, X. Low-cost bioanalysis on paper-based and its hybrid microfluidic platforms, *Talanta* **2015**, *145*, 43-54.
(56) Gubala, V.; Harris, L. F.; Ricco, A. J.; Tan, M. X.; Williams, D. E. Point of care diagnostics: status and future, *Analytical Chemistry* **2011**, *84*, 487-515.
(57) Xu, X.; Akay, A.; Wei, H.; Wang, S.; Pingguan-Murphy, B., *et al*. Advances in smartphone-based point-of-care diagnostics, *Proceedings of the IEEE* **2015**, *103*, 236-247.
(58) Dou, M.; García, J. M.; Zhan, S.; Li, X. Interfacial nano-biosensing in microfluidic droplets for high-sensitivity detection of low-solubility molecules, *Chemical Communications* **2016**, *52*, 3470-3473.
(59) Liu, P.; Li, X.; Greenspoon, S. A.; Scherer, J. R.; Mathies, R. A. Integrated DNA purification, PCR, sample cleanup, and capillary electrophoresis microchip for forensic human identification, *Lab on a Chip* **2011**, *11*, 1041-1048.
(60) Shen, F.; Li, X.; Li, P. C. Study of flow behaviors on single-cell manipulation and shear stress reduction in microfluidic chips using computational fluid dynamics simulations, *Biomicrofluidics* **2014**, *8*, 014109.
(61) Li, X.; Valadez, A. V.; Zuo, P.; Nie, Z. Microfluidic 3D cell culture: potential application for tissue-based bioassays, *Bioanalysis* **2012**, *4*, 1509-1525.
(62) Li, X. J.; Zhou, Y. *Microfluidic devices for biomedical applications*; Elsevier, 2013.
(63) Fu, G.; Sanjay, S. T.; Dou, M.; Li, X. J. Nanoparticle-mediated photothermal effect enables a new method for quantitative biochemical analysis using a thermometer, *Nanoscale* **2016**, *8*, 5422-5427.
(64) Zhang, J.; Sheng, W.; Fan, Z. H. An ensemble of aptamers and antibodies for multivalent capture of cancer cells, *Chemical Communications* **2014**, *50*, 6722-6725.
(65) Hu, J.; Wang, S.; Wang, L.; Li, F.; Pingguan-Murphy, B., *et al*. Advances in paper-based point-of-care diagnostics, *Biosensors and Bioelectronics* **2014**, *54*, 585-597.
(66) Tian, T.; Li, J.; Song, Y.; Zhou, L.; Zhu, Z., *et al*. Distance-based microfluidic quantitative detection methods for point-of-care testing, *Lab on a Chip* **2016**, *16*, 1139-1151.
(67) Sanjay, S. T.; Dou, M.; Fu, G.; Xu, F.; Li, X. Controlled drug delivery using microdevices, *Current Pharmaceutical Biotechnology* **2016**, *17*, 772-787.
(68) Wang, C.; Ye, M.; Cheng, L.; Li, R.; Zhu, W., *et al*. Simultaneous isolation and detection of circulating tumor cells with a microfluidic silicon-nanowire-array integrated with magnetic upconversion nanoprobes, *Biomaterials* **2015**, *54*, 55-62.
(69) Herranz-Blanco, B.; Arriaga, L. R.; Mäkilä, E.; Correia, A.; Shrestha, N., *et al*. Microfluidic assembly of multistage porous silicon–lipid vesicles for controlled drug release, *Lab on a Chip* **2014**, *14*, 1083-1086.
(70) Choi, H.; Kim, K. B.; Jeon, C. S.; Hwang, I.; Lee, S., *et al*. A label-free DC impedance-based microcytometer for circulating rare cancer cell counting, *Lab on a Chip* **2013**, *13*, 970-977.
(71) Li, X.; Chen, Y.; Li, P. C. A simple and fast microfluidic approach of same-single-cell analysis (SASCA) for the study of multidrug resistance modulation in cancer cells, *Lab on a Chip* **2011**, *11*, 1378-1384.
(72) Li, X.; Ling, V.; Li, P. C. Same-single-cell analysis for the study of drug efflux modulation of multidrug resistant cells using a microfluidic chip, *Analytical Chemistry* **2008**, *80*, 4095-4102.

(73) Tennico, Y. H.; Koesdjojo, M. T.; Kondo, S.; Mandrell, D. T.; Remcho, V. T. Surface modification-assisted bonding of polymer-based microfluidic devices, *Sensors and Actuators B: Chemical* **2010**, *143*, 799-804.
(74) Wang, J. D.; Douville, N. J.; Takayama, S.; ElSayed, M. Quantitative analysis of molecular absorption into PDMS microfluidic channels, *Annals of biomedical engineering* **2012**, *40*, 1862-1873.
(75) Hong, T.-F.; Ju, W.-J.; Wu, M.-C.; Tai, C.-H.; Tsai, C.-H., *et al*. Rapid prototyping of PMMA microfluidic chips utilizing a CO2 laser, *Microfluidics and nanofluidics* **2010**, *9*, 1125-1133.
(76) Ashley, J. F.; Cramer, N. B.; Davis, R. H.; Bowman, C. N. Soft-lithography fabrication of microfluidic features using thiol-ene formulations, *Lab on a Chip* **2011**, *11*, 2772-2778.
(77) Xia, Y.; Whitesides, G. M. Soft lithography, *Annual review of materials science* **1998**, *28*, 153-184.
(78) Nie, Z.; Nijhuis, C. A.; Gong, J.; Chen, X.; Kumachev, A., *et al*. Electrochemical sensing in paper-based microfluidic devices, *Lab on a Chip* **2010**, *10*, 477-483.
(79) Leclerc, E.; Sakai, Y.; Fujii, T. Cell culture in 3-dimensional microfluidic structure of PDMS (polydimethylsiloxane), *Biomed Microdevices* **2003**, *5*, 109-114.
(80) Huh, D.; Matthews, B. D.; Mammoto, A.; Montoya-Zavala, M.; Hsin, H. Y., *et al*. Reconstituting organ-level lung functions on a chip, *Science* **2010**, *328*, 1662-1668.
(81) Huh, D.; Hamilton, G. A.; Ingber, D. E. From 3D cell culture to organs-on-chips, *Trends in Cell Biology* **2011**, *21*, 745-754.
(82) Sia, S. K.; Whitesides, G. M. Microfluidic devices fabricated in poly (dimethylsiloxane) for biological studies, *Electrophoresis* **2003**, *24*, 3563-3576.
(83) Toepke, M. W.; Beebe, D. J. PDMS absorption of small molecules and consequences in microfluidic applications, *Lab on a Chip* **2006**, *6*, 1484-1486.
(84) Fujii, T. PDMS-based microfluidic devices for biomedical applications, *Microelectronic Engineering* **2002**, *61*, 907-914.
(85) Devaraju, N. S. G. K.; Unger, M. A. Multilayer soft lithography of perfluoropolyether based elastomer for microfluidic device fabrication, *Lab on a Chip* **2011**, *11*, 1962-1967.
(86) Mathur, A.; Roy, S. S.; Tweedie, M.; Mukhopadhyay, S.; Mitra, S. K., *et al*. Characterisation of PMMA microfluidic channels and devices fabricated by hot embossing and sealed by direct bonding, *Current Applied Physics* **2009**, *9*, 1199-1202.
(87) Rasooly, R.; Bruck, H. A.; Balsam, J.; Prickril, B.; Ossandon, M., *et al*. Improving the sensitivity and functionality of mobile webcam-based fluorescence detectors for point-of-care diagnostics in global health, *Diagnostics* **2016**, *6*, 19.
(88) Bai, Y.; Koh, C. G.; Boreman, M.; Juang, Y.-J.; Tang, I. C., *et al*. Surface modification for enhancing antibody binding on polymer-based microfluidic device for enzyme-linked immunosorbent assay, *Langmuir* **2006**, *22*, 9458-9467.
(89) Wu, N.; Zhu, Y.; Brown, S.; Oakeshott, J.; Peat, T. S., *et al*. A PMMA microfluidic droplet platform for in vitro protein expression using crude E. coli S30 extract, *Lab on a Chip* **2009**, *9*, 3391-3398.
(90) Graß, B.; Neyer, A.; Jöhnck, M.; Siepe, D.; Eisenbeiß, F., *et al*. A new PMMA-microchip device for isotachophoresis with integrated conductivity detector, *Sensors and Actuators B: Chemical* **2001**, *72*, 249-258.
(91) Becker, H.; Heim, U. Hot embossing as a method for the fabrication of polymer high aspect ratio structures, *Sensors and Actuators A: Physical* **2000**, *83*, 130-135.

(92) Comina, G.; Suska, A.; Filippini, D. PDMS lab-on-a-chip fabrication using 3D printed templates, *Lab on a Chip* **2014**, *14*, 424-430.
(93) Yang, C.-S.; Lin, C.-H.; Zaytsev, A.; Teng, K.-C.; Her, T.-H., *et al*. Femtosecond laser ablation of polymethylmethacrylate via dual-color synthesized waveform, *Applied Physics Letters* **2015**, *106*, 051902.
(94) Martinez, A. W.; Phillips, S. T.; Butte, M. J.; Whitesides, G. M. Patterned paper as a platform for inexpensive, low‐volume, portable bioassays, *Angewandte Chemie International Edition* **2007**, *46*, 1318-1320.
(95) Yetisen, A. K.; Akram, M. S.; Lowe, C. R. based microfluidic point-of-care diagnostic devices, *Lab on a Chip* **2013**, *13*, 2210-2251.
(96) Lu, Y.; Shi, W.; Jiang, L.; Qin, J.; Lin, B. Rapid prototyping of paper‐based microfluidics with wax for low‐cost, portable bioassay, *Electrophoresis* **2009**, *30*, 1497-1500.
(97) Li, X.; Tian, J.; Garnier, G.; Shen, W. Fabrication of paper-based microfluidic sensors by printing, *Colloids and Surfaces B: Biointerfaces* **2010**, *76*, 564-570.
(98) Dungchai, W.; Chailapakul, O.; Henry, C. S. A low-cost, simple, and rapid fabrication method for paper-based microfluidics using wax screen-printing, *Analyst* **2011**, *136*, 77-82.
(99) He, Q.; Ma, C.; Hu, X.; Chen, H. Method for fabrication of paper-based microfluidic devices by alkylsilane self-assembling and UV/O3-patterning, *Analytical chemistry* **2013**, *85*, 1327-1331.
(100) Olkkonen, J.; Lehtinen, K.; Erho, T. Flexographically printed fluidic structures in paper, *Analytical chemistry* **2010**, *82*, 10246-10250.
(101) Fu, E.; Lutz, B.; Kauffman, P.; Yager, P. Controlled reagent transport in disposable 2D paper networks, *Lab on a Chip* **2010**, *10*, 918-920.
(102) Thuo, M. M.; Martinez, R. V.; Lan, W.-J.; Liu, X.; Barber, J., *et al*. Fabrication of low-cost paper-based microfluidic devices by embossing or cut-and-stack methods, *Chemistry of Materials* **2014**, *26*, 4230-4237.
(103) Becker, H.; Locascio, L. E. Polymer microfluidic devices, *Talanta* **2002**, *56*, 267-287.
(104) Wongkaew, N.; He, P.; Kurth, V.; Surareungchai, W.; Baeumner, A. J. Multi-channel PMMA microfluidic biosensor with integrated IDUAs for electrochemical detection, *Analytical and Bioanalytical Chemistry* **2013**, *405*, 5965-5974.
(105) Nogi, M.; Iwamoto, S.; Nakagaito, A. N.; Yano, H. Optically transparent nanofiber paper, *Advanced materials* **2009**, *21*, 1595-1598.
(106) Zhu, H.; Fang, Z.; Preston, C.; Li, Y.; Hu, L. Transparent paper: fabrications, properties, and device applications, *Energy & Environmental Science* **2014**, *7*, 269-287.
(107) Zuo, P.; Li, X.; Dominguez, D. C.; Ye, B.-C. A PDMS/paper/glass hybrid microfluidic biochip integrated with aptamer-functionalized graphene oxide nano-biosensors for one-step multiplexed pathogen detection, *Lab on a Chip* **2013**, *13*, 3921-3928.
(108) Choi, J. R.; Liu, Z.; Hu, J.; Tang, R.; Gong, Y., *et al*. Polydimethylsiloxane-paper hybrid lateral flow assay for highly sensitive point-of-care nucleic acid testing, *Analytical chemistry* **2016**, *88*, 6254-6264.
(109) Darain, F.; Wahab, M. A.; Tjin, S. C. Surface activation of poly (methyl methacrylate) by plasma treatment: stable antibody immobilization for microfluidic enzyme-linked immunosorbent assay, *Analytical Letters* **2012**, *45*, 2569-2579.

(110) Hosseini, S.; Ibrahim, F.; Djordjevic, I.; Koole, L. H. Recent advances in surface functionalization techniques on polymethacrylate materials for optical biosensor applications, *Analyst* **2014**, *139*, 2933-2943.
(111) Bai, Y.; Koh, C. G.; Boreman, M.; Juang, Y.-J.; Tang, I.-C., *et al*. Surface modification for enhancing antibody binding on polymer-based microfluidic device for enzyme-linked immunosorbent assay, *Langmuir* **2006**, *22*, 9458-9467.
(112) Kim, D.; Herr, A. E. Protein immobilization techniques for microfluidic assays, *Biomicrofluidics* **2013**, *7*, 041501.
(113) Llopis, S. L.; Osiri, J.; Soper, S. A. Surface modification of poly (methyl methacrylate) microfluidic devices for high‐resolution separations of single‐stranded DNA, *Electrophoresis* **2007**, *28*, 984-993.
(114) Liu, Y.; Wang, H.; Huang, J.; Yang, J.; Liu, B., *et al*. Microchip-based ELISA strategy for the detection of low-level disease biomarker in serum, *Analytica chimica acta* **2009**, *650*, 77-82.
(115) Nugen, S. R.; Asiello, P. J.; Connelly, J. T.; Baeumner, A. J. PMMA biosensor for nucleic acids with integrated mixer and electrochemical detection, *Biosensors and Bioelectronics* **2009**, *24*, 2428-2433.
(116) Goddard, J. M.; Hotchkiss, J. Polymer surface modification for the attachment of bioactive compounds, *Progress in polymer science* **2007**, *32*, 698-725.
(117) Song, F.; Chan, W. C. Principles of conjugating quantum dots to proteins via carbodiimide chemistry, *Nanotechnology* **2011**, *22*, 494006.
(118) Thorek, D. L.; Tsourkas, A. Comparative analysis of nanoparticle-antibody conjugations: carbodiimide versus click chemistry, *Molecular imaging* **2009**, *8*, 7290.2009. 00021.
(119) Gao, Y.; Kyratzis, I. Covalent immobilization of proteins on carbon nanotubes using the cross-linker 1-ethyl-3-(3-dimethylaminopropyl) carbodiimide—a critical assessment, *Bioconjugate chemistry* **2008**, *19*, 1945-1950.
(120) Jeon, O.; Kang, S.-W.; Lim, H.-W.; Chung, J. H.; Kim, B.-S. Long-term and zero-order release of basic fibroblast growth factor from heparin-conjugated poly (L-lactide-co-glycolide) nanospheres and fibrin gel, *Biomaterials* **2006**, *27*, 1598-1607.
(121) Cobo, I.; Li, M.; Sumerlin, B. S.; Perrier, S. Smart hybrid materials by conjugation of responsive polymers to biomacromolecules, *Nature materials* **2015**, *14*, 143-159.
(122) Riccardi, C. M.; Cole, K. S.; Benson, K. R.; Ward, J. R.; Bassett, K. M., *et al*. Toward "Stable-on-the-Table" Enzymes: Improving Key Properties of Catalase by Covalent Conjugation with Poly (acrylic acid), *Bioconjugate chemistry* **2014**, *25*, 1501-1510.
(123) Khnouf, R.; Karasneh, D.; Albiss, B. A. Protein immobilization on the surface of polydimethylsiloxane and polymethyl methacrylate microfluidic devices, *Electrophoresis* **2016**, *37*, 529-535.
(124) Sapsford, K. E.; Francis, J.; Sun, S.; Kostov, Y.; Rasooly, A. Miniaturized 96-well ELISA chips for staphylococcal enterotoxin B detection using portable colorimetric detector, *Analytical and bioanalytical chemistry* **2009**, *394*, 499-505.
(125) Sun, S.; Yang, M.; Kostov, Y.; Rasooly, A. ELISA-LOC: lab-on-a-chip for enzyme-linked immunodetection, *Lab on a Chip* **2010**, *10*, 2093-2100.
(126) Martinez, A. W. Microfluidic paper-based analytical devices: from POCKET to paper-based ELISA, *Bioanalysis* **2011**, *3*, 2589-2592.
(127) Li, Z.; Li, F.; Hu, J.; Wee, W. H.; Han, Y. L., *et al*. Direct writing electrodes using a ball pen for paper-based point-of-care testing, *Analyst* **2015**, *140*, 5526-5535.

(128) Cheng, C. M.; Martinez, A. W.; Gong, J.; Mace, C. R.; Phillips, S. T., *et al*. paper - based elisa, *Angewandte Chemie International Edition* **2010**, *49*, 4771-4774.
(129) Li, X.; Nie, Z.; Cheng, C.; Goodale, A.; Whitesides, G. 2010; 1487-1489.
(130) Murdock, R. C.; Shen, L.; Griffin, D. K.; Kelley-Loughnane, N.; Papautsky, I., *et al*. Optimization of a paper-based ELISA for a human performance biomarker, *Analytical chemistry* **2013**, *85*, 11634-11642.
(131) Wang, S.; Ge, L.; Song, X.; Yu, J.; Ge, S., *et al*. based chemiluminescence ELISA: lab-on-paper based on chitosan modified paper device and wax-screen-printing, *Biosensors and bioelectronics* **2012**, *31*, 212-218.
(132) Yang, Q.; Gong, X.; Song, T.; Yang, J.; Zhu, S., *et al*. Quantum dot-based immunochromatography test strip for rapid, quantitative and sensitive detection of alpha fetoprotein, *Biosensors and Bioelectronics* **2011**, *30*, 145-150.
(133) Zhou, M.; Yang, M.; Zhou, F. Paper based colorimetric biosensing platform utilizing cross-linked siloxane as probe, *Biosensors and Bioelectronics* **2014**, *55*, 39-43.
(134) Lei, K. F.; Huang, C.-H.; Kuo, R.-L.; Chang, C.-K.; Chen, K.-F., *et al*. based enzyme-free immunoassay for rapid detection and subtyping of influenza A H1N1 and H3N2 viruses, *Analytica chimica acta* **2015**, *883*, 37-44.
(135) Zhao, X.; Dong, T. Design and fabrication of low-cost 1536-chamber microfluidic microarrays for mood-disorders-related serological studies, *Sensors* **2013**, *13*, 14570-14582.
(136) Yu, C.; Kim, G.-B.; Clark, P. M.; Zubkov, L.; Papazoglou, E. S., *et al*. A microfabricated quantum dot-linked immuno-diagnostic assay (μQLIDA) with an electrohydrodynamic mixing element, *Sensors and Actuators B: Chemical* **2015**, *209*, 722-728.
(137) Liu, Y.; Wang, H.; Chen, J.; Liu, C.; Li, W., *et al*. A Sensitive Microchip - Based Immunosensor for Electrochemical Detection of Low - Level Biomarker S100B, *Electroanalysis* **2013**, *25*, 1050-1055.
(138) Yang, M.; Sun, S.; Kostov, Y.; Rasooly, A. Lab-on-a-chip for carbon nanotubes based immunoassay detection of Staphylococcal Enterotoxin B (SEB), *Lab on a Chip* **2010**, *10*, 1011-1017.
(139) Xu, T.; Miao, J.; Wang, Z.; Yu, L.; Li, C. M. Micro-piezoelectric immunoassay chip for simultaneous detection of Hepatitis B virus and α-fetoprotein, *Sensors and Actuators B: Chemical* **2011**, *151*, 370-376.
(140) Kamińska, A.; Witkowska, E.; Winkler, K.; Dzięcielewski, I.; Weyher, J. L., *et al*. Detection of hepatitis B virus antigen from human blood: SERS immunoassay in a microfluidic system, *Biosensors and Bioelectronics* **2015**, *66*, 461-467.
(141) Akama, K.; Shirai, K.; Suzuki, S. Droplet-Free Digital Enzyme-Linked Immunosorbent Assay Based on a Tyramide Signal Amplification System, *Analytical Chemistry* **2016**, *88*, 7123-7129.
(142) Shen, G.; Zhang, Y. Highly sensitive electrochemical stripping detection of hepatitis B surface antigen based on copper-enhanced gold nanoparticle tags and magnetic nanoparticles, *Analytica chimica acta* **2010**, *674*, 27-31.
(143) Lee, B. S.; Lee, J.-N.; Park, J.-M.; Lee, J.-G.; Kim, S., *et al*. A fully automated immunoassay from whole blood on a disc, *Lab on a Chip* **2009**, *9*, 1548-1555.
(144) Fu, G.; Sanjay, S. T.; Dou, M.; Li, X. Nanoparticle-mediated photothermal effect enables a new method for quantitative biochemical analysis using a thermometer, *Nanoscale* **2016**, *8*, 5422-5427.

(145) Fu, G.; Sanjay, S. T.; Li, X. Cost-effective and sensitive colorimetric immunosensing using an iron oxide-to-Prussian blue nanoparticle conversion strategy, *Analyst* **2016**, *141*, 3883-3889.
(146) T Sanjay, S.; Dou, M.; Fu, G.; Xu, F.; Li, X. Controlled drug delivery using microdevices, *Current pharmaceutical biotechnology* **2016**, *17*, 772-787.
(147) Sanjay, S. T.; Zhou, W.; Dou, M.; Tavakoli, H.; Ma, L., *et al*. Recent advances of controlled drug delivery using microfluidic platforms, *Advanced drug delivery reviews* **2017**.
(148) Dou, M.; Sanjay, S. T.; Dominguez, D. C.; Liu, P.; Xu, F., *et al*. Multiplexed instrument-free meningitis diagnosis on a polymer/paper hybrid microfluidic biochip, *Biosensors and Bioelectronics* **2017**, *87*, 865-873.
(149) Dou, M.; Sanjay, S. T.; Dominguez, D. C.; Zhan, S.; Li, X. A paper/polymer hybrid CD-like microfluidic SpinChip integrated with DNA-functionalized graphene oxide nanosensors for multiplex qLAMP detection, *Chemical Communications* **2017**, *53*, 10886-10889.
(150) Dye, C. After 2015: infectious diseases in a new era of health and development, *Phil. Trans. R. Soc. B* **2014**, *369*, 20130426.
(151) Shah, K.; Maghsoudlou, P. Enzyme-linked immunosorbent assay (ELISA): the basics, *British Journal of Hospital Medicine* **2016**, *77*, C98-C101.
(152) Chin, C. D.; Laksanasopin, T.; Cheung, Y. K.; Steinmiller, D.; Linder, V., *et al*. Microfluidics-based diagnostics of infectious diseases in the developing world, *Nature medicine* **2011**, *17*, 1015.
(153) Martinez, A. W.; Phillips, S. T.; Whitesides, G. M.; Carrilho, E.; ACS Publications, 2009.
(154) Zhang, S.; Garcia-D'Angeli, A.; Brennan, J. P.; Huo, Q. Predicting detection limits of enzyme-linked immunosorbent assay (ELISA) and bioanalytical techniques in general, *Analyst* **2014**, *139*, 439-445.
(155) Duan, G.; Zhang, C.; Li, A.; Yang, X.; Lu, L., *et al*. Preparation and characterization of mesoporous zirconia made by using a poly (methyl methacrylate) template, *Nanoscale research letters* **2008**, *3*, 118.
(156) Wingerchuk, D. M.; Banwell, B.; Bennett, J. L.; Cabre, P.; Carroll, W., *et al*. International consensus diagnostic criteria for neuromyelitis optica spectrum disorders, *Neurology* **2015**, *85*, 177-189.
(157) van Gerven, N. M.; de Boer, Y. S.; Mulder, C. J.; van Nieuwkerk, C. M.; Bouma, G. Auto immune hepatitis, *World journal of gastroenterology* **2016**, *22*, 4651.
(158) Slama, N. B.; Ahmed, S. S.; Zoulim, F. Quantification de l'antigène HBs: signification virologique, *Gastroentérologie Clinique et Biologique* **2010**, *34*, S112-S118.
(159) Jaroszewicz, J.; Serrano, B. C.; Wursthorn, K.; Deterding, K.; Schlue, J., *et al*. Hepatitis B surface antigen (HBsAg) levels in the natural history of hepatitis B virus (HBV)-infection: a European perspective, *Journal of hepatology* **2010**, *52*, 514-522.
(160) Yazdani, Y.; Roohi, A.; Khoshnoodi, J.; Shokri, F. Development of a sensitive enzyme-linked immunosorbent assay for detection of hepatitis B surface antigen using novel monoclonal antibodies, *Avicenna journal of medical biotechnology* **2010**, *2*, 207.
(161) Toy, M. Cost-effectiveness of viral hepatitis B & C treatment, *Best Practice & Research Clinical Gastroenterology* **2013**, *27*, 973-985.
(162) Chou, R.; Dana, T.; Bougatsos, C.; Blazina, I.; Khangura, J., *et al*. Screening for hepatitis B virus infection in adolescents and adults: a systematic review to update the US

Preventive Services Task Force recommendation, *Annals of internal medicine* **2014**, *161*, 31-45.
(163) Yildiz, U. H.; Inci, F.; Wang, S.; Toy, M.; Tekin, H. C., *et al*. Recent advances in micro/nanotechnologies for global control of hepatitis B infection, *Biotechnology advances* **2015**, *33*, 178-190.
(164) Yeh, Y.-T.; Nisic, M.; Yu, X.; Xia, Y.; Zheng, S.-Y. Point-of-care microdevices for blood plasma analysis in viral infectious diseases, *Annals of biomedical engineering* **2014**, *42*, 2333-2343.
(165) Ghorbel, E.; Hadriche, I.; Casalino, G.; Masmoudi, N. Characterization of thermo-mechanical and fracture behaviors of thermoplastic polymers, *Materials* **2014**, *7*, 375-398.
(166) Florescu, O.; Wang, K.; Au, P.; Tang, J.; Harris, E., *et al*. On-chip magnetic separation of superparamagnetic beads for integrated molecular analysis, *Journal of applied physics* **2010**, *107*, 054702.
(167) Kivity, S.; Gilburd, B.; Agmon-Levin, N.; Carrasco, M. G.; Tzafrir, Y., *et al*. A novel automated indirect immunofluorescence autoantibody evaluation, *Clinical rheumatology* **2012**, *31*, 503-509.
(168) Wild, D. *The Immunoassay Handbook: Theory and applications of ligand binding, ELISA and related techniques*; Newnes, 2013.
(169) Fu, G.; Sanjay, S. T.; Dou, M.; Li, X. J. Nanoparticle-mediated photothermal effect enables a new method for quantitative biochemical analysis using a thermometer, *Nanoscale* **2016**.
(170) Verbarg, J.; Plath, W. D.; Shriver-Lake, L. C.; Howell Jr, P. B.; Erickson, J. S., *et al*. Catch and release: Integrated system for multiplexed detection of bacteria, *Analytical chemistry* **2013**, *85*, 4944-4950.
(171) Wang, H.; Li, J.; Zhang, X.; Hu, B.; Liu, Y., *et al*. A Microfluidic Indirect Competitive Immunoassay for Multiple and Sensitive Detection of Testosterone in Serum and Urine, *Analyst* **2015**.
(172) Chin, C. D.; Laksanasopin, T.; Cheung, Y. K.; Steinmiller, D.; Linder, V., *et al*. Microfluidics-based diagnostics of infectious diseases in the developing world, *Nature medicine* **2011**, *17*, 1015-1019.
(173) Dou, M.; Sanjay, S. T.; Benhabib, M.; Xu, F.; Li, X. Low-cost bioanalysis on paper-based and its hybrid microfluidic platforms, *Talanta* **2015**.
(174) Li, X.; Chen, Y.; Li, P. C. A simple and fast microfluidic approach of same-single-cell analysis (SASCA) for the study of multidrug resistance modulation in cancer cells, *Lab Chip* **2011**, *11*, 1378-1384.
(175) Li, X.; Li, P. C. Strategies for the real-time detection of Ca2+ channel events of single cells: recent advances and new possibilities, *Expert Rev Clin Pharmacol* **2010**, *3*, 267-280.
(176) Lee, G.-H.; Kim, S.-H.; Kang, A.; Takayama, S.; Lee, S.-H., *et al*. Deformable L-shaped microwell array for trapping pairs of heterogeneous cells, *Journal of Micromechanics and Microengineering* **2015**, *25*, 035005.
(177) Andersen, A. S. e.; Zheng, W.; Sutherland, D. S.; Jiang, X. Versatile multiple protein nanopatterning within a microfluidic channel for cell recruitment studies, *Lab on a Chip* **2015**, *15*, 4524-4532.

(178) Lai, D.; Takayama, S.; Smith, G. D. Recent microfluidic devices for studying gamete and embryo biomechanics, *Journal of biomechanics* **2015**, *48*, 1671-1678.
(179) Roelofs, S. H.; van den Berg, A.; Odijk, M. Microfluidic desalination techniques and their potential applications, *Lab on a Chip* **2015**, *15*, 3428-3438.
(180) De, A.; Sparreboom, W.; van den Berg, A.; Carlen, E. T. Rapid microfluidic solid-phase extraction system for hyper-methylated DNA enrichment and epigenetic analysis, *Biomicrofluidics* **2014**, *8*, 054119.
(181) Dou, M.; Dominguez, D. C.; Li, X.; Sanchez, J.; Scott, G. A Versatile PDMS/Paper Hybrid Microfluidic Platform for Sensitive Infectious Disease Diagnosis, *Anal. Chem.* **2014**, *86*, 7978-7986.
(182) Zuo, P.; Li, X.; Dominguez, D. C.; Ye, B.-C. A PDMS/paper/glass hybrid microfluidic biochip integrated with aptamer-functionalized graphene oxide nano-biosensors for one-step multiplexed pathogen detection, *Lab Chip* **2013**, *13*, 3921-3928.
(183) Choi, J. R.; Liu, Z.; Hu, J.; Tang, R.; Gong, Y., *et al*. A PDMS-Paper Hybrid Lateral Flow Assay for Highly Sensitive Point-of-Care Nucleic Acid Testing, *Analytical Chemistry* **2016**.
(184) Choi, S.; Park, J.-K. Two-step photolithography to fabricate multilevel microchannels, *Biomicrofluidics* **2010**, *4*, 046503.
(185) Nam, K.-H.; Eddington, D. T. Size-based separation of microparticles in a multilayered microfluidic device, *Microelectromechanical Systems, Journal of* **2010**, *19*, 375-383.
(186) Lakos, G.; Soós, L.; Fekete, A.; Szabó, Z.; Zeher, M., *et al*. Anti-cyclic citrullinated peptide antibody isotypes in rheumatoid arthritis: association with disease duration, rheumatoid factor production and the presence of shared epitope, *Clinical and experimental rheumatology* **2008**, *26*, 253.
(187) Shors, T. *Understanding viruses*; Jones & Bartlett Publishers, 2011.
(188) Pittock, S. J.; Lennon, V. A.; de Seze, J.; Vermersch, P.; Homburger, H. A., *et al*. Neuromyelitis optica and non–organ-specific autoimmunity, *Archives of Neurology* **2008**, *65*, 78-83.
(189) Rodella, A.; Galli, C.; Terlenghi, L.; Perandin, F.; Bonfanti, C., *et al*. Quantitative analysis of HBsAg, IgM anti-HBc and anti-HBc avidity in acute and chronic hepatitis B, *Journal of clinical virology* **2006**, *37*, 206-212.
(190) Jaroszewicz, J.; Serrano, B. C.; Wursthorn, K.; Deterding, K.; Schlue, J., *et al*. Hepatitis B surface antigen (HBsAg) levels in the natural history of hepatitis B virus (HBV)-infection: a European perspective, *Journal of hepatology* **2010**, *52*, 514-522.
(191) Ben Slama, N.; Si Ahmed, S.; Zoulim, F. Quantification de l'antigène HBs: signification virologique, *Gastroentérologie Clinique et Biologique* **2010**, *34*, S112-S118.
(192) Yazdani, Y.; Roohi, A.; Khoshnoodi, J.; Shokri, F. Development of a sensitive enzyme-linked immunosorbent assay for detection of hepatitis B surface antigen using novel monoclonal antibodies, *Avicenna journal of medical biotechnology* **2011**, *2*, 207-214.
(193) Liang, M.; Wang, L.; Ma, C.; Zhang, M.; Xie, G. Sandwich immunoassay for hepatitis C virus non-structural 5A protein using a glassy carbon electrode modified with an Au-MoO3/chitosan nanocomposite, *Analytical Letters* **2013**, *46*, 1241-1254.
(194) van Amsterdam, P.; Companjen, A.; Brudny-Kloeppel, M.; Golob, M.; Luedtke, S., *et al*. The European Bioanalysis Forum community's evaluation, interpretation and implementation of the European Medicines Agency guideline on Bioanalytical Method Validation, *Bioanalysis* **2013**, *5*, 645-659.

(195) Fu, G.; Sanjay, S. T.; Li, X. Cost-effective and sensitive colorimetric immunosensing using an iron oxide-to-Prussian blue nanoparticle conversion strategy, *Analyst* **2016**.
(196) Xiang, A.; Wei, F.; Lei, X.; Liu, Y.; Guo, Y. A simple and rapid capillary chemiluminescence immunoassay for quantitatively detecting human serum HBsAg, *European journal of clinical microbiology & infectious diseases* **2013**, *32*, 1557-1564.
(197) Ehsani, M.; Chaichi, M. J.; Hosseini, S. N. Comparison of CuO nanoparticle and CuO/MWCNT nanocomposite for amplification of chemiluminescence immunoassay for detection of the hepatitis B surface antigen in biological samples, *Sensors and Actuators B: Chemical* **2017**, *247*, 319-328.
(198) Sabouri, S.; Ghourchian, H.; Shourian, M.; Boutorabi, M. A gold nanoparticle-based immunosensor for the chemiluminescence detection of the hepatitis B surface antigen, *Analytical Methods* **2014**, *6*, 5059-5066.
(199) Alberti, A.; Pontisso, P.; Chemello, L.; Fattovich, G.; Benvegnu, L., *et al*. The interaction between hepatitis B virus and hepatitis C virus in acute and chronic liver disease, *Journal of hepatology* **1995**, *22*, 38-41.
(200) Ma, C.; Xie, G.; Zhang, W.; Liang, M.; Liu, B., *et al*. Label-free sandwich type of immunosensor for hepatitis C virus core antigen based on the use of gold nanoparticles on a nanostructured metal oxide surface, *Microchimica Acta* **2012**, *178*, 331-340.
(201) Jeong, M.-S.; Ahn, D.-R. A microwell plate-based multiplex immunoassay for simultaneous quantitation of antibodies to infectious viruses, *Analyst* **2015**, *140*, 1995-2000.
(202) Bissonnette, L.; Bergeron, M. Diagnosing infections－－current and anticipated technologies for point‐of‐care diagnostics and home‐based testing, *Clinical Microbiology and Infection* **2010**, *16*, 1044-1053.
(203) Lozano, R.; Naghavi, M.; Foreman, K.; Lim, S.; Shibuya, K., *et al*. Global and regional mortality from 235 causes of death for 20 age groups in 1990 and 2010: a systematic analysis for the Global Burden of Disease Study 2010, *The Lancet* **2013**, *380*, 2095-2128.
(204) Lee, W. G.; Kim, Y.-G.; Chung, B. G.; Demirci, U.; Khademhosseini, A. Nano/Microfluidics for diagnosis of infectious diseases in developing countries, *Advanced drug delivery reviews* **2010**, *62*, 449-457.
(205) Fu, G.; Sanjay, S. T.; Zhou, W.; Brekken, R. A.; Kirken, R. A., *et al*. Exploration of Nanoparticle-Mediated Photothermal Effect of TMB-H2O2 Colorimetric System and Its Application in a Visual Quantitative Photothermal Immunoassay, *Analytical chemistry* **2018**.
(206) Giordano, B. C.; Burgi, D. S.; Hart, S. J.; Terray, A. On-line sample pre-concentration in microfluidic devices: a review, *Analytica chimica acta* **2012**, *718*, 11-24.
(207) Yeh, S.-H.; Chou, K.-H.; Yang, R.-J. Sample pre-concentration with high enrichment factors at a fixed location in paper-based microfluidic devices, *Lab on a Chip* **2016**, *16*, 925-931.
(208) Payán, M. D. R.; Jensen, H.; Petersen, N. J.; Hansen, S. H.; Pedersen-Bjergaard, S. Liquid-phase microextraction in a microfluidic-chip–High enrichment and sample clean-up from small sample volumes based on three-phase extraction, *Analytica chimica acta* **2012**, *735*, 46-53.
(209) Bai, H.-Y.; Lin, S.-L.; Chung, Y.-T.; Liu, T.-Y.; Chan, S.-A., *et al*. Quantitative determination of 8-isoprostaglandin F2α in human urine using microfluidic chip-based

nano-liquid chromatography with on-chip sample enrichment and tandem mass spectrometry, *Journal of Chromatography A* **2011**, *1218*, 2085-2090.
(210) Zhang, B.-T.; Zheng, X.; Li, H.-F.; Lin, J.-M. Application of carbon-based nanomaterials in sample preparation: a review, *Analytica chimica acta* **2013**, *784*, 1-17.
(211) Sanjay, S. T.; Dou, M.; Fu, G.; Xu, F.; Li, X. Controlled Drug Delivery using Microdevices, *Current pharmaceutical biotechnology* **2016**, *17*, 000-000.
(212) Nge, P. N.; Rogers, C. I.; Woolley, A. T. Advances in microfluidic materials, functions, integration, and applications, *Chemical reviews* **2013**, *113*, 2550-2583.
(213) Chang, C.-W.; Cheng, Y.-J.; Tu, M.; Chen, Y.-H.; Peng, C.-C., *et al*. A polydimethylsiloxane–polycarbonate hybrid microfluidic device capable of generating perpendicular chemical and oxygen gradients for cell culture studies, *Lab on a Chip* **2014**, *14*, 3762-3772.
(214) Ahmed, R.; Gray, D. Immunological memory and protective immunity: understanding their relation, *Science* **1996**, *272*, 54.
(215) Sanjay, S. T.; Dou, M.; Sun, J.; Li, X. A paper/polymer hybrid microfluidic microplate for rapid quantitative detection of multiple disease biomarkers, *Scientific Reports* **2016**, *6*.
(216) Liaw, Y.-F.; Chu, C.-M. Hepatitis B virus infection, *The Lancet* **2009**, *373*, 582-592.
(217) Lavanchy, D. Hepatitis B virus epidemiology, disease burden, treatment, and current and emerging prevention and control measures, *Journal of viral hepatitis* **2004**, *11*, 97-107.
(218) Schweitzer, A.; Horn, J.; Mikolajczyk, R. T.; Krause, G.; Ott, J. J. Estimations of worldwide prevalence of chronic hepatitis B virus infection: a systematic review of data published between 1965 and 2013, *The Lancet* **2015**, *386*, 1546-1555.
(219) Sardesai, N. P.; Kadimisetty, K.; Faria, R.; Rusling, J. F. A microfluidic electrochemiluminescent device for detecting cancer biomarker proteins, *Analytical and bioanalytical chemistry* **2013**, *405*, 3831-3838.
(220) Wu, L.; Qu, X. Cancer biomarker detection: recent achievements and challenges, *Chemical Society Reviews* **2015**, *44*, 2963-2997.
(221) Pires, N. M. M.; Dong, T.; Hanke, U.; Hoivik, N. Recent developments in optical detection technologies in lab-on-a-chip devices for biosensing applications, *Sensors* **2014**, *14*, 15458-15479.
(222) Barbosa, A. I.; Gehlot, P.; Sidapra, K.; Edwards, A. D.; Reis, N. M. Portable smartphone quantitation of prostate specific antigen (PSA) in a fluoropolymer microfluidic device, *Biosensors and Bioelectronics* **2015**, *70*, 5-14.
(223) Jia, X.; Song, T.; Liu, Y.; Meng, L.; Mao, X. An immunochromatographic assay for carcinoembryonic antigen on cotton thread using a composite of carbon nanotubes and gold nanoparticles as reporters, *Analytica chimica acta* **2017**, *969*, 57-62.
(224) Chen, Y.; Chu, W.; Liu, W.; Guo, X. Distance-based carcinoembryonic antigen assay on microfluidic paper immunodevice, *Sensors and Actuators B: Chemical* **2018**.
(225) Fragoso, A.; Latta, D.; Laboria, N.; von Germar, F.; Hansen-Hagge, T. E., *et al*. Integrated microfluidic platform for the electrochemical detection of breast cancer markers in patient serum samples, *Lab on a Chip* **2011**, *11*, 625-631.
(226) Li, B.; Yu, L.; Qi, J.; Fu, L.; Zhang, P., *et al*. Controlling capillary-driven fluid transport in paper-based microfluidic devices using a movable valve, *Analytical chemistry* **2017**, *89*, 5707-5712.

Vita

Sanjay Sharma Timilsina was born in Pokhara, Kaski, Nepal. He earned his Bachelor of Science in Biotechnology from Bangalore University in 2010. In 2012, he received his Master of Science degree in Biotechnology from Bangalore University, India. In August 2013, he joined the doctoral program in Chemistry & Biochemistry at the University of Texas at El Paso under the mentorship of Dr. XiuJun (James) Li. His dissertation project focuses on detection of disease biomarkers in surface modified polymer and paper/polymer hybrid microfluidic devices.

Sanjay was the recipient of the Graduate Award for Academic and Research Excellence in Chemistry in 2018. Besides, College of Science, UTEP chose Sanjay's Dissertation as the 'Best Dissertation' for Spring 2018. He also participated in NSF Innovation Corp for Technology commercialization and also won the third place for the Paso del Norte Venture Competition for a start-up company. In addition, he received several grants from SGA, college of science, and UTEP graduate school for his oral and poster presentations at several international conference meetings and workshops. Besides, he was also the recipient of Frank B. Cotton Trust Scholarship in 2017-2018.

His research interest is bio-analytical chemistry focusing on low-cost detection of infectious diseases and cancer biomarkers in microfluidic platforms. He has 19 published papers in high impact journals such as Advanced Drug Delivery Reviews, Biosensors and Bioelectronics, Nanoscale, and Scientific reports, of which 14 are from his doctoral degree. In addition, he has 3-filed patents and several other manuscripts under revision.

Mr. Timilsina's dissertation entitled, "Integrated Immunoassays on Paper/polymer Hybrid Microfluidic Devices for Low-cost Detection of Disease Biomarkers," was supervised by Dr. XiuJun (James) Li.

Contact Information: sanjaytimilsina@gmail.com

This thesis/dissertation was typed by Sanjay Sharma Timilsina.